# UNIVERSITY OF NAPOLI FEDERICO II

**Doctorate School in Molecular Medicine**

**Doctorate Program in**
**Genetics and Molecular Medicine**
**Coordinator: Prof. Lucio Nitsch**
**XXV Cycle**

# "A specific immunophenotype and an increased adipogenic potential characterized human amniotic mesenchymal stem cells (hA-MSCs) isolated from obese pregnant women at delivery"

**Laura Iaffaldano**


**Napoli 2013**

# "A specific immunophenotype and an increased adipogenic potential characterized human amniotic mesenchymal stem cells (hA-MSCs) isolated from obese pregnant women at delivery"

# TABLE OF CONTENTS

# LIST OF PUBLICATIONS

**Paper in extenso:**

1. Delia Zanzi, Rosita Stefanile, Sara Santagata, **Laura Iaffaldano**, Gaetano Iaquinto, Nicola Giardullo, Giuliana Lania, Ilaria Vigliano, Aufiero Rotondi Vera, Katia Ferrara, Salvatore Auricchio, Riccardo Troncone and Giuseppe Mazzarella. IL-15 interferes with suppressive activity of intestinal regulatory T cells expanded in celiac disease. **Am J Gastroenterol. 2011;106 (7): 1308-17.**

2. Marina Capuano, **Laura Iaffaldano**, Nadia Tinto, Donatella Montanaro, Valentina Capobianco, Valentina Izzo, Francesca Tucci, Giancarlo Troncone, Luigi Greco and Lucia Sacchetti. MicroRNA-449a overexpression is associated with weak NOTCH1 signals and scarce goblet cells in celiac small intestine. **PLoS One. 2011;6 (12): e29094.**

3. Valentina Capobianco, Carmela Nardelli, Maddalena Ferrigno, **Laura Iaffaldano**, Vincenzo Pilone, Pietro Forestieri, Nicola Zambrano, Lucia Sacchetti. miRNA and Protein Expression Profiles of Visceral Adipose Tissue Reveal miR-141/YWHAG and miR-520e/RAB11A as Two Potential miRNA/Protein Target Pairs Associated with Severe Obesity. **J. Proteome Res. 2012, 11, 3358−3369.**

4. **Laura Iaffaldano**, Carmela Nardelli, Maddalena Raia, Elisabetta Mariotti, Maddalena Ferrigno, Filomena Quaglia, Giuseppe Labruna, Valentina Capobianco, Angela Capone, Giuseppe Maria Maruotti, Lucio Pastore, Rosa Di Noto, Pasquale Martinelli, Lucia Sacchetti, Luigi Del Vecchio. High Aminopeptidase N/CD13 Levels Characterize Human Amniotic Mesenchymal Stem Cells and Drive Their Increased Adipogenic Potential in Obese Women. **Stem Cells Dev. 2013. In press.**

# ABSTRACT

Maternal obesity is associated to increased fetal risk of obesity and other metabolic diseases. Human amniotic mesenchymal stem cells (hA-MSC) have not been characterized in obese women. The aim of this study was to isolate and compare hA-MSC immunophenotypes from obese (Ob-) and normal weight control (Co-) women to identify alterations possibly predisposing the foetus to obesity. We enrolled 16 Ob- and 7 Co-women at delivery (mean/SEM pre-pregnancy BMI: 40.3/1.8 kg/$m^2$ and 22.4/1.0 kg/$m^2$, respectively). hA-MSCs were phenotyped by flow cytometry; several maternal and newborn clinical and biochemical parameters were also measured.

The expression of membrane antigen CD13 was higher on Ob-hA-MSCs than on Co-hA-MSCs (P=0.0043). Also serum levels of CD13 at delivery were higher in Ob- versus Co-pregnant women and correlated with CD13 antigen expression on Ob-hA-MSCs ($r^2$=0.84, P<0.0001). Adipogenesis induction experiments revealed that Ob-hA-MSCs had a higher adipogenic potential than Co-hA-MSCs as witnessed by higher PPARγ and aP2 mRNA levels (P=0.02 and P=0.03, respectively) at post-induction day 14 associated with an increase of CD13 mRNA from baseline to day 4 post-induction (P<0.05). Adipogenesis was similar in the two sets of hA-MSCs after CD13 silencing, whereas it was increased in Co-hA-MSCs after CD13 overexpression. Pretreatment of Co- and Ob-hA-MSCs with IFN-γ (12.5 ng/mL) for 24 h induced upregulation of CD13 expression.

In conclusion, antigen CD13, by influencing the adipogenic potential of hA-MSCs could be an *in-utero* risk factor for obesity. Our data strengthen the hypothesis that high levels of serum and MSC CD13 are obesity markers.

# BACKGROUND

## Epidemic Obesity and Definition

Obesity is an epidemic health problem worldwide that affects virtually all age and socioeconomic groups and threatens to overwhelm both developed and developing countries. In 1995, there were an estimated 200 million obese adults worldwide and another 18 million under-five children classified as overweight. As of 2000, the number of obese adults has increased to over 300 million. Contrary to conventional wisdom, the obesity epidemic is not restricted only to industrialized societies but also in developing countries, when it is estimated that over 115 million people suffer from obesity-related problems [WHO. Fact sheet No 311].

Obesity causes morbidity and mortality associated with increased risk of cardiovascular disease, metabolic syndrome, and cancer [Maury et al. 2010, Gesta et al. 2006]. It is a multifactorial disease caused by a complex interaction between environmental, genetic and behavioral factors. The environment is likely the major contributor to the obesity epidemic. It is certain that obesity develops when there is an altered imbalance between energy intake and energy expenditure, but the underlying mechanism is poorly understood, even if it is known that both excess energy intake and decreased energy expenditure contributed in the obesity insurgence. In addition to environment, also genetic factors play an important role in the predisposition to obesity. In fact, it is known that gene mutations are responsible for monogenic or polygenic forms of obesity [Dang et al. 2010, Choquet and Meyre 2011].

The obesity is characterized by an increased body weight. The body mass index (BMI), defined as the weight in kilograms divided by the height in meters squared ($kg/m^2$), is the more used index from the World Health Organization (WHO) for the definition of obesity grade. This classification provides that a person is overweight when the BMI is greater or equal to 25 and obese when the BMI is greater or equal to 30 [WHO. Fact sheet No 311]. Waist circumference can be used in combination with a BMI value to evaluate health risk for individuals [Mitchell et al. 2011].

The overweight and obesity consist in an adipose tissue expansion, increased adipocyte size and number, and increased macrophage infiltration that, together, lead to increased free fatty acid release, dysregulated secretion from adipocytes of a variety of adipokines, including adiponectin, leptin, resistin, and retinol binding protein 4 (RBP4), and increased release from resident macrophages of the inflammatory cytokines, tumor necrosis factor α (TNFα) and interleukin 6 (IL6). Dysregulated secretion of these adipokines elicits a variety of adverse effects on numerous tissues including the hypothalamus, liver, skeletal muscle, pancreas, and vasculature [Harwood et al. 2012].

**Table 1:** International Classification of adult underweight, overweight and obese according to BMI.

| Classification | BMI (kg/m²) |
|---|---|
| Underweight | <18.50 |
| Normal Range | 18.50 - 24.99 |
| Overweight | ≥25.00 |
| Obesity | ≥30.00 |
| Type I | 30.00 - 34-99 |
| Type II | 35.00 - 39.99 |
| Type III | ≥40.00 |

## Obesity in pregnancy

The incidence of obesity and overweight is increasing worldwide also during pregnancy, in fact recent data show that ~30% of American women of reproductive age are obese and 8% have reached extreme obesity [Ogden et al. 2006]. Maternal obesity is associated with adverse consequences both in mother and child. [Catalano et al. 2007, Huda et al. 2010]. The related risks include infertility, fetal anomalies, gestational hypertensive diseases, gestational diabetes, intrauterine fetal death, cesarean birth, macrosomia, and long-term risks of adult disease for the foetus. [Nodine et al. 2012]

Normally, the pregnancy is characterized by marked increases in plasma lipid concentrations, due to the strong lipolytic activity, to meet the feto-placental and maternal demands of late gestation and lactation. In normal weight women the majority of fat is accumulated centrally in the subcutaneous compartment. Instead, obese women, who will have more saturated subcutaneous fat stores, tend to accumulate fat more centrally (visceral) than lean women, an observation which may reflect their more insulin-resistant state. Visceral adiposity, in pregnancy, appears to be strongly correlated with adverse metabolic outcomes in pregnancy including gestational diabetes mellitus, gestational hypertension and pre-eclampsia [Huda et al. 2010].

Furthermore, the hyperlipidemia of pregnancy is exaggerated in obesity with higher serum triglyceride and very low density lipoprotein cholesterol concentrations than those observed in lean women. Maternal obesity is also accompanied by alterations in glucose metabolism and by perturbations in inflammatory markers, adipokines and vascular dysfunction [Huda et al. 2010].

Interestingly, the mother, placenta and foetus interact to modulate fetal growth during pregnancy. Maternal obesity appears to induce modifications in adipose tissue and in placenta, in fact both showed to have increased expression of proinflammatory cytokines and a marked accumulation of a heterogeneous macrophage population. Additionally, placenta from obese women compared with

that from lean women demonstrated a significant increase in the expression of the placental lipoprotein lipase, leptin and TNF-α. How this might impact placental function is not well established, however, the activation of phospholipase activity suggests that the inflammation may be one mechanism by which excess fat accumulates in obese neonates (Figure1). [Heerwagen et al. 2010].

The placenta maintains fetal homeostasis by carrying out a wide range of physiological functions. Therefore, placental perturbations, by affecting one or more aspects of placental structure and function, may determine long-term health outcomes into adulthood [Murphy et al. 2010]. For example, placental weight correlates with fetal weight, and since fetal growth is related to adult outcomes, placental weight and low birth weight could predict adult diseases as obesity, diabetes 2 and hypertension [Barker et al. 2005, Godfrey et al. 2002, Osmond et al. 2000, Lewis et al. 2006]. In addition, changes in placental structure (thicker placental exchange barrier and increased placental vascular resistance) are directly involved in the fetal programming of cardiovascular diseases [Thornburg and Louey 2010]. The placenta could act as a nutrient sensor, in fact it could modify nutrient and hormone availability to foeto-placental tissues in relation to environmental conditions in a manner that maximises fetal growth [Jansson et al. 2007]. Intrauterine growth retardation induced in animal models by a variety of methods (including over- and under-nutrition, isocalorific manipulation of the macro- and micro-nutrient content of the diet, maternal stress, hypoxemia, glucocorticoid administration, and restriction of uterine blood flow) has been shown to cause abnormalities in postnatal physiological functions [Fowden et al. 2006, Fowden et al. 2006, McMillen et al. 2005]. The exaggerated inflammatory response demonstrated in the placenta during obesity appears have critical consequences for the short- and long-term programming of obesity. [Challier et al. 2008]. The above observations led to the concept that adult disease can originate in utero as a result of changes in development during suboptimal intrauterine conditions that lead to permanent changes in tissue morphology and function - this process is called "intrauterine or fetal programming" [Fowden et al. 2008].

Fetal programming involves developmental plasticity that allows the foetus to respond to present or predicted environmental influences, by adaptive mechanisms (that is, by changing its metabolism and growth). The process whereby a developing individual makes permanent changes to its physiology or anatomy that could be advantageous in later life, is known as "predictive adaptive response". However, the predictive adaptive response of the foetus may be inappropriate if postnatal conditions are different from those expected, and this mismatch may result in adult life disease [Gluckman et al. 2008]. Because the placenta is the active interface between the maternal and fetal blood circulations, perturbation in the maternal compartment, such as altered nutrition, cytokine and hormonal levels and reduced utero-placental blood flow must be transmitted across

the placenta in order to affect the foetus. The mechanisms linking an adverse intrauterine environment to adult disease are under investigation, however studies in animal models have shown that epigenetic regulation of fetal genes in key metabolic pathways is an important mechanism in fetal programming [Pham et al. 2003, Lillycrop et al. 2005].

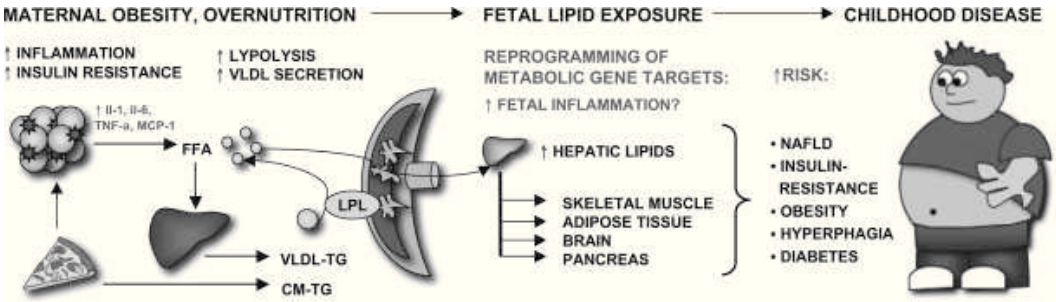


**Figure 1. Maternal metabolism undergoes profound adjustments to meet the nutrient needs of the developing foetus.** Obesity is associated with adipose tissue inflammation and systemic insulin resistance, resulting in increased adipose tissue lipolysis and hepatic very-low-density lipoprotein (VLDL) secretion. When combined with pregnancy, this leads to an increase in maternal circulating lipids with advancing gestation. Subsequent hydrolysis of maternal triglycerides (TGs) by placental lipoprotein lipase (LPL) and increased free fatty acid (FFA) uptake and transport by the placenta results in excess lipid transfer to the developing foetus. This increase in fetal lipid exposure may impact the liver, skeletal muscle, adipose tissue, brain, and pancreas to increase the risk for metabolic disease in childhood. MCP-1, monocyte chemotractant protein-1; CM, chylomicron; NAFLD, nonalcoholic fatty liver disease. [Heerwagen et al. 2010]

## Placenta

The placenta is the site of exchange between mother and foetus and regulates fetal growth. Placenta, fetal membranes and umbilical cord are fetal adnexa. The term placenta is discoid in shape with a diameter from 15 cm to 20 cm and a thickness from 2 cm to 3 cm. The fetal component, which includes the amniotic and chorionic fetal membranes, separates the foetus from the endometrium. The amniochorionic membrane forms the outer limits of the sac that encloses the foetus, while the innermost layer of the sac is the amniotic membrane (AM). The AM thickness varies from 0.02 mm to 0.5 mm and consists of an epithelial monolayer, a thick basement membrane, and an avascular stroma (Figure 2).

The innermost layer, nearest to the foetus, is the amniotic epithelium and consists of a single layer of cells uniformly arranged on the basement membrane. The basement membrane is one of the thickest membranes found in all human tissue. The support provided to the foetus by the basement membrane throughout gestation stands testimony to the structural integrity of this remarkable membrane. The compact layer of stromal matrix adjacent to the basement membrane forms the

main fibrous skeleton of the AM. The collagens of the compact layer are secreted by mesenchymal cells situated in the fibroblast layer. Interstitial collagens (types I and III) predominate and form parallel bundles that maintain the mechanical integrity of AM. Collagens type V and VI form filamentous connections between interstitial collagens and the epithelial basement membrane. The intermediate layer (spongy layer or *zona spongiosa*) of the stromal matrix sits adjacent to the chorionic membrane. Its abundant content of proteoglycans and glycoproteins produces a spongy appearance in histologic preparations, and it contains a nonfibrillar meshwork of mostly type III collagen. The spongy layer is loosely connected to the chorionic membrane; hence, the AM is easily separated from the chorion by means of blunt dissection.

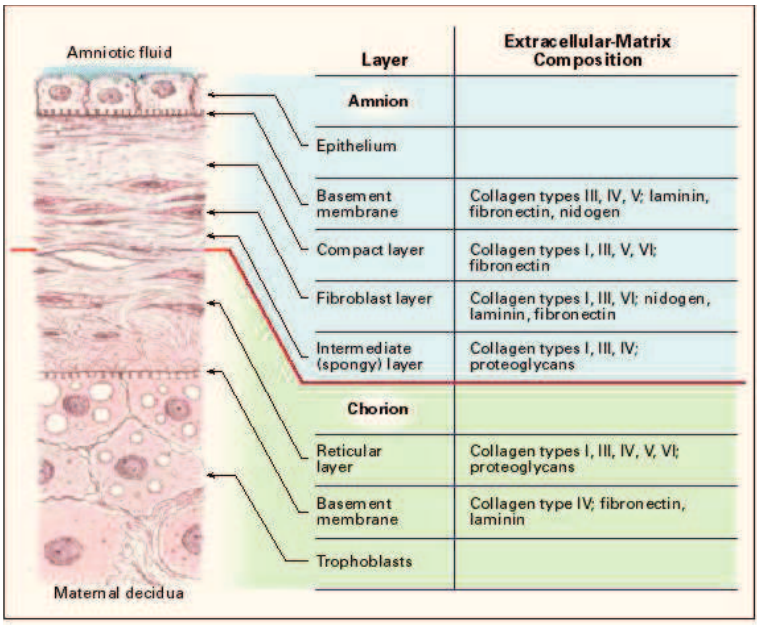


**Figure 2**: Schematic presentation of the structure of the fetal membrane at term. The Extracellular matrix components of each layer are shown [NiKnejad et al. 2008].

AM is not just a simple avascular structure (no blood vessels or nerves); it has multiple metabolic functions such as the transport by diffusion out of the amniotic fluid and/or from the underlining decidua of water and soluble materials and the production of bioactive factors, including vasoactive peptides, growth factors and cytokines [NiKnejad et al. 2008]. The AM provides protection to the developing embryo against desiccation and an environment of suspension, in which the embryo can grow free from pressures of the structures that surround its body. Furthermore, the presence of interstitial collagens, one of the important properties of AM is its resistance to proteolytic factors [NiKnejad et al. 2008]. AM

also has an important role during birth, because the substances produced by the epithelium of AM allow the initiation and maintenance of uterine contractility.

**Placental Stem Cells**

Mesenchymal stem cells (MSCs) have been thoroughly studied for over 40 years, ever since Friedenstein's initial description in 1966 [Klein and Fauza 2011]. MSCs were initially identified in the bone marrow of adult subjects. The plasticity, self-renewal and multi-lineage potential of MSCs have generated growing interest in their use in a constantly expanding variety of experimental regenerative applications [Klein and Fauza 2011]. A number of reports have identified diverse sources of MSCs, i.e. fat tissue, placental, amniotic fluid [Mihu et al. 2008]. Furthermore, it is accepted that these cells have the capacity to regenerate mesenchymal tissue and blood cells.

Human placenta, besides playing a fundamental and essential role in fetal development, nutrition, and tolerance, may also represent a reserve of progenitor/stem cells. Four regions of fetal placenta can be distinguished: amniotic epithelial, amniotic mesenchymal, chorionic mesenchymal, and chorionic trophoblastic. From these regions can be isolated: human amniotic epithelial cells (hA-EC), human amniotic mesenchymal stromal cells (hA-MSC), human chorionic mesenchymal stromal cells (hC-MSC), and human chorionic trophoblastic cells (hC-TC) [Parolini et al. 2008]. Cells from each layer demonstrate variable plasticity. Because of their plasticity, the term stem cell has been used in the literature to describe a number of cells isolated from placenta. Self renewal and "hierarchy," which are normally considered a hallmark of stem cells, have not been clearly demonstrated in the different placenta derived cell types, and therefore the term "stem cell" at this time is not always appropriate. However, it may be interesting to mention that recent reports propose an alternative stem cell concept whereby plasticity is essential to define stemness, and self renewal and hierarchy are optional characteristics [Parolini et al. 2008].

According to criteria recently proposed by Dominici et al. for bone marrow-derived mesenchymal stromal cells [Parolini et al. 2008], mesenchymal cells isolated from fetal membranes should be termed mesenchymal stromal cells (hA-MSC and hC-MSC). Minimal criteria for defining hA-MSC are as follows:

- Adherence to plastic;
- Formation of fibroblast colony-forming units;
- A specific pattern of surface antigen expression ($CD90^+$, $CD73^+$, $CD105^+$ and $CD45^-$, $CD34^-$, $CD14^-$, $HLA\text{-}DR^-$);
- Differentiation potential toward one or more lineages, including osteogenic, adipogenic, chondrogenic, and vascular/endothelial;
- Fetal origin.

# AIMS OF THE STUDY

Experimental observations and epidemiological studies led to the concept that adult disease can originate *in utero* as a result of changes in development during suboptimal intrauterine conditions that lead to permanent changes in tissue morphology and function - this process is called "intrauterine or fetal programming".

The aim of this study is to determine whether human amniotic mesenchymal stromal cells (hA-MSCs) of obese pregnant women, at delivery, differed from those of control pregnant women in term of clinical/biochemical parameters, cell morphology, immunophenotypes, adipogenic differentiation potential.

# MATERIALS AND METHODS

### *Patients and controls*

Sixteen Ob- (age range: 26–39 years) and seven Co-pregnant women, (age range: 26–38 years), pre-pregnancy BMI (mean/SEM) 40.3/1.8 kg/m$^2$ and 22.4/1.0 kg/m$^2$, respectively and thirty-two not pregnant women (16 obese and 16 normal weight, BMI >30 kg/m$^2$ and <25 kg/m$^2$, respectively) were recruited at the Dipartimento of Neuroscienze and Scienze Riproduttive and Odontostomatologiche, University of Naples Federico II. The clinical, personal and family history of the 23 women was recorded during a medical interview conducted by an expert upon hospitalization. Data relative to each pregnancy follow-up and delivery were also recorded. The general characteristics of the newborn and clinical data (birth weight, length, head circumference, Apgar score) were recorded at birth.

### *Sample collection*

Two fasting peripheral blood samples were collected in the morning from not pregnant women and from Ob- and Co-pregnant women, immediately before delivery. One sample was used for DNA extraction, whereas the other was centrifuged at 2,500 rpm for 15 min and serum was stored at -80°C until further processing. At delivery, placentas were collected by C-section from each enrolled women and immediately processed.

All patients and controls gave their informed consent to the study and both parents gave consent for their newborns. The study was performed according to the Helsinki II Declaration and was approved by the Ethics Committee of our Faculty.

### *Biochemical evaluations*

The main serum biochemical parameters were evaluated by routine assays. Leptin and adiponectin were measured in maternal serum with Luminex xMAP Technology on a BioRad Multiplex Suspension Array System (Bio-Rad, Hemel Hempstead, Herts., UK), according to the manufacturer's instructions. The ratio leptin/adiponectin (L/A) was also calculated.

### *Aminopeptidase N/CD13 ELISA assay*

Aminopeptidase N (APN)/CD13 serum levels were measured by ELISA (Life Science, Houston). Briefly, the microtiter plate was pre-coated with a specific anti-CD13 antibody. Standards or samples were then added to the appropriate microtiter plate wells with a biotin-conjugated polyclonal antibody preparation specific for CD13. Next, avidin conjugated to horseradish peroxidase was added to each microplate well and incubated for 15 min at room temperature. A TMB substrate solution (3,3´,5,5´-tetramethylbenzidine) was then added to each

well. The enzyme-substrate reaction was terminated by the addition of a sulphuric acid solution and the color change was measured spectrophotometrically at a wavelength of 450 nm. The amount of CD13 in each sample was determined by comparing the absorbance of the sample to a standard curve.

### *Cell isolation from placenta tissue*

Placentas were collected and immediately processed, according to Parolini et al. [2008]. After removal of the maternal decidua, the amnion was manually separated from the chorion and extensively washed 5 times in 40 mL of phosphate-buffered saline (PBS) containing 100 U/mL penicillin, 100 μg/mL streptomycin and 250 μg/mL amphotericin B (all from Sigma-Aldrich) after which it was mechanically minced into small pieces [Parolini et al. 2008]. Amnion fragments were digested overnight at 4°C in ACCUMAX® reagent (Innovative Cell Technology, San Diego), a combination of DNase, protease and collagenolytic enzymes [Grant et al. 2005], containing 100 U/mL penicillin, 100 μg/mL streptomycin and 250 μg/mL amphotericin B. The next day, digestion enzymes were inactivated with complete culture medium constituted by low glucose D-MEM (Sigma-Aldrich) supplemented with 10% of heat-inactivated bovine serum (FBS), 1% of non-essential amino acids and 2% of Ultraglutamine (all from Lonza, Basel, Switzerland). After centrifugation at 300g for 10 min, cell pellets and digested tissue fragments were seeded in a cell culture dish (BD Falcon, New York) in complete culture medium and incubated at 37°C in 5% $CO_2$. One week later, digested tissue pieces were removed from the dish and discarded, and isolated cells formed distinct fibroblast colony-forming units. When the colonies reached 70% confluence, they were washed with PBS and detached with trypsin/EDTA (Sigma-Aldrich), counted and reseeded in complete medium for expansion at a concentration of about 5,000/$cm^2$ [Parolini et al. 2008].

### *Cell preparation*

hA-MSCs were expanded for several passages. Absence of mycoplasma contamination was assessed as described previously [Mariotti et al. 2008]. The population-doubling level was calculated for each subcultivation with the following equation: population doubling= $[\log_{10} (N_H) - \log_{10} (N_I)]/ \log_{10} (2)$, where $N_I$ is the cell inoculum number and $N_H$ is cell harvest number [Bieback et al. 2004]. The increase in population doubling was added to the population doubling levels of the previous passages to yield the cumulative population doubling level. When 70%-80% confluent cultures reached about 4 population doublings they were detached with trypsin/EDTA, resuspended in PBS with 10% FBS, and processed for flow cytometry, and DNA, RNA and protein extraction. Cellular viability was assessed by both Trypan blue dye exclusion and the analysis of light scatter proprieties in flow cytometry, and it was never lower than 90%.

### *DNA typing*

The fetal origin of both amnion and hA-MSCs was verified by DNA typing. Genomic DNA was extracted from the mother's peripheral blood, from amnion samples and from hA-MSCs using the Nucleon BACC2 extraction kit (Illustra DNA Extraction Kit BACC2, GE Healthcare, Calfont St. Giles, Bucks., UK). DNA concentration was evaluated using the NanoDrop® ND-1000 UV-Vis spectrophotometer (NanoDrop Technologies, Wilmington, DE). Genomic DNA (1 ng) was amplified in a final volume of 25 μL using the AmpFlSTR® Identifiler™ PCR Amplification Kit (Applied Biosystems, Foster City). The AmpFlSTR® Identifiler™ PCR Amplification Kit is a short tandem repeat (STR) multiplex assay that amplifies 15 repeat loci and the Amelogenin gender determining marker in a single PCR amplification using a primer set labeled with four fluorescent molecules. The amplification was performed with the GeneAmp PCR System 9700 (Applied Biosystems) instrument. PCR products were then analyzed by capillary electrophoresis on the ABI Prism 3130 Genetic Analyzer (Applied Biosystems) together with an allelic ladder that contained all the most common alleles for the analyzed loci that were present in Caucasian populations and both a negative- and a positive-quality control sample. Typically, 1μL of each sample was diluted in 18.7μL of deionized formamide; each sample was supplemented with 0.3μL of an internal size standard (LIZ 500 Applied Biosystems) labeled with an additional fluorophore. The samples were denatured at 95 °C for 4 min and then placed in the auto sampler tray (maximum of 96 samples) on the ABI Prism 3130 for automatic injection in the capillaries. The data were analyzed by Gene Mapper Software (Applied Biosystems).

### *Immunophenotyping of hA-MSCs by flow cytometry*

We analyzed the expression of 38 hematopoietic, mesenchymal, endothelial, epithelial and no-lineage membrane antigens on the surface of hA-MSCs by four-color flow cytometry (Table 2).

The antibody cocktails contained in each tube are detailed in Table 3. All monoclonal antibodies (MoAbs) were from Becton Dickinson (San Jose) except anti-CD338-APC, which was from R&D (Minneapolis), anti-CD-133-PE and anti-CD271-APC MoAbs, which were from Milenyi Biotec (Bergisch Gladbach, Germany). For all antibody staining experiments, at least $1x10^5$ hA-MSCs isolated from each placenta sample were incubated at 4°C for 20 min with the appropriate amount of MoAbs, washed twice with PBS and finally analyzed with an unmodified Becton-Dickinson FACSCanto II flow cytometer (Becton-Dickinson, San Jose), that was set up according to published guidelines [Perfetto et al. 2006]. For each sample the respective control was prepared in order to determine the level of background cellular autofluorescence without antibody staining.

CaliBRITE beads (Becton-Dickinson, catalog no. 340486) were used as quality controls across the study as described elsewhere [Lmoreaux et al. 2006, Maeker et al. 2006], according to the manufacturer's instructions. Daily control of CaliBRITE intensity showed no change in instrument sensitivity throughout the study. The relative voltage range for each detector was assessed *una tantum* using the "eight-peak" technology (Rainbow Calibration Particles, Becton-Dickinson, catalog no. 559123) at the beginning of the study.

Compensation was set in the FACS-DiVa (Becton-Dickinson) software, and compensated samples were analyzed. Samples were acquired immediately after staining using the FACSCanto II instrument, and at least 10,000 events were recorded for each monoclonal combination. Levels of CD antigen expression were displayed as median fluorescence intensity (MFI). The FACS-DiVa software (Becton-Dickinson) was used for cytometric analysis.

**Table 2.** Surface immunophenotypic profile investigated in hA-MSCs by flow cytometry

| Fluorochrome | CD Antigen | Other Names | Molecular Weigth (kDa) | Cell expression | Function |
|---|---|---|---|---|---|
| **FITC** | **CD9** | Tspan-29 | 24-26 | Platelets, pre-B, activated T | Adhesion, migration, platelet activation |
| **APC** | **CD10** | CALLA | 100 | B/T precursors, stromal cells | Endopeptidase |
| **PE** | **CD13** | APN | 150 | Granulocytes, monocytes and their precursors, endothelial, epithelial cells, mesenchymal stem cells | Metalloproteinase |
| **PE** | **CD14** | LPS-R | 53-55 | Monocytes, macrophages | Receptor for LPS/LPB complex |
| **APC** | **CD15** | Lewis X | – | Granulocyte, monocyte, epithelial cells | Cell adhesion |
| **PE** | **CD16** | FCγRIIIa | 50-65 | Neutrophils, NK, macrophages | Low affinity with FCγ receptor, mediates phagocytosis |
| **APC** | **CD19** | Bgp95 | 95 | B, not on plasma cells | Signal transduction |
| **FITC** | **CD26** | DPP IV | 110 | Mature thymocytes, T, B, NK cells | Exoprotease, costimulation |
| **APC** | **CD28** | Tp44 | 44 | Most T, thymocyte,NK and plasma cells | Costimulation |
| **APC** | **CD29** | VLA β1-chain | 130 | T, B, Granulocytes, monocytes, fibroblast, endothelial, NK , platelet | Adhesion activation, embryogenesis and development |
| **FITC** | **CD31** | PECAM-1 | 130-140 | Monocytes, platelets, granulocytes and endothelial cells | Cell adhesion |
| **APC** | **CD33** | My9 | 67 | Monocytes, granulocytes, masocytes and myeloid progenitors | Cell adhesion |
| **APC** | **CD34** | My10 | 105-120 | Hematopoietic stem cells and progenitors, endothelial cells | Cell adhesion |
| **APC** | **CD36** | Platelet GPIV | 85 | Platelets, monocytes, macrophages, endothelial cells, erythroid precursors | Adhesion and phagocytosis |
| **FITC** | **CD40** | Bp50 | 48 | Monocytes, macrophage, B, endothelial, fibroblast cells, keratinocytes | Costimulation to B cells, growth, differentiation and isotype switching |
| **APC** | **CD44** | H-CAM | 90 | Leukocytes, erythrocytes and epithelial cells | Rolling, homing and aggregation |
| **Per Cp** | **CD45** | LCA | 180-220 | hematopoietic cells, except erythrocyte and platelet | Critical for T and B cell receptor mediated activation |
| **FITC** | **CD47** | IAP I | 50-55 | Hematopoietic, epithelial, endothelial, brain mesenchymal cells | Adhesion |
| **FITC** | **CD49d** | VLA-4 | 150 | B and T , monocytes, eosinophils, basophils, NK, dendritic cells | Adhesion, migration, homing, activation |
| **APC** | **CD54** | ICAM-1 | 80-114 | Epithelial and endothelial cells monocyte. Low on resting lymphocyte, upregulate on activated | T cell activation |
| **PE** | **CD56** | NCAM | 175-220 | Neural, tumors, embryonic tissue, NK | Homophilic and heterophilic adhesion |
| **PE** | **CD58** | LFA-3 | 40-70 | Leucocyte, erythrocyte, epithelial endothelial cells and fibroblast | Costimulation |
| **FITC** | **CD71** | Transferrin recepor | 95 | Reticulocytes, erythroid precursor | Controls iron intake during cell proliferation |
| **APC** | **CD81** | TAPA-1 | 26 | B, T, monocytes, endothelial cells | Signal transduction |
| **FITC** | **CD90** | Thy-1 | 25-35 | Hematopoietic stem cells, neurons, mesenchymal stem cells | Inhibition of hematopoietic stem cells and neurons differentiation |
| **PE** | **CD99** | MIC2 | 32 | Leucocyte, NK, monocytes, endothelial and epithelial cells | Leucocyte migration, T cell activation,cell adhesion |
| **PE** | **CD105** | Endoglin | 90 | Endothelia and mesenchymal stem cells erythroid precursors, monocytes | Angiogenesis, modulates cellular response to TGFβ1 |
| **PE** | **CD117** | c-kit | 145 | Hematopoietic stem cells and progenitors | Crucial for hematopoietic stem cells |
| **PE** | **CD133** | Prominin-1 | 120 | Hematopoietic stem cell, endothelial, epithelial and neural precursors | Unknown function, stem cells marker |
| **PE** | **CD151** | PETA-3 | 32 | Endothelial and epithelial cells, megakaryocye, platelets | Adhesion |
| **PE** | **CD166** | ALCAM | 100-105 | Neurons, activated T cells, epithelial cells, MSC | Adhesion, T cells activation |
| **PE** | **CD200** | OX-2 | 33 | B , activated T, Thymocytes, neurons endothelium | Down regulatory signal for myeloid cell functions |
| **FITC** | **CD243** | MDR-1 | 170 | Stem cells, multi drug resistant tumours | Influences the up-take, distribution, elimination of drugs |
| **APC** | **CD271** | NGFR | 75 | Neurons, stromal and dendritic follicular cells | Low affinity for NGF receptor |

| | | | | | |
|---|---|---|---|---|---|
| **APC** | **CD324** | E-cadherin | 120 | Epithelial, keratinocytes, platelet | Adhesion, growth, differentiation |
| **APC** | **CD338** | ABCG-2 | 72 | Hematopoietic stem cells, liver, kidney, intestine, side population of stem cells | Absorbition and excretion of xenobiotics |
| **FITC** | **HLA-ABC** | Class I MHC | 46 | All nucleated cells and platelets | Antigen presentation |
| **FITC** | **HLA-DR** | Class II MHC | 30 | B cells, monocytes, myeloid progenitors, activated T and dendritic cells | Antigen presentation |

**Table 3:** Antibody cocktails contained in each tube for hA-MSCs immunophenotyping by flow cytometry.

| Tube | CD Antigens |
|---|---|
| 1 | Anti-CD90-FITC (clone 5E10)/anti-CD13-PE (clone L138)/anti-CD45-PerCP (clone 2D1)/anti-CD34-APC (clone 8G12) |
| 2 | Anti-HLA-DR-FITC (clone l243)/anti-CD14-PE (clone MΦP9)/anti-CD45-PerCP (clone 2D1)/anti-CD29-APC (clone MAR4) |
| 3 | Anti-CD243-FITC (clone17F9)/anti-CD56-PE (clone MY31)/anti-CD45-PerCP (clone 2D1)/anti-CD44-APC (clone g44-26) |
| 4 | Anti-CD324-FITC (clone 36)/anti-CD105-PE (clone 266)/anti-CD45-PerCP (clone 2D1)/anti-CD338-APC (clone 5D3) |
| 5 | Anti-CD71-FITC (clone L01.1)/anti-CD56-PE (clone MY31)/anti-CD45-PerCP (clone 2D1)/anti-CD28-APC (clone CD28.2) |
| 6 | Anti-CD90-FITC (clone 5E10)/anti-CD200-PE (clone MRC OX-104)/anti- CD45-PerCP (clone 2D1)/anti-CD33-APC (clone p67.6) |
| 7 | Anti-HLA-A,B,C-FITC (clone G46-2.6)/anti-CD16-PE (clone B73.1)/anti-CD45-PerCP (clone 2D1)/anti-CD36-APC (clone CB38 NL07) |
| 8 | Anti-CD90-FITC (clone 5E10)/anti-CD200-PE (clone MRC OX-104)/anti-CD45-PerCP (clone 2D1)/anti-CD34-APC (clone 8G12) |
| 9 | Anti-CD9-FITC (clone ML-13)/anti-CD133-PE (clone ACC133/1)/anti-CD45-PerCP (clone 2D1)/anti-CD10-APC (clone HI10A) |
| 10 | Anti-49d-FITC (clone R1-2)/anti-CD58-PE (clone L306.4)/anti-CD45-PerCP (clone 2D1)/anti-CD271-APC (clone ME20.4-1.H4) |
| 11 | Anti-CD31-FITC (clone WM59)/anti-CD117-PE (clone 104D2)/anti-CD45-PerCP (clone 2D1)/anti-CD81-APC (clone JS-81) |
| 12 | Anti-CD26-FITC (clone L272)/anti-CD99-PE (clone TU12)/anti-CD45-PerCP (clone 2D1)/anti-CD19-APC (clone SJ25C1) |
| 13 | Anti-CD40-FITC (clone 53C)/anti-CD151-PE (clone 14A.H1)/anti-CD45-PerCP (clone 2D1)/anti-CD54-APC (clone HA58) |
| 14 | Anti-CD47-FITC (clone B6H12)/anti-CD166-PE (clone 3A6)/anti-CD45-PerCP (clone 2D1)/anti-CD15-APC (clone HI98) |

FITC: fluorescein isothiocyanat; PE: R-Phycoerythrin; PerCP: peridinin-chlorophyll-protein complex; APC: allophycocyanin

### *Differentiation potential towards the adipogenic lineage*

hA-MSCs were cultured in low glucose D-MEM (Sigma-Aldrich) supplemented with 10% of FBS, 2% of ultraglutamine and 1% of non-essential amino acids at 37°C in 5% $CO_2$ (all from Lonza, Basel, Switzerland). The cells were passaged twice before the addition of differentiation medium composed of DMEM with the addition of 10% FBS, 1 µM dexamethasone, 0.5 mM 3-isobutyl-1-methylxhantine, 200 µM indomethacin and 10 µg/mL insulin. Media were changed every two days and cells were either stained or collected for RNA extraction.

### *CD13 RNA interference and overexpression*

hA-MSCs plated at a density of 5,000 cells/$cm^2$ were transfected using 20 µL Lipofectamine 2000 according to the manufacturer's instructions (Invitrogen, Paisley, UK) with 8 µg short hairpin RNAs (shRNAs)-expressing plasmids (Open Biosystem, Huntsville) or with 8 µg pCMV-Sport 6 Vector (Invitrogen, Paisley, UK), to silence or to overexpress CD13 mRNA, respectively. Transfected cells were induced to differentiate towards the adipogenic lineage up to 4 days.

### *Effect of IFN-γ on the expression of CD13 on the surface of hA-MSCs*

The expression of CD13 on the surface of Co- and of Ob-hA-MSCs was measured after exposure of cells to 0.8 and 12.5 ng/mL IFN-γ at 37° C for 24 h, using untreated Co- and Ob-hA-MSCs as controls. At the end of incubation, the cells were harvested by trypsin, washed in PBS, counted, and adjusted to the same concentrations of $1x10^5$ hA-MSCs. Subsequently, their immunophenotype was examined by flow cytometry.

### Adipocyte staining

After 14 days of differentiation, the adipocyte cultures were stained for lipid droplets, which are an index of differentiation. The cells were washed in PBS and fixed in 10% formalin for 1 h. Then they were washed in PBS and the lipids were stained for 15 min with Oil-red-O prepared by mixing vigorously three parts of stock solution (0.5% Oil-red-O in 98% isopropanol) with two parts of water and then eliminating undissolved particles with a 0.4-µm filter. Cells were then washed with water and the number of adipocytes was evaluated with a microscope. Relative lipid levels were assessed by redissolving the Oil-Red-O present in stained cells in 98% isopropanol and then determining absorbance at 550 nm.

### RNA isolation

Total RNA was purified from hA-MSCs isolated from term placentas of Co- and of Ob-pregnant women using the mirVana™ miRNA isolation kit

(Ambion, Austin) and its concentration was evaluated with the NanoDrop® ND-1000 UV-Vis spectrophotometer (NanoDrop Technologies, Wilmington).

### *Quantitative real-time polymerase chain reaction (qRT-PCR) of mRNAs*

Real-time quantitative PCR was carried out on the Applied Biosystems 7900HT Sequence Detection system (Applied Biosystems). cDNAs were synthesized from 2 μg of total RNA using hexamer random primers and M-MuLV Reverse Transcriptase (New England BioLabs, Beverly). The PCR reaction was performed in a 20 μL final volume containing cDNA, 1X SYBR Green PCR mix, 10 μM of each specific primer. Table 4 lists the oligonucleotide primers used for PCR of selected genes: peroxisome proliferator-activated receptor gamma (PPARγ), CD13, protein homologous to myelin P2 (aP2), and glyceraldehyde-3-phosphate dehydrogenase (GAPDH). The PCR conditions for reverse transcription were: stage 1: 50°C, 2 min; stage 2: 95°C, 10 min; stage 3: 95°C, 15 s; 60°C, 1 min/40 cycles; and stage 4: 95°C, 15 s; 60°C, 1 min. Levels of target genes were quantified using specific oligonucleotide primers and normalized for GAPDH expression.

**Table 4**: PCR oligonucleotide primers

| **Primers** | **Sequence** |
|---|---|
| CD13 Forward | GGACAGCGAGTTCGAGGGGGA |
| CD13 Reverse | AGTGGCCACCACCTTTCTGACA |
| PPARγ Forward | CATACATAAAGTCCTTCCCGCTG |
| PPARγ Reverse | CGAATGGTGATTTGTCTGTTGTCT |
| aP2 Forward | GGTGGTGGAATGCGTCATG |
| aP2 Reverse | CAACGTCCCTTGGCTTATGC |
| GAPDH Forward | GTCGGAGTCAACGGATTTGG |
| GAPDH Reverse | AAAAGCAGCCCTGGTGACC |

### *Statistical analysis*

The parameters investigated were expressed as mean and standard error of the mean (SEM) (parametric distributions) or as median value and 25$^{th}$ and 75$^{th}$ percentiles (non parametric distributions). Student's "t" and Mann-Whitney tests were used to compare parametric and nonparametric data, respectively. P values $<0.05$ were considered statistically significant. Correlation analysis was performed with the SPSS package for Windows (ver. 18; SPSS Inc., Headquarters, Chicago).

# RESULTS

The clinical and biochemical characteristics of the mothers and their newborns are reported in Table 5 (A and B, respectively). Weight gain was lower (P=0.025) and diastolic blood pressure was higher (P=0.039) in Ob- than in Co-pregnant women. Both leptin concentration (P<0.0001) and the L/A ratio (P<0.0001) were higher in Ob- than in Co-pregnant women at delivery. Biometric characteristics did not differ significantly between Ob- and Co-newborns.

**Table 5.** Clinical and biochemical characteristics of obese (Ob-) and normal weight control (Co-) pregnant women at delivery and their newborns.

| **A** | | |
|---|---|---|
| **Mother's parameters** | **Ob-pregnant women (n=16)** | **Co-pregnant women (n=7)** |
| Age (years) | 32.6 (0.9) | 30.7 (1.5) |
| Weight (kg) [a] | 110.1 (5.4) | 65.2 (3.6) |
| Height (m) | 163.3(1.6) | 169.0 (1.7) |
| BMI pre-pregnancy (kg/m$^2$) [a] | 40.3 (1.8) | 22.4 (1.0) |
| Weight gain in pregnancy [b] | 8.4 (1.3) | 14.3 (1.8) |
| Systolic blood pressure (mmHg) | 124.3 (2.7) | 117.1 (5.1) |
| Diastolic blood pressure (mmHg) [c] | 82.5 (2.2) | 74.2 (2.0) |
| Frequency cardiac. | 79.6 (1.7) | 79.0 (3.7) |
| Gestational age | 38.4 (0.3) | 38.7 (0.2) |
| Glucose (mmol/L) | 4.3 (0.1) | 4.0 (0.3) |
| Total cholesterol (mmol/L) | 6.9 (0.4) | 7.3 (0.1) |
| Triglycerides (mmol/L) | 2.8 (0.2) | 2.3 (0.3) |
| AST (U/L) | 15 [d] (12.2-26.5[d]) | 14.8 (0.7) |
| ALT (U/L) | 13 [d] (9.2-17.7[d]) | 12.1 (1.1) |
| ALP (U/L) | 124.2 (11.1) | 115.0 (12.6) |
| GGT (U/L) | 11.0 (1.7) | 8.8 (1.5) |
| Leptin (L)(ng/ml) [a] | 38.5 (2.2) | 15.2 (3.3) |
| Adiponectin (A)(mg/ml) | 6.0 (0.7) | 7.5 (1.4) |
| L/A [a] | 7.7 (0.6) | 2.6 (0.5) |
| **B** | | |
| **Newborn's parameters** | **Ob-newborns (n=16)** | **Co-newborns (n=7)** |
| Birth weight (kg) | 3162 (0.1) | 3401 (0.1) |
| Length (cm) | 49.6 (0.7) | 50.8 (0.7) |
| Head circumference (cm) | 34.0 (0.4) | 34.8 (0.3) |
| Apgar 1' | 7.0 [d] (7.0-8.0 [d]) | 7.8 (0.2) |
| Apgar 5' | 9.0 [d] (8.5-9.0 [d]) | 8.7 (0.1) |

Data are expressed as mean (SEM) (parametric distributions).
Statistically significant difference at "t Student" test: [a] P<0.0001, [b] P =0.025 and [c] P=0.039.
[d] median value and 25$^{th}$ – 75$^{th}$ percentiles (non parametric distributions).

## Isolation of hA-MSCs

We isolated hA-MSCs from the mesenchymal layer of amniotic membranes obtained from our Ob- and Co-pregnant women at delivery. The fetal origin of all isolated hA-MSCs was confirmed by STR typing of DNA of the mother and of the hA-MSCs. Mycoplasma contamination of cultures was checked and excluded (data not shown). All isolated hA-MSCs were characterized by a high proliferation potential and collected after 4 population doublings. Morphologically, cultured Ob- and Co-hA-MSCs showed a similar fibroblastic-like morphology after 4 population doublings (Figure 3).

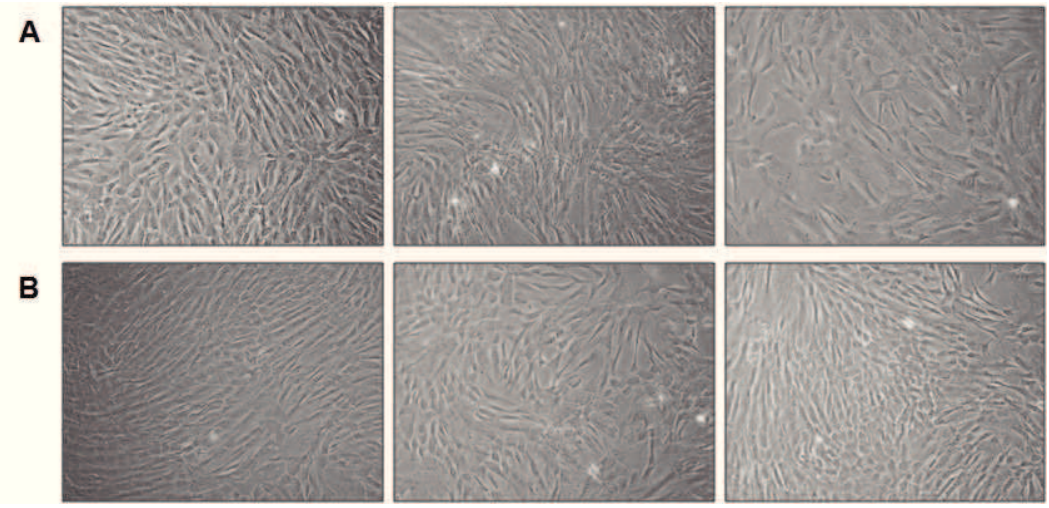


**Figure 3: Morphology of hA-MSCs isolated from pregnant women.** A similar fibroblastic-like shape was observed in three Ob- **(A)** and three Co- **(B)** hA-MSCs after 4 population doublings by phase contrast light microscopy (magnification 10x).

## Immunophenotyping of placental hA-MSCs

The antigenic mosaic displayed by Ob- and Co-hA-MSCs is shown in Table 5. Seventeen of the 38 antigens investigated were not expressed on the surface of hA-MSCs (hematopoietic antigens: CD14, CD15, CD16, CD19, CD28, CD33, CD34, CD45 and CD117; the endothelial marker PECAM-1/CD31; and no-lineage markers: thrombospondin receptor/CD36, Bp50/CD40, Prominin-1/CD133, MDR-1/CD243, NGFR/CD271, ABCG-2/CD338 and HLA-DR). Both Ob- and Co-hA-MSCs were positive for the following mesenchymal markers: CD9, CD10, CD13, CD26, CD29, CD44, CD47, CD49d, CD54, CD56, CD58, CD71, CD81, CD90, CD99, CD105, CD151, CD166, CD200 and HLA-ABC. A very weak positivity for the epithelial antigen E-cadherin/CD324 was also observed. Interestingly, CD13 expression was significantly higher in Ob-hA-MSCs than in Co-hA-MSCs, i.e., MFI: 9,802.0 and 3,950.0, respectively (P=0.0043) (Table 6 and Figure 4A).

**Table 6.** Immunophenotyping of hA-MSCs isolated from obese (Ob-) and control (Co-) pregnant women

| | | Ob-hA-MSCs | | Co-hA-MSCs | | |
|---|---|---|---|---|---|---|
| **Not expressed antigens** | | | | | | |
| **Fluorochrome** | **Antigen** | **MFI** | **25th-75th Percentiles** | **MFI** | **25th-75th Percentiles** | **p Value** |
| **FITC** | **CD31** | 364.0 | 278.3-511.3 | 306.5 | 286.8-368.0 | 0.3254 |
| | **CD40** | 444.0 | 336.5-568.3 | 388.0 | 357.0-457.8 | 0.4824 |
| | **CD243** | 363.0 | 292.3-528.3 | 307.5 | 274.0-378.3 | 0.2061 |
| | **HLA-DR** | 355.0 | 283.8-530.0 | 297.0 | 272.5-374.8 | 0.2415 |
| | **NC** | 325.0 | 250.0-516.3 | 279.0 | 218.8-418.8 | 0.4260 |
| **PE** | **CD14** | 166.5 | 125.5-197.8 | 134.5 | 124.5-157.8 | 0.2815 |
| | **CD16** | 36.0 | 11.5-71.7 | 65.5 | 50.5-72.0 | 0.2407 |
| | **CD117** | 142.5 | 109.5-189.3 | 121.0 | 116.0-176.8 | 0.6065 |
| | **CD133** | 95.5 | 80.5-112.8 | 87.5 | 76.50-110.5 | 0.5423 |
| | **NC** | 115.5 | 91.75-181.5 | 102.5 | 93.25-135.0 | 0.5427 |
| **APC** | **CD15** | 122.0 | 91.0-283.5 | 122.5 | 80.0-162.5 | 0.6065 |
| | **CD36** | 241.5 | 194.0-388.5 | 200.5 | 145.5-267.3 | 0.2417 |
| | **CD271** | 208.0 | 127.0-296.5 | 170.0 | 127.5-233.3 | 0.6065 |
| | **CD338** | 200.5 | 106.5-373.0 | 107.5 | 101.8-146.8 | 0.1223 |
| | **CD19** | 192.0 | 154.0-241.3 | 144.0 | 120.3-182.2 | 0,1012 |
| | **CD28** | 91.0 | 5.2-228.5 | 85.5 | 0-122.0 | 0.1722 |
| | **CD33** | 147.5 | 10.0-189.5 | 105.5 | 90.0-132.3 | 0.6734 |
| | **CD34** | 186.5 | 105.0-241.5 | 133.0 | 17.5-206.0 | 0.4250 |
| | **NC** | 169.0 | 99.5-244.8 | 92.0 | 64.0-204.0 | 0.2061 |
| **Per Cp** | **CD45** | 215.5 | 133.8-251.3 | 167.0 | 146.0-208.0 | 0.6734 |
| | **NC** | 305.0 | 252.0-483.3 | 288.5 | 261.3-348.8 | 0.7431 |
| **Expressed antigens** | | | | | | |
| **Fluorochrome** | **Antigen** | **MFI** | **25th-75th Percentiles** | **MFI** | **25th-75th Percentiles** | **p Value** |
| **FITC** | **CD9** | 3,538.0 | 2,172.0-6,871.0 | 2,156.0 | 1,743.0-3,495.0 | 0.2417 |
| | **CD26** | 1,287.0 | 651.8-3,235.0 | 1,308.0 | 742.3-1,920.0 | 0.9626 |
| | **CD47** | 1,339.0 | 980.3-2,312.0 | 1,287.0 | 1,106.0-1,344.0 | 0.4824 |
| | **CD49d** | 1,185.0 | 946.8-1,393.0 | 941.0 | 708.3-1,140.0 | 0.2061 |
| | **CD71** | 1,271.0 | 796.5-2,147.0 | 1,093.0 | 897.0-1,538.0 | 0.7431 |
| | **CD90** | 37,140.0 | 22,740.0-52,690.0 | 36,210.0 | 21,640.0-50,260.0 | 0.8149 |
| | **CD324** | 517.0 | 463.0-551.0 | 436.0 | 375.0-545.0 | 0.3027 |
| | **HLA-ABC** | 9,363.0 | 4,033.0-14,180.0 | 5,424.0 | 3,987.0-6,539.0 | 0.1223 |
| | **NC** | 325.0 | 250.0-516.3 | 279.0 | 218.8-418.8 | 0.4260 |
| **PE** | **CD13** | 9,802.0 | 6,786.0-17,130.0 | 3,950.0 | 3,634.0-4,961.0 | 0.0043 [a] |
| | **CD56** | 496.0 | 293.8-711.0 | 528.0 | 151.0-1,048.0 | 0.9626 |
| | **CD58** | 2,432.0 | 1,723.0-2,792.0 | 2,009.0 | 1,798.0-2,459.0 | 0.5427 |
| | **CD99** | 405.0 | 296.5-586.3 | 467.5 | 360.5-651.0 | 0.3736 |
| | **CD105** | 652.0 | 507.0-1,329.0 | 790.0 | 746.0-847.8 | 0.6734 |
| | **CD151** | 16,010.0 | 10,970.0-21,430.0 | 19,410.0 | 11,090.0-23,690.0 | 0.4260 |

| | | | | | | |
|---|---|---|---|---|---|---|
| | **CD166** | 5,215.0 | 3,551.0-7,382.0 | 4,634.0 | 3,962.0-5,608.0 | 0.6734 |
| | **CD200** | 722.5 | 205.8-1,699.0 | 1,137.0 | 631.5-1,444.0 | 0.3736 |
| | **NC** | 115.5 | 91.7-181.5 | 102.5 | 93.2-135.0 | 0.5427 |
| **APC** | **CD10** | 1,247.0 | 999.3-2,319.0 | 1,890.0 | 1,122.0-3,031.0 | 0.3736 |
| | **CD29** | 45,150.0 | 25,130.0-54,610.0 | 24,240.0 | 17,660.0-40,000.0 | 0.0832 |
| | **CD44** | 11,440.0 | 8,186.0-16,290.0 | 7,259.0 | 6,613.0-9,753.0 | 0.0678 |
| | **CD54** | 9,910.0 | 5,404.0-14,260.0 | 10,660.0 | 9,486.0-24,670.0 | 0.3736 |
| | **CD81** | 31,240.0 | 19,110.0-55,050.0 | 38,890.0 | 24,500.0-44,640.0 | 0.8149 |
| | **NC** | 169.0 | 99.5-244.8 | 92.0 | 64.0-204.0 | 0.2061 |

MFI, Median fluorescence intensity; [a] significant P value at Mann-Whitney test.

## APN/CD13 serum levels

We first measured baseline serum levels of CD13 in a small group of not pregnant obese and normal weight women and found significantly higher values in the obese subset (medians: 6.00 U/L and 1.00 U/L, P=0.02, respectively) (Figure 4B). The serum levels of CD13 were also significantly higher in Ob- than in Co-pregnant women at delivery (medians: 24.00 U/L and 7 U/L, P=0.002, respectively), (Fiure 4B). CD13 levels were significantly higher in Ob- and Co-pregnant women than in not pregnant Ob- and Co-women: 4 (P=0.0003) and 7 times (P=0.003), respectively. Furthermore, in Ob-pregnant women, serum CD13 levels were significantly correlated to the levels of CD13 on the surface of hA-MSCs ($r^2$=0.84; P<0.0001) (Figure 4C).

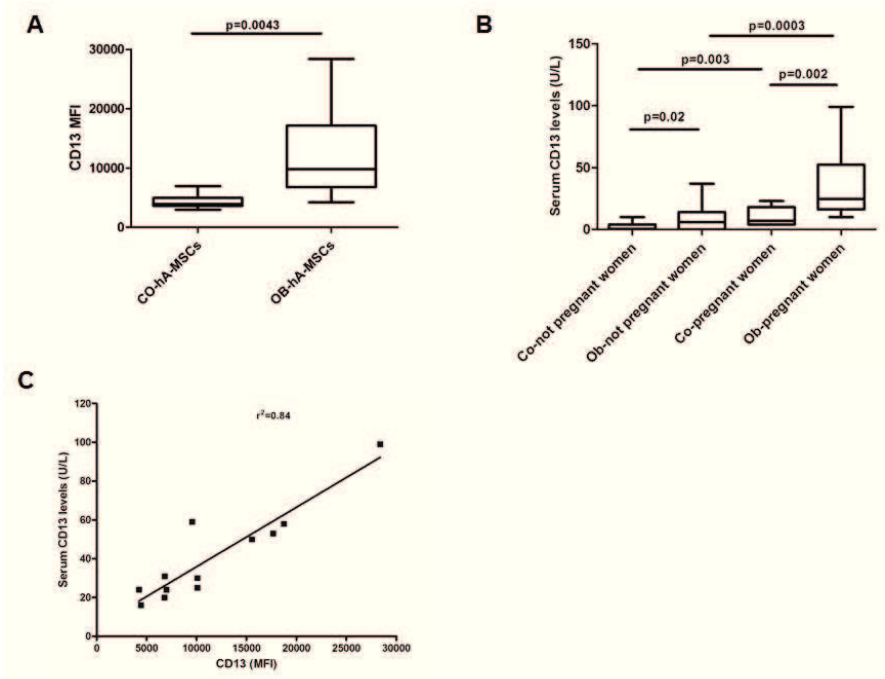


**Figure 4. Expression of CD13 antigen in control (Co-) and obese (Ob-) pregnant women. A**: Ob-hA-MSCs expressed significantly higher amounts (at Mann-Whitney test) of CD13 surface antigen compared with Co-hA-MSCs (P=0.0043); **B**: serum levels of CD13 were significantly higher in Ob-women than in Co-women at delivery (P=0.002); **C**: Serum CD13 levels were correlated with CD13 surface expression levels in Ob-pregnant women ($r^2$=0,84; P<0.0001). The box plots provide a vertical view of the data expressed as median, 25th percentile, 75th percentile and extreme values.

## CD13 hA-MSC expression during adipogenic differentiation

To investigate whether CD13 is involved in adipogenesis, we cultured Ob- and Co-hA-MSCs for 14 days in adipogenic induction medium. At the end of incubation, the adipogenic potential, as measured by PPARγ and aP2 mRNA levels, was higher in Ob- than in Co-hA-MSCs. In fact, as shown in Figure 5A and 5B, the mean RQs at day 14 were 0.04 and 0.02, respectively for PPARγ (P=0.02), and 0.02 and 0.01, respectively for aP2 (P=0.03). The same results were obtained by Oil-Red staining, this latter being higher incorporated in Ob- than in Co-hA-MSCs at day 14 of differentiation [Abs (550 nm) = 0.6 and 0.4, P=0.02, respectively] (Figure 5C).

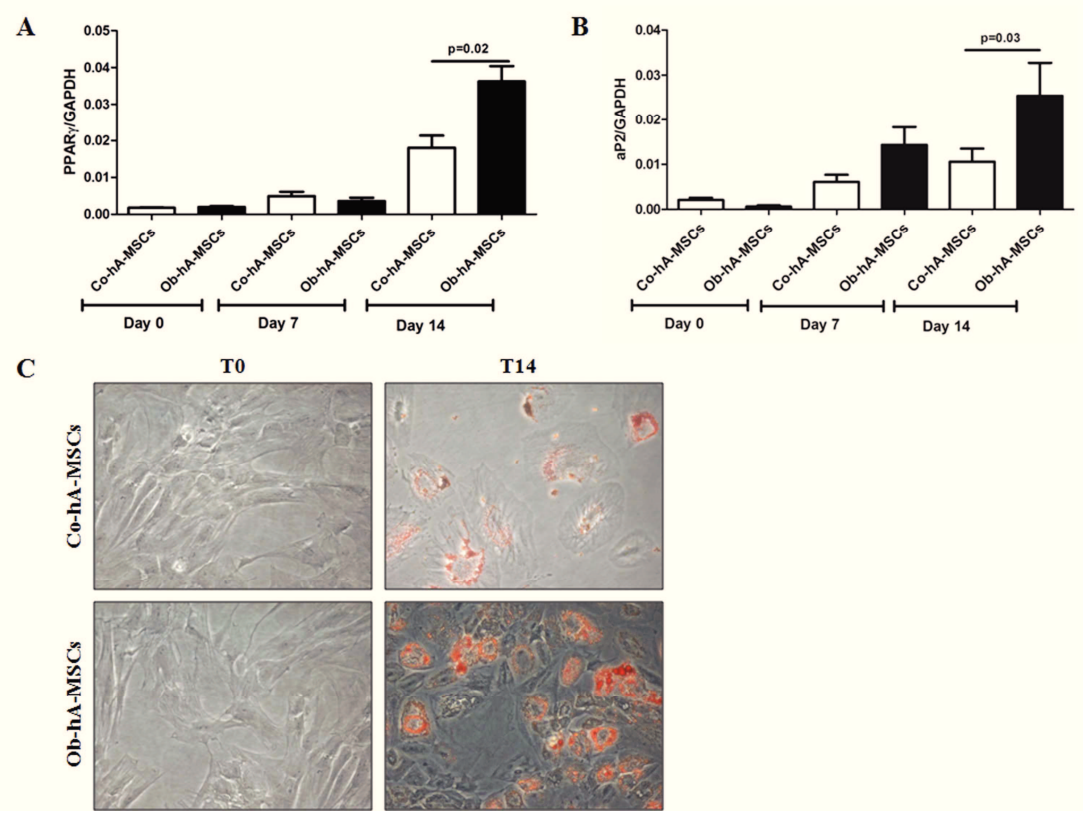


**Figure 5. Adipogenic potential in Ob-hA-MSCs and in Co-hA-MSCs.** The statistically significant higher mRNA expression levels of PPARγ (P=0.02) (A) and of aP2 (P=0.03) (B) measured 14 days after the adipogenic induction, indicated increased adipogenesis in Ob- versus Co-hA-MSCs. The higher adipogenesis in Ob- than in Co-hA-MSCs was also confirmed by Oil-Red staining [Abs (550 nm) = 0.6 and 0.4, P=0.02, respectively] (C).

During adipogenesis, CD13 mRNA levels remained higher in Ob- than in Co-hA-MSCs. When we silenced CD13 by shRNA in Ob-hA-MSCs we observed a switch-off of CD13 mRNA expression, as evaluated by RT-PCR (Figure 6A), and at the same time, the adipogenic potential of these cells did not differ from that observed in Co-hA-MSCs, as shown by similar PPARγ mRNA levels measured in silenced Ob-hA-MSCs and in Co-hA-MSCs (P=0.71) (Figure 6B). In agreement to CD13 involvement in adipogenesis, we overexpressed CD13 in Co-hA-MSCs (mRNA CD13 mean RQ=7.23) and observed at day 4 of differentiation higher PPARγ mRNA levels in treated (mean RQ=0.015) than in untreated (mean RQ=0.001) Co-hA-MSCs.

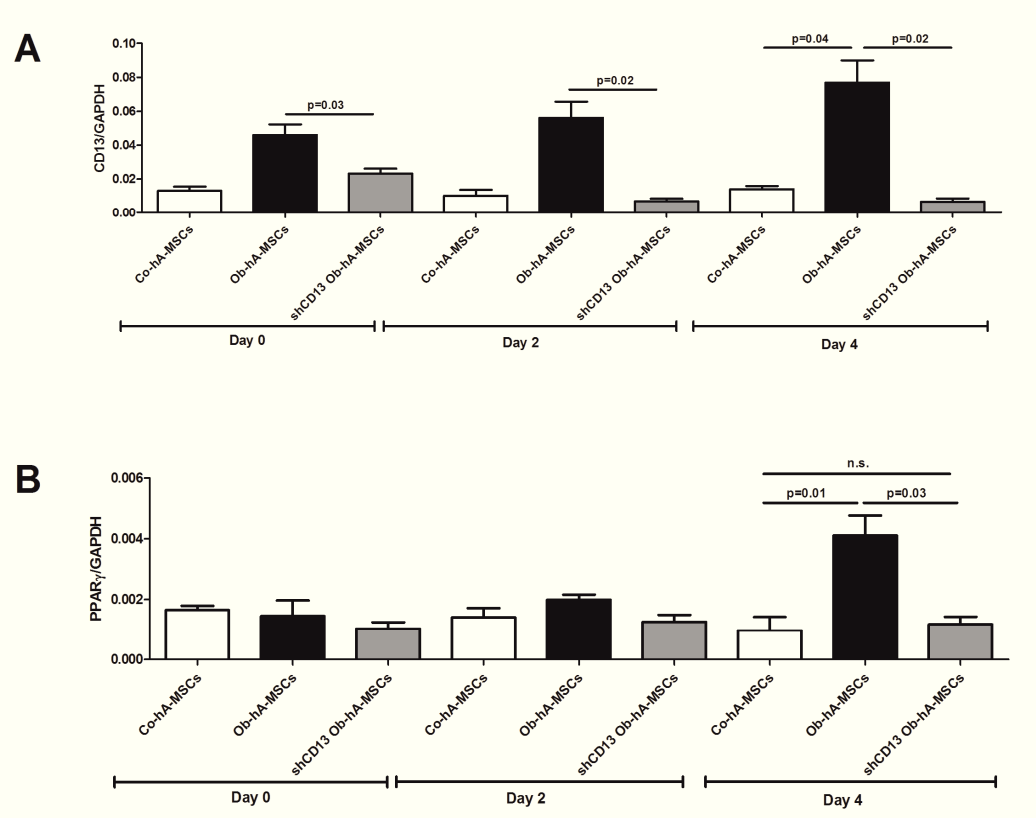


**Figure 6. Role of CD13 in adipogenesis.** (**A**) mRNA expression levels of CD13 were significantly higher in Ob- than in Co-hA-MSCs at day 0 (P=0.02), day 2 (P=0.02) and day 4 (P=0.04) when cultured with adipogenic medium. CD13 mRNA expression was switched-off in Ob-hA-MSCs after CD13 silencing with shRNA. (**B**) At day 4 of adipogenic induction, PPARγ mRNA expression levels that were significantly higher in Ob-hA-MSCs than in Co-hA-MSCs (P=0.01), decreased to the levels detected in Co-hA-MSCs after CD13 silencing (P=0.71), which indicates that CD13 enhances adipogenesis in hA-MSCs. n.s.: not statistically significant difference.

**Upregulation of CD13 hA-MSC expression by IFN-γ**

We next evaluated if CD13 expression could be upregulated in h-MSCs by IFN-γ as occurs in murine cellular models [Gabrilovac et al. 2011]. To this aim, we treated the Co- and Ob-hA-MSCs with 0.8 ng/mL or 12.5 ng/mL IFN-γ for 24 h. We found that CD13 expression was significantly higher on membranes of Co-hA-MSCs treated with 12.5 ng/mL IFN-γ (P=0.04) than in untreated cells, whereas there was a slight, not significant, increase in treated Ob-hA-MSCs (Figure 7) versus the untreated counterpart cells. Our results suggest that high levels of INF-γ drive the up-regulation of CD13 expression in Co-h-MSCs, whereas its effect on Ob-h-MSCs CD13 expression during obesity is ambiguous.

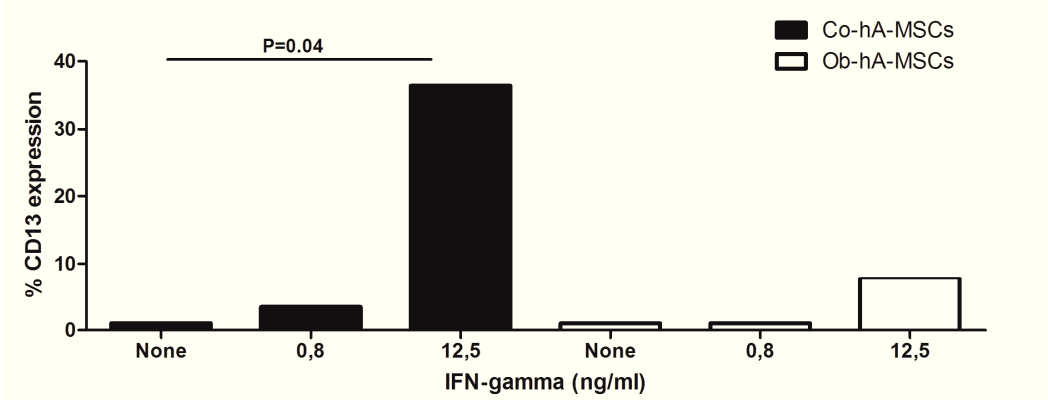


**Figure 7. CD13 expression on Co- and Ob-hA-MSCs treated with 0.8 ng/mL or 12.5 ng/mL IFN-γ for 24 h.** CD13 expression significantly increased on membrane of Co-hA-MSCs treated with 12.5 ng/mL IFN-γ (P=0.04) versus untreated, whereas slight even if not significant increase was observed in treated Ob-hA-MSCs respect to untreated.

# DISCUSSION

Human amniotic membrane is a readily available source of abundant fetal mesenchymal stem cells that are free from ethical concerns [Miki et al. 2005]. hA-MSCs isolated from normal weight healthy women at delivery have been characterized [Parolini et al. 2008, Marioti et al. 2008, Roubelakis et al. 2012], but, to our knowledge, the features of hA-MSCs from obese women are largely unknown. In this study, we used flow cytometry to characterize hA-MSCs isolated at delivery from two groups of women: pre pregnancy normal weight and pre pregnancy severely obese women. The immunophenotypic characterization confirmed the mesenchymal origin of the isolated cells [Delorme et al. 2008]. In particular, the distribution of CD56 was in agreement with the placental origin of the isolated hA-MSCs. In fact, this marker is absent from bone marrow [Mariotti et al. 2008] and from adipose tissue-derived mesenchymal stem cells [Gronthos et al. 2001]. Similarly, the endothelial marker PECAM-1/CD31, and the hematopoietic antigens CD14, CD15, CD16, CD19, CD28, CD33, CD34, CD45 and CD117 were absent from isolated Ob- and Co-hA-MSCs. Staining for the E-cadherin/CD324 epithelial antigen was very weak in our Ob- and Co-hA-MSC preparations; the co-expression of epithelial, albeit at a low intensity, and mesenchymal markers on our h-AMSCs was in agreement with previous findings [Sakuragawa et al. 2004, Soncini et al. 2007]. Overall, our results are similar to those reported by Parolini et al. [2008] and/or Roubelakis et al. [2012] for the expressed (CD49d, CD90, HLA-ABC, CD13, CD56, CD105, CD166, CD10, CD29, CD44 and CD54) and not expressed (PECAM-1/CD31, HLA-DR, CD14, Prominin-1/CD133, NGFR/CD271, CD34 and CD45) membrane-bound antigens in hA-MSCs. We found that the Ob-hA-MSC immunophenotype is characterized by a significantly higher expression of the APN/CD13 antigen with respect to the Co-hA-MSC phenotype.

Type II metalloprotease APN/CD13 (EC. 3.4.11.2) is a heavily glycosylated membrane-bound protein (~ 960aa, ~ 150 kDA) that is encoded by the human ANPEP gene located in chromosome 15 (q25-q26) [Watt and Willard 1990]. This protein exists also in a soluble form. CD13 is a ubiquitous enzyme present in a wide variety of human organs, tissues and cell types including placenta, human umbilical vein endothelial cells, monocytes, lymphocytes T, hypothalamus, and epithelial intestinal cells [Osorio et al. 2008]. It has various mechanisms of action: enzymatic cleavage of peptides, endocytosis and signal transduction [Luan et al. 2007]. CD13 is involved in inflammation, cellular differentiation and proliferation, apoptosis, cell adhesion and motility [Osorio et al. 2008]. Dysregulated expression of membrane and/or soluble forms of CD13 has been observed in many diseases [Luan et al. 2007], but until now it has never been associated with obesity. Here, we provide the first demonstration that the

CD13 antigen is increased on hA-MSCs during obesity and could play a role in adipogenesis. In fact, we first detected a higher adipogenic potential in Ob- than in Co-hA-MSCs after 14 days of adipogenic differentiation and then observed that the adipogenic potential of Ob-hA-MSCs was comparable to that of Co-hA-MSCs after CD13 silencing. Conversely, the adipogenic potential increased in Co-hA-MSCs after CD13 overexpression. Further, we showed evidence that INFγ upregulated CD13 expression also in Co-hA-MSCs.

Intriguingly, in Ob-pregnant women CD13 serum levels at delivery were higher than in Co-pregnant women and correlated with CD13 surface Ob-hA-MSC expression ($r^2$=0.89, P<0.0001) supporting that the placenta is the major source of the high CD13 levels measured in maternal serum [Kawai et al. 2009]. Further increased biochemical markers in Ob-maternal serum at delivery were leptin concentration and the L/A ratio. This finding confirms the concept that these two parameters are obesity risk markers [Labruna et al. 2009, Labruna et al. 2011].

# CONCLUSIONS

The prevalence of obesity has increased in the world, in both men and women. Considering the prevalence of obese in women in reproductive age and that the pregnancy itself induces a state of insulin resistance and inflammation, maternal obesity may be the most common health risk for the developing foetus. Since the placenta is the main interface between foetus and mother, the study of changes in this tissue may help you understand how it regulates intrauterine development and modulates adaptive responses to suboptimal *in utero* conditions.

We succeeded in isolating and culturing mesenchymal cells from amnion. The fibroblast morphology of these cells in culture is characteristic to mesenchymal cells. The immunophenotypic characterization showed an antigen expressed differently in hA-MSCs isolated from obese compared to controls, and that this antigen, CD13, influences the adipogenic potential of these cells. CD13 could be an in-utero risk factor for obesity. Furthermore, we find this antigen increased in the serum of obese women.

Together, our data strengthen the hypothesis that high serum CD13 and mesenchymal stem cell CD13 are markers of obesity.

# Acknowledgments

*I would like to thank Prof.ssa Lucia Sacchetti, who guided me through this project with optimism and great enthusiasm. Thanks for showing me the most fascinating side of research. I owe her so much.*

*I would also like to thank Prof.ssa Nadia Tinto for welcoming me as a PhD student.*

*I also owe a lot to Prof. Lucio Pastore, Prof.ssa Rosa Di Noto and Prof. Luigi Del Vecchio and their groups for making me feel at home and for teaching me so much.*

*Many thanks also go to Carmela Nardelli. An exceptional person, she has managed to transmit her great knowledge with patience and generously. You are a great researcher.*

*Thanks to Maddalena Ferrigno and Valentina Capobianco for opening their world and for helping and supporting me. I could not have hoped for anyone better or more helpful.*

*Thanks to Giuseppe Labruna for being my companion in this important journey.*

*A special thanks goes to Silvia Parisi, Eleonora Leggiero and Carolina Tarantino for their availability, their knowledge, their great friendship and their disinterested help and for being a really comforting presence, even from afar, in laboratory hours and not only.*

*Thanks to all the other members of the group, always available for advice and a joke. They made our days in the laboratory more pleasant.*

*I would also like to thank my parents, my grandfather, my sister, Fabio, my brother and Fabrizia. Any words of gratitude would never be sufficient to express all they did for me. Their constant presence and support have always been fundamental in carrying out ever the smallest step. Thanks for everything; you have made me a better and more complete person.*

*Thank you Martina, my little great angel, for having been my strength in the worst moment of my life and for making me experience emotions I have never felt before. You are my greatest joy!*

*Thanks also to Corinna, my best friend, for her friendship and her strong desire to look at the world from the most interesting and optimistic point of view. I owe her a lot.*

*Thanks to Cecilia, a constant example of loyalty for showing me that real deep and disinterested relationships really do exist.*

*Thanks also to Simone's family for loving me as a daughter!*

*..and thanks to you, Simone .. my partner for life.. You have managed to change my life, seasoning it with a "pinch of sugar"!*

***Finally, my thoughts full of love go to my aunts,***
***Carolina and Lidia, to whom this thesis is dedicated.***

# References

Barker DJ. (2005). The developmental origins of insulin resistance. Horm Res 64 Suppl 3:2-7.

Bieback K, Kern S, Klüter H, Eichler H. (2004). Critical parameters for the isolation of mesenchymal stem cells from umbilical cord blood. Stem Cells 22:625-34.

Catalano PM. (2007). Increasing maternal obesity and weight gain during pregnancy: the obstetric problems of plentitude. Obstet Gynecol 110(4):743-4.

Challier JC, Basu S, Bintein T, Minium J, Hotmire K, Catalano PM, Hauguel-de Mouzon S. (2008). Obesity in pregnancy stimulates macrophage accumulation and inflammation in the placenta. Placenta 29(3):274-81.

Choquet H, Meyre D. (2011). Genetics of Obesity: What have we Learned? Curr Genomics 12(3):169-79.

Delorme B, Ringe J, Gallay N, Le Vern Y, Kerboeuf D, Jorgensen C, Rosset P, Sensebé L, Layrolle P, Häupl T, Charbord P. (2008). Specific plasma membrane protein phenotype of culture-amplified and native human bone marrow mesenchymal stem cells. Blood 111:2631-5.

Fowden AL, Forhead AJ, Coan PM, Burton GJ. (2008). The placenta and intrauterine programming. J Neuroendocrinol 20(4):439-50.

Fowden AL, Giussani DA, Forhead AJ. (2006). Intrauterine programming of physiological systems: causes and consequences. Physiology 21, 29-37.

Fowden AL, Ward JW, Wooding FP, Forhead AJ, Constancia M. (2006). Programming placental nutrient transport capacity. J Physiol 572 (Pt 1):5-15.

Gabrilovac J, Cupić B, Zivković E, Horvat L, Majhen D. (2011). Expression, regulation and functional activities of aminopeptidase N (EC 3.4.11.2; APN; CD13) on murine macrophage J774 cell line. Immunobiology 216:132-44.

Gesta S, Blüher M, Yamamoto Y, Norris AW, Berndt J, Kralisch S, Boucher J, Lewis C, Kahn CR. (2006). Evidence for a role of developmental genes in the origin of obesity and body fat distribution. Proc Natl Acad Sci U S A 25;103(17):6676-81.

Gluckman PD, Hanson MA. (2004). Living with the past: evolution, development, and patterns of disease. Science 305(5691):1733-6.

Godfrey KM. (2002). The role of the placenta in fetal programming-a review. Placenta 23 Suppl A:S20-7.

Grant A, Palzer S, Hartnett C, Bailey T, Tsang M, Kalyuzhny AE. (2005). A cell-detachment solution can reduce background staining in the ELISPOT assay. Methods Mol Biol 302:87-94.

Gronthos S, Franklin DM, Leddy HA, Robey PG, Storms RW, Gimble JM. (2001). Surface protein characterization of human adipose tissue-derived stromal cells. J Cell Physiol 189:54-63.

Harwood HJ Jr. (2012. The adipocyte as an endocrine organ in the regulation of metabolic homeostasis. Neuropharmacology 63(1):57-75.

Heerwagen MJ, Miller MR, Barbour LA, Friedman JE. (2010). Maternal obesity and fetal metabolic programming: a fertile epigenetic soil. Am J Physiol Regul Integr Comp Physiol 299(3):R711-22.

Huda SS, Brodie LE, Sattar N. (2010). Obesity in pregnancy: prevalence and metabolic consequences. Semin Fetal Neonatal Med 15(2):70-6.

Jansson T, Powell TL. (2007). Role of the placenta in fetal programming: underlying mechanisms and potential interventional approaches. Clin. Sci 113, 1-13.

Kawai M, Araragi K, Shimizu Y, Hara Y. (2009). Identification of placental leucine aminopeptidase and triton-slowed aminopeptidase N in serum of pregnant women. Clin Chim Acta 400:37-41.

Klein JD and Fauza DO. (2011). Amniotic and placental mesenchymal stem cell isolation and culture. Methods Mol Biol 698:75-88.

Labruna G, Pasanisi F, Nardelli C, Caso R, Vitale DF, Contaldo F, Sacchetti L. (2011). High leptin/adiponectin ratio and serum triglycerides are associated with an "at-risk" phenotype in young severely obese patients. Obesity (Silver Spring) 19:1492-6.

Labruna G, Pasanisi F, Nardelli C, Tarantino G, Vitale DF, Bracale R, Finelli C, Genua MP, Contaldo F, Sacchetti L. (2009). UCP1 -3826 AG+GG genotypes, adiponectin, and leptin/adiponectin ratio in severe obesity. J Endocrinol Invest 32:525-9.

Lai A, Ghaffari A, Ghahary A. (2010). Inhibitory effect of anti-aminopeptidase N/CD13 antibodies on fibroblast migration. Mol Cell Biochem 343:191-9.

Lamoreaux L, Roederer M, Koup R. (2006). Intracellular cytokine optimization and standard operating procedure. Nat Protocols 1:1507–1516.

Lewis RM, Poore KR, Godfrey KM. (2006). The role of the placenta in the developmental origins of health and disease - implications for practice. Reviews in Gynaecology & Perinatal Practice 6:70-9.

Lillycrop KA, Phillips ES, Jackson AA, Hanson MA, Burdge GC. (2005). Dietary protein restriction of pregnant rats induces and folic acid supplementation prevents epigenetic modification of hepatic gene expression in the offspring. J Nutr 135(6):1382-6.

Luan Y, Xu W. (2007). The structure and main functions of aminopeptidase N. Curr Med Chem 14:639-47.

Maeker HT, Trotter J. (2006). Flow cytometry controls, instrument setup, and the determination of positivity. Cytometry Part A 69A:1037–1042.

Mariotti E, Mirabelli P, Abate G, Schiattarella M, Martinelli P, Fortunato G, Di Noto R, Del Vecchio L. (2008). Comparative characteristics of mesenchymal stem cells from human bone marrow and placenta: CD10, CD49d, and CD56 make a difference. Stem Cells Dev 17:1039-41.

Mariotti E, Mirabelli P, Di Noto R, Fortunato G, Salvatore F. (2008). Rapid detection of mycoplasma in continuous cell lines using a selective biochemical test. Leuk Res 32:323-6.

Maury E, Brichard SM. (2010). Adipokine dysregulation, adipose tissue inflammation and metabolic syndrome. Mol Cell Endocrinol 15;314(1):1-16.

McMillen IC, Robinson JS. (2005). Developmental origins of the metabolic syndrome: prediction, plasticity, and programming. Physiol Rev 85(2):571-633.

Mihu CM, Mihu D, Costin N, Rus Ciucă D, Suşman S, Ciortea R. (2008). Isolation and characterization of stem cells from the placenta and the umbilical cord. Rom J Morphol Embryol 49(4):441-6.

Miki T, Lehmann T, Cai H, Stolz DB and Stromk SC. (2005). Stem cell characteristics of amniotic epithelial cells. Stem Cells 23:1549-1559.

Mitchell NS, Catenacci VA, Wyatt HR, Hill JO. (2011). Obesity: overview of an epidemic. Psychiatr Clin North Am. Dec;34(4):717-32.

Murphy VE, Smith R, Giles WB, Clifton VL. (2006). Endocrine regulation of human fetal growth: the role of the mother, placenta, and fetus. Endocr Rev 27(2):141-69.

Nguyen DM, El-Serag HB. (2010). The epidemiology of obesity. Gastroenterol Clin North Am. 39(1):1-7.

Niknejad H, Peirovi H, Jorjani M, Ahmadiani A, Ghanavi J, Seifalian AM. (2008). Properties of the amniotic membrane for potential use in tissue engineering. Eur Cell Mater 29;15:88-99.

Nodine PM, Hastings-Tolsma M. (2012). Maternal obesity: improving pregnancy outcomes. MCN Am J Matern Child Nurs 37(2):110-5.

Ogden CL, Carroll MD, Curtin LR, McDowell MA, Tabak CJ, Flegal KM. (2006). Prevalence of overweight and obesity in the United States, 1999-2004. JAMA 295(13):1549-55

Osmond C, Barker DJ. (2000). Fetal, infant, and childhood growth are predictors of coronary heart disease, diabetes, and hypertension in adult men and women. Environ Health Perspect 108 Suppl 3:545-53.

Paola Mina-Osorio. (2008). The moonlighting enzyme CD13: old and new functions to target. Trends in Molecular Medicine 14:361-371.

Parolini O, Alviano F, Bagnara GP, Bilic G, Bühring HJ, Evangelista M, Hennerbichler S, Liu B, Magatti M, Mao N, Miki T, Marongiu F, Nakajima H, Nikaido T, Portmann-Lanz CB, Sankar V, Soncini M, Stadler G, Surbek D, Takahashi TA, Redl H, Sakuragawa N, Wolbank S, Zeisberger S, Zisch A, Strom SC. (2008). Concise review: isolation and characterization of cells from human

term placenta: outcome of the first international Workshop on Placenta Derived Stem Cells. Stem Cells 26:300-11.

Perfetto SP, Ambrozak D, Nguyen R, Chattopadhyay P, Roederer M. (2006). Quality assurance for polychromatic flow cytometry. Nat Protocols 1:1522–1530.

Pham TD, MacLennan NK, Chiu CT, Laksana GS, Hsu JL, Lane RH. (2003). Uteroplacental insufficiency increases apoptosis and alters p53 gene methylation in the full-term IUGR rat kidney. Am J Physiol Regul Integr Comp Physiol. 285(5):R962-70.

Roubelakis MG, Trohatou O, Anagnou NP. (2012) Amniotic fluid and amniotic membrane stem cells: marker discovery. Stem Cells Int 2012:107836.

Sakuragawa N, Kakinuma K, Kikuchi A, Okano H, Uchida S, Kamo I, Kobayashi M, Yokoyama Y. (2004). Human amnion mesenchyme cells express phenotypes of neuroglial progenitor cells. J Neurosci Res 78:208-14.

Soncini M, Vertua E, Gibelli L, Zorzi F, Denegri M, Albertini A, Wengler GS, Parolini O. (2007). Isolation and characterization of mesenchymal cells from human fetal membranes. J Tissue Eng Regen Med 1:296-305.

Thornburg KL, Louey S. (2005). Fetal roots of cardiac disease. Heart 91(7):867-8.

Watt, V.M. and Willard, H.F. (1990). The human aminopeptidase N gene: isolation, chromosome localization, and DNA polymorphism analysis. Hum Genet 85:651–654.

WHO. Fact sheet No 311: Obesity and overweight. March 2013. Available at: http://www.who.int/mediacentre/factsheets/fs311/en/

# IL-15 Interferes With Suppressive Activity of Intestinal Regulatory T Cells Expanded in Celiac Disease

Delia Zanzi, MS[1,2,5], Rosita Stefanile, PhD[3,5], Sara Santagata, PhD[1], Laura Iaffaldano, MS[1], Gaetano Iaquinto, MD[4], Nicola Giardullo, MD[4], Giuliana Lania, MS[1], Ilaria Vigliano, MS[1], Aufiero Rotondi Vera, BS[3], Katia Ferrara, BS[1], Salvatore Auricchio, MD[1,2], Riccardo Troncone, MD[1,2] and Giuseppe Mazzarella, MS[2,3]

OBJECTIVES: **Celiac disease (CD) is a condition in which the regulation of the mucosal immune response to dietary gliadin might be altered. The transcription factor forkhead box P3 (Foxp3) has been identified as a marker of a subset of regulatory T cells (Treg). In this study, we have investigated the presence and the suppressive function of Treg cells in the celiac small intestinal mucosa, their correlation with the disease state, and the inducibility by gliadin in an organ culture system; moreover, we tried to define whether interleukin 15 (IL-15), overexpressed in CD, could influence the regulatory activity of such cells.**

METHODS: **The expression of Foxp3, CD3, CD4, and CD8 were analyzed by immunohistochemistry and flow cytometry in duodenal biopsies taken from patients with untreated CD, treated CD, and from non-CD controls, as well as *in vitro* cultured biopsy samples from treated CD patients, upon challenge with gliadin. Furthermore, we analyzed the suppressive function of CD4+CD25+ T cells, isolated from untreated CD biopsy samples, on autologous responder CD4+CD25− T cells, in the presence of a polyclonal stimulus, with or without IL-15.**

RESULTS: **Higher density of CD4+CD25+Foxp3+ T cells was seen in duodenal biopsy samples from active CD patients in comparison with treated CD and non-CD controls. In coculture, CD4+CD25+ T cells were functionally suppressive, but their activity was impaired by IL-15. Cells from CD subjects showed increased sensitivity to the IL-15 action, likely due to enhanced expression of IL-15 receptor. Finally, we demonstrated an expansion of Foxp3 in treated CD mucosa following *in vitro* challenge with gliadin.**

CONCLUSIONS: **These data suggest that CD4+CD25+Foxp3+ T cells are induced *in situ* by gliadin. However, their suppressor capacity might be impaired *in vivo* by IL-15; this phenomenon contributes to maintain and expand the local inflammatory response in CD.**

**SUPPLEMENTARY MATERIAL** is linked to the online version of the paper at http://www.nature.com/ajg

*Am J Gastroenterol* 2011; 106:1308–1317; doi:10.1038/ajg.2011.80; published online 5 April 2011

## INTRODUCTION

Celiac disease (CD) is a chronic disorder caused by the ingestion of the gluten prolamines of wheat, rye, and barley in genetically predisposed individuals (1). Although the pathogenesis of CD is not fully understood, it has been clearly shown that in the CD mucosa, gluten peptides deamidated by tissue transglutaminase trigger CD4+ T cells to produce large amounts of interferon gamma (IFN-γ) (2,3). This mucosal inflammatory response leads to a profound remodeling of the intestinal mucosa, up to complete villous atrophy. However, the spectrum of histological changes is quite wide and there are CD patients, indicated as potential CD, who present the genetic and immunological features of CD, but whose small-bowel mucosa is architecturally normal (4,5).

In addition to the Th1 response, it has highlighted the fundamental role of other pro-inflammatory cytokines, such as interleukin 15 (IL-15) (6). More recently, also other cytokines, such as IL-21, bridging innate, and adaptive immunity, have been found to have an important role (6). In these studies, an important contribution to the comprehension of the mechanisms

[1]Department of Paediatrics University Federico II, Naples, Italy; [2]European Laboratory for the Investigation of Food-Induced Diseases, University Federico II, Naples, Italy; [3]Institute of Food Science, CNR, Immunobiology, Avellino, Italy; [4]Gastroenterology and Digestive Endoscopy Service, San G. Moscati Hospital, Avellino, Italy; [5]These authors contributed equally to this manuscript and should be considered joint first authors. **Correspondence:** Giuseppe Mazzarella, MS, Institute of Food Science, CNR, Immunobiology, via Roma 64, Avellino, Italy. E-mail: gmazzarella@isa.cnr.it
**Received 30 April 2010; accepted 4 February 2011**

leading to disease has come from *in vitro* studies based on *ex vivo* organ cultures of intestinal biopsies taken from CD patients on a gluten-free diet (6).

CD can be seen as the result of a break of tolerance in which the regulation of the mucosal immune response to dietary gliadin might be altered. Several Tregs subsets are involved in immune tolerance (7). These subsets include natural Treg cells expressing the forkhead box P3 (Foxp3) transcription factor that is able to maintain tolerance to self components, and antigen-induced Foxp3+ cells that are able to contain the activity of Th1 and Th17 cells (8). Tr1 cells that downregulate naive and memory T-cell responses upon local secretion of IL-10 and transforming growth factor-β (TGF-β) (9), and TGFβ-producing Treg cells (Th3) (10) are other important subsets that possess regulatory properties. Many factors may interfere with the function of Treg cells. For CD, it is relevant to know that IL-15, largely expressed in the CD mucosa, interferes with immune regulation, functioning on TGF-β1 activity, thus contributing to the loss of intestinal homeostasis and promoting chronic inflammation (11). Nevertheless, concomitantly with this pro-inflammatory response, high amount of the anti-inflammatory cytokines IL-10 and IL-4 are also produced in the untreated CD intestinal mucosa (12). This apparent paradoxical milieu of both pro-inflammatory and suppressive cytokines strongly suggests that regulatory mechanisms might operate to counterbalance the gliadin-triggered, abnormal immune activation in untreated mucosa (13). Our recent studies have revealed that the treatment with IL-10 of small intestinal mucosa from CD patients in remission prevents the massive immune activation induced by gliadin challenge (14). Moreover, we have observed that celiac intestinal mucosa harbors a subset of Treg cells, Tr1 cells, which, through the release of both IL-10 and TGF-β, inhibit the pathogenic response to *in vitro* gliadin challenge (15). Although Tr1 cells, identified in CD, have some properties similar to that of Treg cells, they do not express Foxp3 (16). This suggests that they are functionally distinct and may represent another level of regulation of the inflammatory response. Several studies have found that the number of Foxp3+ T cells is significantly increased in the small intestinal mucosa with active CD (17–19). Futhermore, although the functional activity of circulating CD4+CD25+ T cells from CD patients has been recently investigated (20–22), the suppressive capacity relative to their intestinal counterparts has never been reported.

The aim of our study was to investigate the presence of Foxp3 cells in the celiac small intestinal mucosa and their correlation with the disease state by combined immunohistochemistry and flow cytometry (FACS) *ex vivo* analysis. Furthermore, we used an *in vitro* organ culture to investigate the induction of Foxp3 by gluten. Finally, we evaluated the functional capacity of intestinal Treg cells from celiac patients, and the effects that IL-15 exerts on their suppressive function.

## METHODS

### Patients and controls

Biopsy specimens were obtained from the distal duodenum of 25 untreated CD patients (seven male and eighteen female patients; median age, 29 years; range 17–54). They were snap-frozen in liquid nitrogen or immediately processed. Diagnosis was based on typical mucosal lesions with crypt cell hyperplasia and total villous atrophy. All untreated CD patients were positive for serum anti-endomysial antibodies. Duodenal biopsy samples were also obtained from 15 treated CD patients (seven male and eight female patients; median age 35 years; range 21–51), who were in clinical and histological remission, and negative for anti-endomysial antibodies. Finally, 10 non-celiac individuals (six male and four female patients; median age 41 years; range 25–57) with normal intestinal mucosa and negative serology for anti-endomysial were recruited. Functional studies were performed on both intestinal CD4+CD25+ T cells, isolated from biopsy samples of nine untreated CD patients, and on peripheral blood CD4+CD25+ T cells, purified from five untreated CD patients and four non-CD controls. The study received approval from a local ethics committee (Hospital Moscati, Avellino, Italy).

### Immunohistochemistry

Acetone-fixed sections (5 μm), from biopsy samples that were not cultured or after culture, were individually incubated for 1 h with mouse monoclonal antibodies (see **Supplementary Table 1** online), followed by incubation (20 min) in the dark with rabbit anti-mouse tetramethyl-rhodamine isothiocyanate-conjugated (Vector 1:200) antibodies. Costaining experiments were set up by mixing rat anti-human Foxp3 with mouse anti-CD3, -CD8, or -CD4, and incubating the cryosections individually for 1 h with each single mixture. After incubation with primary antibodies, the cryosections were incubated with a mixture of goat anti-rat tetramethyl-rhodamine isothiocyanate-conjugated antibody and horse anti-mouse fluorescein isothiocyanate-conjugated antibody for 30 min. Finally, all the sections were counterstained with ToPro-3 (Molecular Probes, Leiden, The Netherlands), mounted in phosphate-buffered saline:glycerol (1:1), and imaged with a Leica SP confocal microscope (Heidelberg, Germany). Non-immune mouse immunoglobulins were used as isotype controls of primary antibodies. The density of cells expressing Foxp3 in the lamina propria was evaluated within a total area of 1 $mm^2$ of lamina propria. Slides were analyzed by two observers who were blinded.

### Organ culture

The mucosal specimens were cultured as described elsewhere (22). Briefly, biopsy samples taken from 10 patients with inactive CD and from six control patients were placed on iron grids, with the mucosal face upwards in the central well of an organ culture dish. Cultures were prepared with or without the addition of 1 mg/ml of peptic–tryptic digest (Frazer III fraction) of gliadin (PT-gliadin; Sigma, St Louis, MO), and were placed in a tight container with 95% $O_2$/5% $CO_2$ at 37 °C, at 1 bar. After 24 h of culture, the tissue was embedded in Optimal Cutting Temperature and snap-frozen in liquid nitrogen.

### *Ex vivo* cytofluorimetric analysis

Mucosal explants from nine healthy donors, nine CD patients and four gluten-free diet, either following 24 h of gliadin chal-

lenge or freshly processed, were digested with collagenase-A. Immediately after the digestion, the cells were passed through a cell strainer (40 μm Nylon, Becton Dickinson (BD), Bedford, MA) and isolated from mucosal explants. A total of 5–10×$10^4$ cells obtained from fresh biopsy samples were washed in phosphate-buffered saline and labelled with a pre-titrated optimal dilution of each fluorochrome-conjugated mouse monoclonal antibodies against surface antigens (see **Supplementary Table 1** online). Appropriate isotype-matched control antibodies (BD) were included in all experiments. Intracellular cytokine production was detected by using a triple-staining technique and by FACS analysis. Briefly, after washing twice with phosphate-buffered saline, cells were fixed and permeabilized with Cytofix/cytoperm (BD), according to the manufacturer's instructions, followed by staining with fluorescein isothiocyanate (FITC)-anti-Foxp3 antibody (PCH101; eBioscience, San Diego, CA) in permeabilization buffer. Cells were then analyzed by a flow cytometer (FACSCalibur and CellQuest Software, BD), using a live gate set around viable lymphocytes based on their forward-scatter/side-scatter characteristics.

IL-15 receptor-α surface expression (IL-15Rα) was evaluated by incubating peripheral blood mononuclear cells (PBMCs) with optimal concentration of phycoerythrin-conjugated mouse mAb against CD4 (BD Pharmingen, San Jose, CA), phycoerythrin-Cy5-conjugated mAb against CD25 (BD Pharmingen), anti-IL-15Rα goat IgG (R&D System, Minneapolis, MN, USA and Alexa Fluo 488, R&D System), and donkey anti-goat as a secondary mAb (R&D System). Cells were also incubated with the respective mouse isotype controls. After two washings, the cells were fixed with 2% paraformaldehyde and analyzed by flow cytometry.

### Purification of T cell subsets

Autologous PBMCs isolated by heparinized blood obtained from patients with active CD and healthy donors were purified by density-gradient centrifugation (Ficoll, MP Biomedicals, LLC, Solon, OH). However, freshly isolated mucosal cells were processed from intestinal mucosal explants after collagenase digestion. CD4+CD25+ T cells and CD4+CD25− T cells were separated using the Dynabeads Regulatory CD4+ CD25+ T cell kit (Dynal-Biothec, AS, Oslo, Norway). In the first step, CD4+ cells were separated by negative selection, using the Antibody Mix Human CD4 (Dynal-Biothec, AS, Oslo, Norway). In the second step, Depletion MyOne Dynabeads (Dynal-Biothec, AS, Oslo, Norway) was added to remove the non-CD4 cells. In the third step, Dynabeads CD25 (Dynal-Biothec, AS, Oslo, Norway) was added to CD4+ T cells to capture the CD4+CD25+ T cells and the remaining fraction was used as CD4+CD25− T cells. In the last step, Dynabeads CD25 was removed from the cells. All purification steps were performed according to the manufacturer's instructions and collected cells were found to be >95% pure by flow cytometry.

### Suppression assay

The CD4+CD25+ (Treg) and CD4+CD25− responder T cells (Tresp) were cultured, respectively, at different ratios in the suppression experiments (1:1, 1:0.5, 1:0.25, 1:0.125, 1:0). Cells were cultured (1–2×$10^4$ cells/well) in U-bottom 96-well plates with RPMI medium supplemented with 2-mM L-glutamine, 100-U/ml penicillin, 100-μg streptomycin, and 10% fetal bovine serum. Cells were stimulated for 3 days in the presence of Treg suppression Inspector (Miltenyi Biotec, Bergisch Gladbach, Germany) that consists of Anti-Biotin MACSi Bead Particles that are pre-loaded with biotinylated CD2, CD3, and CD28 antibodies. As additional control, Tresp cells were cultured alone with and without the Treg suppression Inspector (Miltenyi Biotec) and Treg cells were cultured alone with Treg suppression Inspector (Miltenyi Biotec). Furthermore, the cocultured Tresp/Treg cells were stimulated with 10-ng/ml of IL-15 (R&D System). On the last day, $^3$H-thymidine (1 uCi/well; Amersham-Pharmacia Biotec, Uppsala, Sweden) was added to the cultures and incubated for 16 h. Radioactivity was assessed with a β-counter (1600 TP, Hewlet Packard California, San Francisco, CA, USA). Percentage proliferation was determined as (cpm incorporated in the coculture)/(cpm of responder population alone)×100%. Percentage of inhibition was calculated as (1 – number of cells in coculture that divide/number of responder cells that divide)×100.

### Cytokine assay

At the end of the cell culture, supernatants were collected and analyzed for the content of IFN-γ by enzyme-linked immunosorbent assay. Briefly, 96-well plates (Immunoplate MaxiSorp, Nunc, Merelbeke, Belgium) were coated by incubating with anti-human IFN-γ monoclonal antibody (Endogen) overnight at 4 °C. After washing, wells were blocked by incubation with phosphate-buffered saline

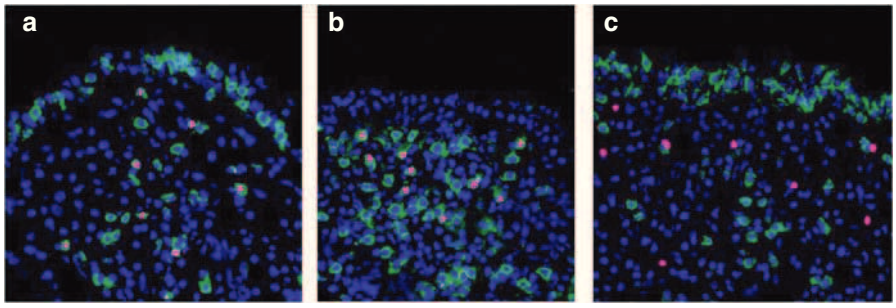


**Figure 1.** Phenotyping of forkhead box P3 (Foxp3+) cells on jejunal biopsy samples from untreated celiac disease (CD). Immunofluorescence costaining experiments revealed that all the Foxp3+ cells were CD3+ (**a**), CD4+ (**b**), and CD8− (**c**). Pink indicates the Foxp3 molecule staining, green indicates the CD3, CD4 and CD8 molecule staining, and blue indicates the nuclei counterstaining by using ToPro-3. Original magnification: ×40.

solution containing 2% bovine serum albumin. Supernatants were added and incubated for 1 h at room temperature. After two washes, the wells were incubated with biotinylated anti-human IFN-γ monoclonal antibody (Endogen) for 30 min at room temperature. Finally, the wells were incubated with streptavidin-horseradish peroxidase (BD Pharmingen) and then was added 100 µl of TMB (3,3′,5,5′-tetramethylbenzidine; Sigma), a chromogenic substrate for horseradish peroxidase. Absorbances were read on an enzyme-linked immunosorbent assay reader at 450 nm.

### Statistical analysis

Data are presented as mean values±s.d.; paired two-tailed Student's *t*-test was used to calculate *P*-values within the same individuals and unpaired two-tailed Student's-*t* test was used to calculate *P*-values between study groups. *P*-values $<0.05$ were considered statistically significant.

## RESULTS

### Increased expression of Foxp3 T cells in untreated CD mucosa

To localize the anatomical site of cells expressing Foxp3, we performed immunohistochemical analysis of untreated CD, treated CD, and non-CD control duodenal sections, using a mouse anti-human Foxp3 antibody. In untreated CD, the number of cells/mm$^2$ of lamina propria expressing the transcription factor Foxp3+ was significantly higher (mean±s.d.: 91±24) in comparison with treated CD (8±2, $P<0.001$) and non-CD controls (6±3, $P<0.001$; see **Supplementary Figure 1** online upper panel online). Foxp3 cells exhibit a nuclear localization in positive cells (see **Supplementary Figure 1** online lower panel). Those cells were not found in the epithelium layer, but only in the lamina propria, particularly in the subepithelial compartment (see **Supplementary Figure 1** online lower panel). No significant differences were noted in the number of Foxp3+ cells in biopsy samples of treated CD in comparison with

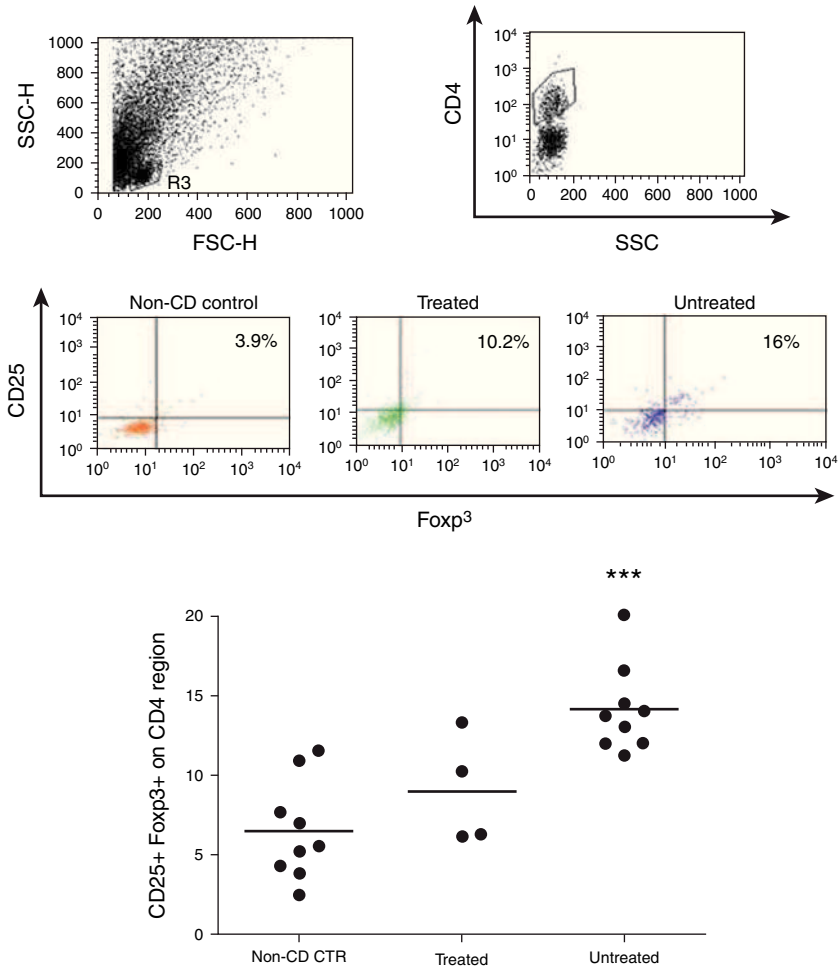


**Figure 2.** Increased CD4+CD25+forkhead box P3 (Foxp3+) intestinal T cells in untreated celiac disease (CD) patients as compared with treated-CD and non-CD control. Freshly isolated human intestinal cells were collected, stained, and analyzed by flow cytometry, as described in Methods, and assessed by a FACSCalibur (BD). Upper panel, representative dot plot from one experiment from non-CD control, treated-CD, and untreated-CD intestinal cells each is shown. Lymphocytes gated on forward- and side-scatter properties to exclude dead and/or granular cells, representative gates of CD4 populations are shown. Dot plot of Foxp3+CD25+ are gated on CD4+cells. Foxp3+ staining was performed after cell permeabilization. Lower panel, the mean percentages of the intestinal whole Foxp3$^+$CD25$^+$ T cells in total CD4$^+$ cells isolated from non-CD control patients ($n=9$), untreated patients ($n=9$), and treated patients ($n=4$) was presented in each scatter plot. Horizontal bars represent mean values. ***$P<0.0001$ comparing the non-CD control vs. untreated-CD patients.

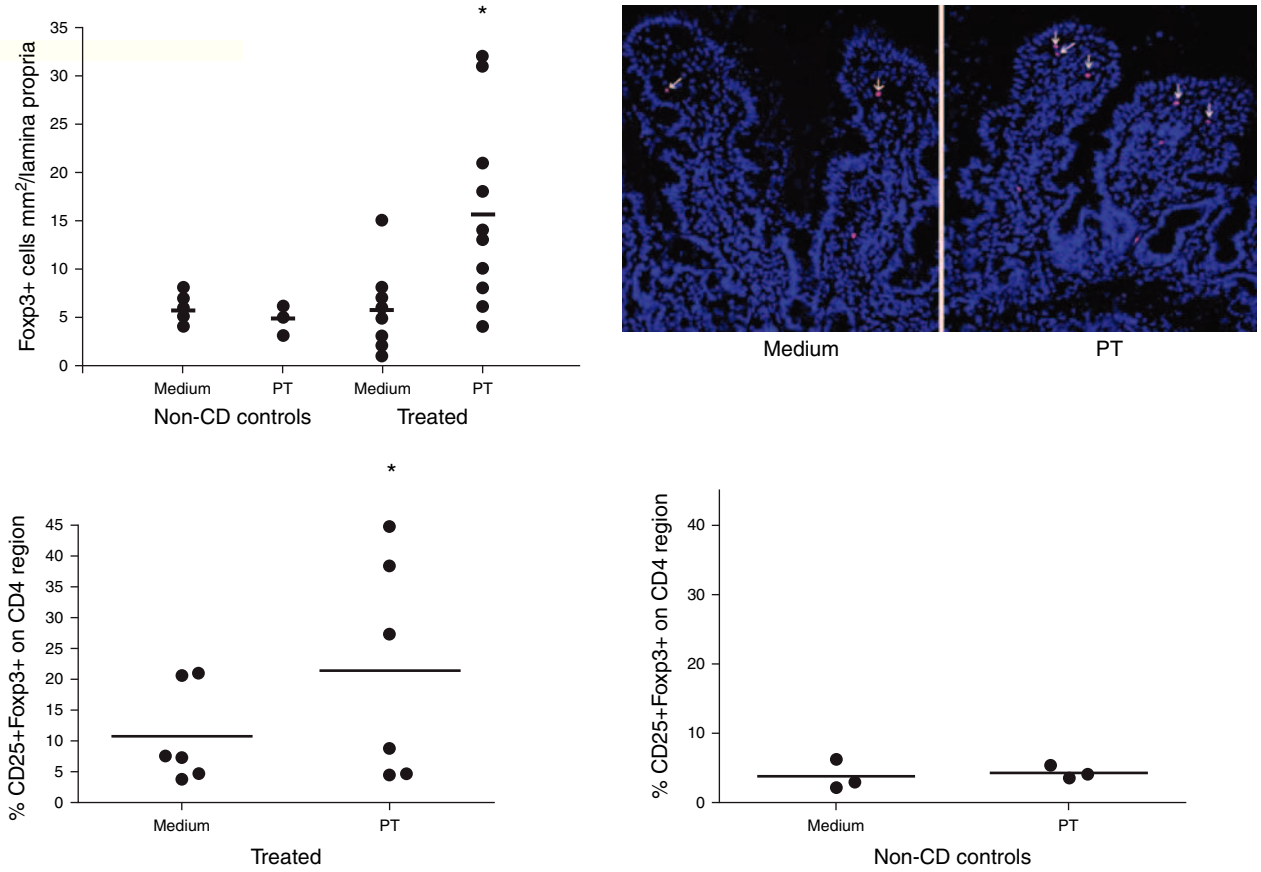


**Figure 3.** PT-gliadin challenge increased Foxp3+ cells in the jejunal biopsy specimens from treated-celiac disease (CD) patients. Upper left panel, number of forkhead box P3 (Foxp3) cells analyzed by immunohistochemistry, in mucosal explants from non-CD controls and treated CD cultured *in vitro* with medium alone or with PT-gliadin. Foxp3+ cells were counted per square millimeter of lamina propria. Dashes indicate the mean values. Statistical significance was evaluated by comparing responses to PT-gliadin with responses to medium alone for each group of subjects. **P*<0.05. Upper right panel, Foxp3+ cells in the jejunal mucosa from a celiac patient cultured *in vitro* with medium only or with a PT-gliadin. In the later, increased numbers of immunostained cells are evident particularly in the subepithelial region (arrows). Original magnification: ×20. Lower panel, CD4+CD25+Foxp3+ cells, analyzed on FACSCalibur, in intestinal biopsies from treated CD patients (left panel) and non-CD controls (right panel) cultured for 24 h in the presence of only medium or PT-gliadin. Data represent the mean of percentages of CD25+Foxp3+ cells in the CD4+ population. Each scatter plot is representative of mean of three or six independent experiments, respectively. Statistical significance was evaluated for lower panel as indicated in the upper left panel. **P*<0.05.

biopsy samples of non-CD controls (see **Supplementary Figure 1** online upper panel). We next explored the phenotype of Foxp3+ cells, with antibodies to CD3, CD4, and CD8, by costaining experiments. Herein, we demonstrated that all the intestinal Foxp3+ cells, in untreated CD, treated CD, and non-CD control duodenal sections, expressed a CD3+CD4+ double-positive phenotype (**Figure 1a**, **b**), whereas CD8+ T cells expressing Foxp3 were not found (**Figure 1c**).

FACS confirmed the findings obtained by immunohistochemistry. Specifically, we analyzed the frequency of Foxp3+CD25+ cells in a CD4+ population. As shown in **Figure 2**, the percentage of Foxp3+CD25+CD4+ cells was significantly higher in untreated celiac patients (mean±s.d.: 14.1±2.7%) compared with treated CD patients (8.9±3.4%, $P<0{,}01$) and non-CD controls (6.8±2.4%, $P<0{,}001$; **Figure 2**). No significant differences were noted in the percentage of Foxp3+CD25+CD4+ cells in treated CD in comparison with non-CD controls (**Figure 2**).

### Foxp3+ cell expansion in treated-CD biopsy samples cultured with gliadin

An *in vitro* gliadin-challenge system was used, which reproduces many features of the mucosal immune response that occurs in the established celiac lesion (23). In the lamina propria of treated-CD biopsy specimens cultured in the presence of PT gliadin, the number of cells/mm$^2$ expressing Foxp3 (16±9) was significantly higher ($P<0.01$) than in those cultured in medium alone (6±4; **Figure 3**, upper left panel). By contrast, no statistically significant differences were noted in the number of Foxp3+ cells, when biopsy samples obtained from non-CD controls were cultured in the presence of PT-gliadin (5±1), compared with those cultured in medium alone (5±2; **Figure 3**, upper left panel). As seen in uncultured biopsy samples taken from untreated CD, Foxp3+ cells in PT-gliadin-challenged mucosa were not found in the epithelium layer, but were found only in the lamina propria, mainly localized beneath the epithelium (**Figure 3**, upper right panel).

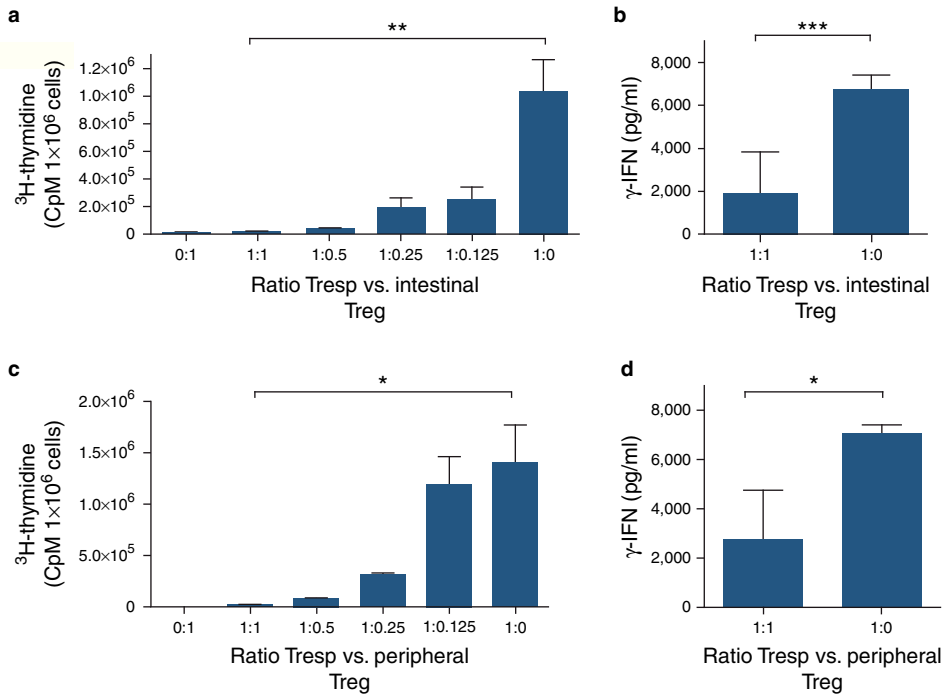


**Figure 4.** In coculture, CD4+CD25+ cells isolated from intestinal or peripheral blood of untreated-celiac disease (CD) patients significantly suppressed the proliferation and interferon gamma (IFN-γ) production of responder T cells (Tresp). Proliferative responses were measured by [$^3$H]thymidine uptake. IFN-γ secretion was evaluated in supernatants of cocultures by an enzyme-linked immunosorbent assay test. Upper panel, *in vitro* study evaluating the suppressive capacity of CD4+CD25+ T cells, purified from intestinal biopsy of seven active CD patients, on the proliferation (**a**) and IFN-γ production (**b**) by Tresp cells. Results are from at least three independent experiments. $^{**}P<0.005$ and $^{***}P<0.001$ comparing the 1:0 vs. 1:1 ratio). Lower panel, *in vitro* study evaluating the suppressive capacity of CD4+CD25+ T cells, purified from peripheral blood of four active CD patients, on the proliferation (**c**) and IFN-γ production (**d**) by Tresp cells. Results are from at least three independent experiments. $^{*}P<0.05$ comparing the 1:0 vs. 1:1 ratio.

The FACS analysis of the frequency of Foxp3+CD25+ cells before and after challenge with PT-gliadin in CD4+ population, confirmed the immunohistochemical data. As shown in **Figure 3**, lower left panel, there was a significantly higher ($P<0,01$) frequency of Foxp3+CD25+ T cells in treated-CD biopsy samples cultured with PT-gliadin (21.4±17.9%) than in those cultured in medium alone (10.8±7.9%). No significant differences were noted in the percentage of Foxp3+CD25+CD4+ cells in biopsy samples of non-CD controls cultured with PT-gliadin (4.2±0.87%), in comparison with biopsy samples cultured with medium alone (3.7±2.1%; **Figure 3**, lower right panel).

### Intestinal CD4+CD25+ cells in CD are regulatory T cells

The high Foxp3 expression by CD4+CD25+ cells from the mucosal explants of active CD raised the possibility that these cells may be Treg cells. Therefore, we co-cultured intestinal CD4+CD25+ T cells from untreated CD patients with CD4+CD25− peripheral Tresp at a ratio of 1:1, in the presence of a polyclonal stimulus. After 3 days, CD4+CD25+ T cells showed a hypoproliferative response (anergy), whereas Tresp cells proliferated vigorously (**Figure 4a**). In coculture, intestinal CD4+CD25+ T cells significantly suppressed the proliferation of Tresp cells (**Figure 4a**)($P<0.005$) in a cell dose-dependent manner, and induced a significant decrease of IFN-γ production ($P<0,001$; **Figure 4b**). Moreover, in line with previous reports (21), we have shown that the peripheral blood CD4+CD25+ T cells of untreated CD patients were Treg cells, being capable of suppressing a significantly autologous responder CD4+CD25− stimulated by anti-CD3/anti-CD28 in a cell dose-dependent manner, in both terms of proliferation ($P<0.05$; **Figure 4c**) and IFN-γ secretion ($P<0.05$) (**Figure 4d**).

### Ability of IL-15 to overcome Treg-mediated immunosuppression in CD patients

As our data show increased number of Foxp3+ cells and a satisfactory suppressive activity to explain the strong inflammatory response in untreated CD patients, we hypothesized that IL-15 hyperexpressed in the untreated CD mucosa could impair such suppression. Therefore, we assessed whether IL-15 could alter Treg-mediated immunosuppression. Freshly isolated Treg cells from intestinal or peripheral blood of untreated CD patients were cocultured, with Tresp at a ratio of 1:1, in a medium containing anti-CD3/CD28, in the presence or absence of IL-15 (10 ng/ml). In CD patients, IL-15 was effective in counteracting both intestinal and peripheral blood Treg cell-mediated suppression of anti-CD3-activated Tresp cells, partially in terms of proliferation (**Figure 5a**, **b**, respectively) and completely in terms of IFN-γ production (**Figure 5c**).

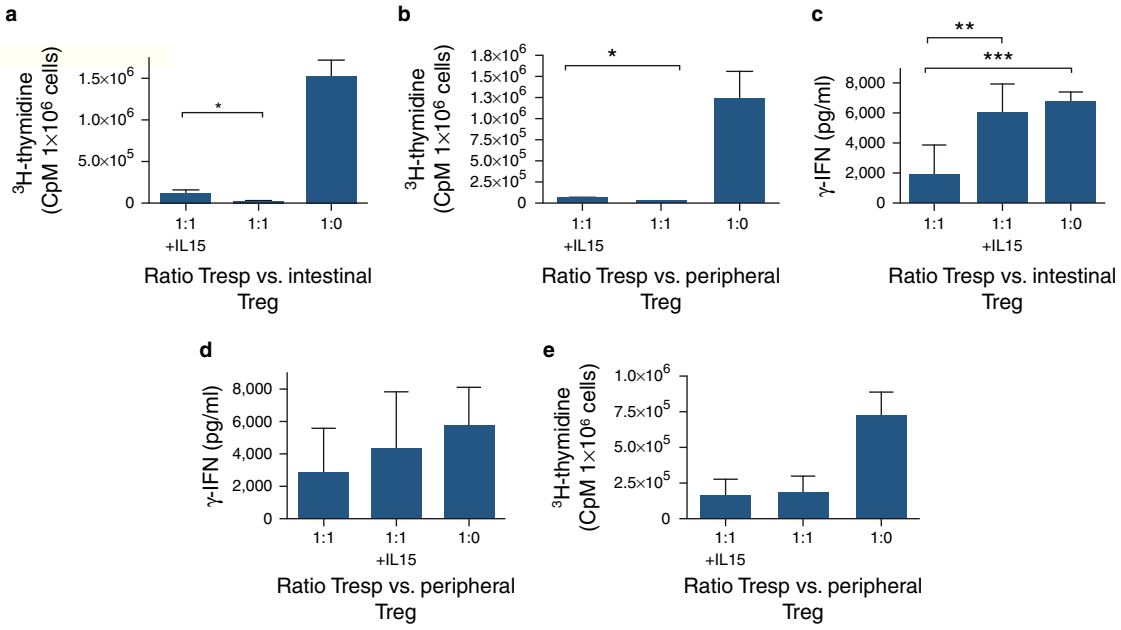


**Figure 5.** Interleukin 15 (IL-15) impairs the suppressive activity of regulatory T cells (Treg). (**a, b**) Effect of IL-15 on suppressive capacity of Treg cells isolated, respectively, from intestinal biopsy and peripheral blood of five active celiac disease (CD) patients assessed on proliferation. (**c**) Effect of IL-15 on suppressive capacity of Treg cells isolated from peripheral blood of five active CD patients assessed on IFN-γ production. Proliferative responses were measured by [$^3$H]thymidine uptake. Interferon gamma (IFN-γ) secretion was evaluated in supernatants of cocultures by an enzyme-linked immunosorbent assay test. (**d** and **e**) Effect of IL-15 on suppressive capacity of Treg cells isolated from peripheral blood of four non-CD controls assessed, respectively, on IFN-γ production and proliferation. Results are from four independent experiments. The Treg and responder T cells (Tresp) were cocultured at 1:1 ratio and stimulated with IL-15 (10 ng/ml). $^*P<0.05$, $^{**}P<0.005$, $^{***}P<0.001$, when compared with the condition in presence of IL-15.

To test whether the inhibitive effect of IL-15 on Treg cells was unique to CD patients, we performed analysis on non-CD controls. We cocultured only peripheral blood CD4+CD25+ T cells with Tresp cells, with or without IL-15, as CD4+CD25+ T cells isolated from the intestinal biopsy samples of non-CD control patients were not enough for functional studies. Our data demonstrated that the phenomenon was nonspecific for CD patients as in non-CD controls IL-15 partially prevented the inhibition of IFN-γ secretion (**Figure 5d**). However, it did not overcome the Treg cell-mediated block of Tresp cell proliferation (**Figure 5e**).

Finally, we wondered whether the greater sensitivity to IL-15 seen in CD patients could be explained by an increased expression of its receptor. Cell-surface IL-15Rα was then monitored by FACS in peripheral blood Treg and Tresp cells of both CD patients and non-CD controls. We found that IL-15Rα was highly expressed on Treg cells in both CD patients and non-CD controls (**Figure 6**), whereas it was moderately detectable in Tresp cells (**Figure 6**). However, a direct comparison of Treg cells from CD patients and non-CD controls revealed that the surface density of IL-15Rα was significantly higher ($P<0.05$) in Treg cells from CD patients (mean±s.d.: 261±150 and 33±28, respectively; **Figure 6**).

## DISCUSSION

In this study, we found, by two complementary methods—immunohistochemistry and FACS *ex vivo* analysis—an increased number of Foxp3+ cells in the intestinal mucosa of patients with active CD compared with both treated CD and non-CD controls. These cells were not found in the epithelium layer, but were mainly localized in the subepithelial layer of the lamina propria. The data obtained in biopsies from active celiac patients are in agreement with recent observations (17–19), indicating an increased density of Foxp3+ cells by immunohistochemistry. In our study, we have confirmed these results also by FACS *ex vivo* analysis.

In general, these data suggest that Foxp3 expression is linked to the Th1-driven mucosal immune response to gliadin. In fact, the expansion of this subset proportional to the intensity of local inflammation, could have a role in the negative feedback loop of T-cell activation. In support of this hypothesis, we found in three CD patients with a partially healed mucosal tissue, an increased number of Foxp3+ cells when compared with the normal mucosa of both treated CD and non-CD controls, but lower with respect to the density found in the mucosa of untreated CD (data not shown). Moreover, the data that we are collecting on duodenal biopsies from "potential" CD patients (patients with positive CD serology, and low local inflammation) point in the same direction. Thus, the increased density of Foxp3+ cells seems to be correlated with the histological lesion, suggesting that the immune system is actively trying to downregulate ongoing inflammation either through the rapid redistribution of Treg cells from the circulation to the inflamed site, or through the local proliferation of these regulatory cells.

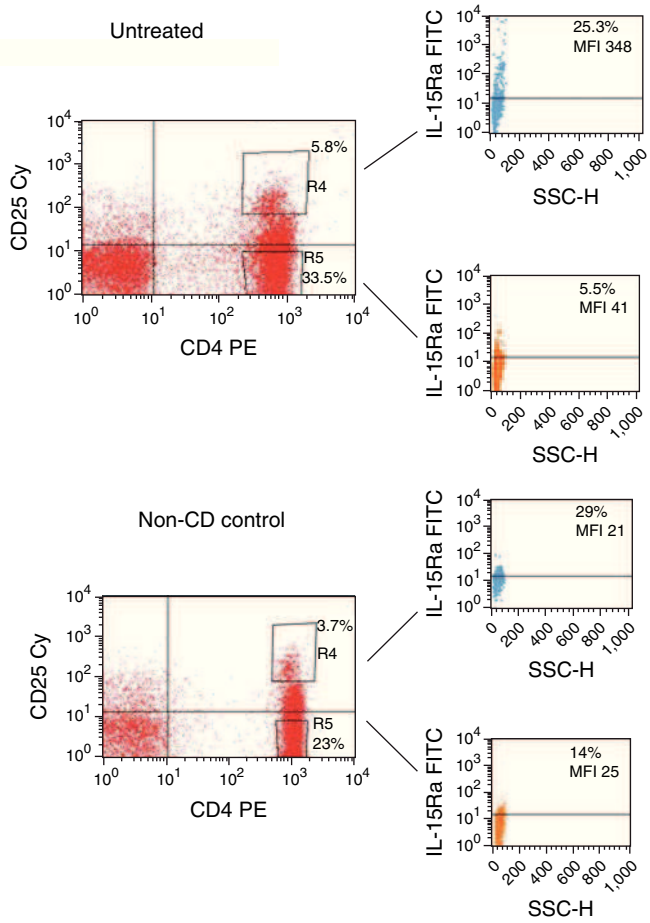


**Figure 6.** Increased expression of interleukin-15 receptor alpha surface expression (IL-15Rα) on CD4+CD25+ T cells from active celiac disease (CD) patients. Freshly isolated peripheral blood mononuclear cells (PBMCs) cells from active celiac patients and non-CD controls stained for CD4, CD25, and IL-15Rα, and analyzed by flow cytometry (FACS). Representative dot plot from one experiment from active CD patients and non-CD control was shown. CD4+CD25+ and CD4+CD25− T cells were analyzed for IL-15Rα expression and mean fluorescence intensity (MFI) of IL-15Rα was indicated. The dot plot shows a higher intensity of IL-15Rα on CD4+CD25+ peripheral blood T cells from active CD patient than non-CD controls ($P<0.05$). Numbers indicate the MFI of at least three experiments.

In humans, the correlation between Foxp3 expression and suppressive capacity is not as clear as in the murine system. In fact, recently it has been shown that expression of Foxp3 does not exclusively occur in CD4+CD25+ Treg cells, as in humans it can also be transiently induced in activated CD4+CD25− T effector cells, which do not express Foxp3 in the resting state (24,25). Therefore, the statement that CD patients are characterized by accumulation of suppressive cells in the intestinal mucosa must be considered carefully, in the absence of a functional suppressive assay. Although the functional activity of CD4+CD25+ T cells isolated from peripheral blood of untreated-CD patients was recently investigated (20–22), the suppressive capacity of such T cells in the intestinal mucosa of CD patients has never been reported. Towards this aim, and to ascertain whether the observed Treg cells are indeed suppressive, we isolated CD4+CD25+ cells from biopsy samples of active CD and tested their suppressive capacity in an *in vitro* coculture assay. Our data show that intestinal CD4+CD25+ T cells of CD patients are able to exert their regulatory effects *in vitro* in terms of inhibition of proliferation and IFN-γ secretion of Tresp cells. Moreover, in line with recent report (21), we confirm the suppressive activity of peripheral blood CD4+CD25+ T cells of CD patients. Therefore, our current results suggest that intestinal and peripheral blood Treg cells of untreated CD patients are not functionally deficient and could be able to control the ongoing immune response to gluten and the consequent inflammation.

On the contrary, despite the increased frequency and suppressive activity *in vitro*, Treg cells fail to control the development of the inflammation in the small intestinal mucosa with active CD. It is possible that the suppressor capacity of these cells may be abrogated *in vivo* or it is insufficient to counterbalance the strong proinflammatory response. Recently, it has been shown that IL-15 not only has a pleiotropic role at the interface between innate and adaptive immunity in CD, but also exerts effects interfering with anti-inflammatory pathways that are normally activated in the small intestinal mucosa by the cytokine TGF-β1 (11). The massive increase of the proinflammatory cytokine IL-15 in CD led us to investigate whether IL-15 might interfere with the suppressive activity of intestinal Treg cells. In active CD patients, we have shown that IL-15 impairs the functions of Treg cells making Tresp cells refractory to the regulatory effects of CD4+CD25+ T cells, in terms of proliferation and production of IFN-γ. This phenomenon was nonspecific for CD patients, as in non-CD controls the addition of IL-15 to cocultures of Treg/Tresp cells prevented the inhibition of IFN-γ secretion. Nevertheless, this effect was less marked than in CD. The greater sensitivity to IL-15 of CD patients is likely to be due to their increased expression of IL-15 receptor. Recently, it has been observed that the mRNA expression of IL-15 receptor-α was increased in duodenal biopsy samples of untreated CD patients as compared with controls (26). How IL-15 can impair the suppressive activity of Treg cells in *vitro* remains to be defined. Previous data indicated that, in active CD, IL-15 was involved in the local downregulation of TGF-β signaling (11), which is required to maintain the regulatory function of Treg cells (27). Studies are now in progress to address in our system whether and how IL-15 might interfere with the regulatory function of TGF-β.

Aside from evidence that natural Foxp3+ Treg cells arise and mature in the thymus, there is mounting evidence that Foxp3+ Treg cells can develop extrathymically under certain conditions. As a consequence of this expansion, Treg cells cause downmodulation of inflammation associated with pathogen-specific immune responses. Recently, it was observed that small intestine lamina propria dendritic cells promote *de novo* generation of Foxp3 Treg cells through retinoic acid, which is a vitamin A metabolite that is highly expressed in gut associated lymphoid tissue (28). Together, these data demonstrate that the intestinal immune system has

evolved a self-contained strategy to promote Treg cell induction. The *in vitro* gliadin challenge system reproduces many features of the mucosal immune response, which occur in the established celiac lesion (29,30). In such a system, we provide evidence that in CD intestinal mucosa, Foxp3 + Treg cell can be expanded locally during gliadin-specific stimulation as a likely attempt to curtail the mucosal immune response. In fact, in the lamina propria of celiac biopsy samples cultured in the presence of a PT-gliadin, but not in those from controls, the number of cells expressing Foxp3 were significantly higher, particularly in the subepithelial compartment, than in samples cultured in medium alone. The FACS analysis of the frequency of Foxp3 + CD25 + cells before and after challenge with PT-gliadin in CD4 + population confirmed the immunohistochemical data.

In conclusion, we have shown that in CD-untreated intestinal mucosa, the expanded CD4 + CD25 + Foxp3 + T cells are regulatory cells. We proved that they are induced *in situ* by gliadin. However, they can be impaired *in vivo* in their suppressor capacity by IL-15. Their sensitivity to the IL-15 action is likely due to enhanced expression of IL-15 receptor.

On the basis of these results and on the finding that IL-15 is overexpressed in intestinal mucosa of patients with active CD, we suggest that, in target tissues, the function of Treg may be substantially limited by these cytokines, and that therapies that aim at neutralizing such cytokines may not only decrease bystander T-cell activation but also reconstitute the suppressor function of regulatory T cells.


## ACKNOWLEDGMENTS

We thank Maria Cristina Bruno (Gastroenterology and Digestive Endoscopy Service, San G Moscati Hospital, Avellino, Italy) and Renata Auricchio (Gastroenterology, Federico II Napoli) for their help in the collection of blood and mucosal samples. The authors are grateful to Dr Giuseppina Ruggiero for her precious scientific support, and to Clemente Meccariello for his technical help.


## CONFLICT OF INTEREST

**Guarantors of the article:** Delia Zanzi, MS and Giuseppe Mazzarella, MS.

**Specific author contributions:** Delia Zanzi was involved in study design, data analysis, and supervised the flow cytometric analyses. Rosita Stefanile contributed to study design and immunohistochemical analyses. Sara Santagata performed flow cytometric analyses. Gaetano Iaquinto and Nicola Giardullo helped in patients' recruitment. Laura Iaffaldano performed flow cytometric analyses. Giuliana Lania and Ilaria Vigliano carried out purification of T Cell subsets and performed suppression assay. Aufiero Rotondi Vera performed organ culture. Katia Ferrara performed the enzyme-linked immunosorbent assay test. Salvatore Auricchio and Riccardo Troncone contributed to study design, data analysis, and critical revision. Giuseppe Mazzarella contributed to study design and data analysis, and supervised immunohistochemical analyses. Riccardo Troncone and Giuseppe Mazzarella were also involved in drafting of the article.

**Financial support:** European Laboratory for the Investigation of Food-Induced Diseases, University Federico II, Naples, Italy.

**Potential competing interests:** None.

## Study Highlights

### WHAT IS CURRENT KNOWLEDGE

- ✓ Coeliac disease (CD) is a condition characterized by a dysregulated mucosal immune response to gliadin.
- ✓ Increased number of Foxp3+ T cells are present in the small-intestine biopsy samples from patients with active CD.
- ✓ Suppressor capacity of circulating CD4 + CD25 + T cells from CD patients are reported, but no functional data are available for their intestinal counterparts.

### WHAT IS NEW HERE

- ✓ Intestinal CD4 + CD25 + T cells from CD patients are functionally suppressive.
- ✓ IL-15 impairs the regulatory activity of both intestinal and peripheral blood Treg cells of CD patients. Their sensitivity to IL-15 is partly explained by the increased expression of IL-15Rα.
- ✓ CD4 + CD25 + Foxp3 + T cells are induced *in situ* by gliadin.

## REFERENCES


1. Green PH, Cellier C. Celiac disease. N Engl J Med 2007;357:1731–43.
2. Nilsen EM, Jahnsen FL, Lundin KE *et al.* Gluten induces an intestinal cytokine response strongly dominated by interferon gamma in patients with celiac disease. Gastroenterology 1998;115:551–63.
3. Salvati VM, MacDonald TT, Del Vecchio Blanco G *et al.* Enhanced expression of interferon regulatory factor-1 in the mucosa of children with celiac disease. Pediatr Res 2003;54:312–8.
4. Ferguson A, Arranz E, O'Mahony S. Clinical and pathological spectrum of coeliac disease –active, silent, latent, potential. Gut 1993;34:150–1.
5. Tosco A, Salvati VM, Auricchio R *et al.* Most Children With Potential Celiac Disease Are Healthy but One-Third of Them Develop Villous Atrophy at 3-Years Follow-Up. Clin Gastroenterol Hepatol 2010; e-pub ahead of print.
6. De Nitto D, Monteleone I, Franzè E *et al.* Involvement of interleukin-15 and interleukin-21, two g-chain-related cytokines, in celiac disease. World J Gastroenterol 2009;15:4609–14.
7. Lan RY, Mackay IR, Gershwin ME. Regulatory T cells in the prevention of mucosal inflammatory diseases: Patrolling the border. J Autoimmun 2007;29:272–80.
8. Awasthi A, Murugaiyan G, Kuchroo VK. Interplay between effector Th17 and regulatory T cells. J Clin Immun 2008;28:660–70.
9. Roncarolo MG, Bacchetta R, Bordignon C *et al.* Type 1 T regulatory cells. Immunol Rev 2001;182:68–79.
10. Allez M, Mayer L. Regulatory T cells – peace keepers in the Gut. Inflamm Bowel Dis 2004;10:666–76.
11. Benhamed M, Bertrand M, Bertrand A *et al.* Inhibition of TGF-β signaling by IL-15: a new role for IL-15 in the loss of immune homeostasis in celiac disease. Gastroenterology 2007;132:994–1008.
12. Lahat N, Shapiro S, Karban R *et al.* Cytokine profile in coeliac disease. Scand J Immunol 1999;49:441–6.
13. Forsberg G, Hernell O, Melgar S *et al.* Paradoxical coexpression of proinflammatory and down-regulatory cytokines in intestinal T-cells in childhood celiac disease. Gastroenterology 2002;123:667–78.
14. Salvati V, Mazzarella G, Gianfrani C *et al.* Recombinant human IL-10 suppresses gliadin-dependent T-cell activation in *ex vivo* cultured celiac intestinal mucosa. Gut 2005;54:46–53.
15. Gianfrani C, Leving M, Sartirana C *et al.* Gliadin-specific type-1 regulatory T-cells from intestinal mucosa of treated celiac patients inhibit pathogenic T-cells. J Immunol 2006;177:4178–86.
16. Vieira PL, Christensen JR, Minaee S *et al.* IL-10-secreting regulatory T cells do not express Foxp3 but have comparable regulatory function

to naturally occurring CD4(R)CD25(R) regulatory T cells. J Immunol 2004;172:5986–93.
17. Tiittanen M, Westerholm-Ormio M, Verkasalo M *et al.* Infiltration of forkhead box P3-expressing cells in small intestinal mucosa in coeliac disease but not in type 1 diabetes. Clin Exp Immunol 2008;152:498–507.
18. Vorobjova T, Uibo O, Heilman K *et al.* Increased FOXP3 expression in small-bowel mucosa of children with coeliac disease and type I diabetes mellitus. Scand J Gastroenterol 2009;44:422–30.
19. Westerholm-Ormio M, Vaarala O, Tiittanen M *et al.* Infiltration of Foxp3- and Toll-like receptor-4-positive cells in the intestines of children with food allergy. J Pediatr Gastroenterol Nutr 2010;50:367–76.
20. Granzotto M, dal Bo S, Quaglia S *et al.* Regulatory T-cell function is impaired in celiac disease. Dig Dis Sci 2009;54:1513–9.
21. Frisullo G, Nociti V, Iorio R *et al.* Increased CD4+CD25+Foxp3+ T cells in peripheral blood of celiac disease patients: correlation with dietary treatment. Hum Immunol 2009;70:430–5.
22. Kivling A, Nilsson L, Fälth-Magnusson K *et al.* Diverse foxp3 expression in children with type 1 diabetes and celiac disease. Ann N Y Acad Sci 2008;1150:273–7.
23. Mazzarella G, Stefanile R, Camarca A *et al.* Gliadin activates HLA class I-restricted $CD8^+$ T-cells in celiac intestinal mucosa and induces the enterocyte apoptosis. Gastroenterology 2008;134:1017–27.
24. Wang J, Ioan-Facsinay A, van der Voort EI *et al.* Transient expression of FOXP3 in human activated nonregulatory CD4+ T cells. Eur J Immunol 2007;37:129.
25. Roncarolo MG, Gregori S. Is FOXP3 a bona fide marker for human regulatory T cells? Eur J Immunol 2008;38:925–7. Review.
26. Bernardo D, Garrote JA, Allegretti Y *et al.* Higher constitutive IL15R alpha expression and lower IL-15 response threshold in coeliac disease patients. Clin Exp Immunol 2008;154:64–73.
27. Marie JC, Letterio JJ, Gavin M *et al.* TGF-beta1 maintains suppressor function and Foxp3 expression in CD4+CD25+ regulatory T cells. J Exp Med 2005;201:1061–7.
28. Sun CM, Hall JA, Blank RB *et al.* Small intestine lamina propria dendritic cells promote *de novo* generation of Foxp3T reg cells via retinoic acid. J Exp Med 2007;204:1775–85.
29. Maiuri L, Picarelli A, Boirivant M *et al.* Definition of initial immunologic modifications upon *in vitro* gliadin challenge in the small intestine of celiac patients. Gastroenterology 1996;110:1368–78.
30. Mazzarella G, Maglio M, Paparo F *et al.* An immunodominant DQ8 restricted gliadin peptide activates small intestinal immune response in *in vitro* cultured mucosa from HLA-DQ8 positive but not HLA-DQ8 negative coeliac patients. Gut 2003;52:57–62.

OPEN ACCESS Freely available online

PLoS one

# MicroRNA-449a Overexpression, Reduced NOTCH1 Signals and Scarce Goblet Cells Characterize the Small Intestine of Celiac Patients

**Marina Capuano[1,2•], Laura Iaffaldano[1,2•], Nadia Tinto[1,2], Donatella Montanaro[1], Valentina Capobianco[3], Valentina Izzo[4], Francesca Tucci[4], Giancarlo Troncone[1,5], Luigi Greco[4], Lucia Sacchetti[1,2]***

**1** CEINGE (Centro di Ingegneria Genetica) Advanced Biotechnology, s. c. a r. l., Naples, Italy, **2** Department of Biochemistry and Medical Biotechnology, University of Naples Federico II, Naples, Italy, **3** Fondazione IRCSS SDN (Istituto di Ricovero e Cura a Carattere Scientifico - Istituto di Ricerca Diagnostica e Nucleare), Naples, Italy, **4** Department of Paediatrics and European Laboratory for the Investigation of Food-Induced Diseases (ELFID), University of Naples Federico II, Naples, Italy, **5** Department of Biomorphological and Functional Sciences, University of Naples Federico II, Naples, Italy

## Abstract

MiRNAs play a relevant role in regulating gene expression in a variety of physiological and pathological conditions including autoimmune disorders. MiRNAs are also important in the differentiation and function of the mouse intestinal epithelium. Our study was aimed to look for miRNA-based modulation of gene expression in celiac small intestine, and particularly for genes involved in cell intestinal differentiation/proliferation mechanisms. A cohort of 40 children (20 with active CD, 9 on a gluten-free diet (GFD), and 11 controls), were recruited at the Paediatrics Department (University of Naples Federico II). The expression of 365 human miRNAs was quantified by TaqMan low-density arrays. We used bioinformatics to predict putative target genes of miRNAs and to select biological pathways. The presence of NOTCH1, HES1, KLF4, MUC-2, Ki67 and beta-catenin proteins in the small intestine of CD and control children was tested by immunohistochemistry. The expression of about 20% of the miRNAs tested differed between CD and control children. We found that high miR-449a levels targeted and reduced both NOTCH1 and KLF4 in HEK-293 cells. NOTCH1, KLF4 signals and the number of goblet cells were lower in small intestine of children with active CD and in those on a GFD than in controls, whereas more nuclear beta-catenin staining, as a sign of the WNT pathway activation, and more Ki67 staining, as sign of proliferation, were present in crypts from CD patients than in controls. In conclusion we first demonstrate a miRNA mediated gene regulation in small intestine of CD patients. We also highlighted a reduced NOTCH1 pathway in our patients, irrespective of whether the disease was active or not. We suggest that NOTCH pathway could be constitutively altered in the celiac small intestine and could drive the increased proliferation and the decreased differentiation of intestinal cells towards the secretory goblet cell lineage.

**Citation:** Capuano M, Iaffaldano L, Tinto N, Montanaro D, Capobianco V, et al. (2011) MicroRNA-449a Overexpression, Reduced NOTCH1 Signals and Scarce Goblet Cells Characterize the Small Intestine of Celiac Patients. PLoS ONE 6(12): e29094. doi:10.1371/journal.pone.0029094

**Editor:** Hang Thi Thu Nguyen, Emory University, United States of America

**Received** May 23, 2011; **Accepted** November 21, 2011; **Published** December 15, 2011



**Funding:** Study supported from European community (PREVENT CD project: EU-FP6-2005-FOOD4B-contract no. 036383). The funder had no role in study design, data collection and analysis, decision to publish, or preparation of the manuscript.

**Competing Interests:** The authors have declared that no competing interests exist.

* E-mail: sacchett@unina.it

• These authors contributed equally to this work.

## Introduction

Celiac disease (CD) is an immunomediated enteropathy and one of the most heritable complex diseases. The concordance rate in monozygotic twins is 75% [1,2]. HLA DQ2/DQ8 haplotypes confer the highest estimated heritability (~35%) [3] reported so far.

Exposure to gliadin triggers an inappropriate immune response in HLA-susceptible individuals. However, the presence of HLA-risk alleles is a necessary but not sufficient condition for the development of CD. In fact, about 30–40% of healthy subjects carry HLA-risk alleles [4,5]. Attempts at identifying non-HLA major genetic risk loci have been unsuccessful [6]. Gluten has also been shown to affect epithelial differentiation-associated genes in the small intestinal mucosa of celiac patients [7,8]. However, the role of miRNA-based regulatory mechanisms in mediating gene expression alteration in CD has not yet been investigated.

MicroRNAs (miRNAs) are small non-coding RNAs, 20–25 nt long, that modulate gene expression through canonical base pairing to complementary sequences in the 3′UTR of target mRNA [9]. Since their identification in 1993 [10], miRNAs have been found to play a relevant role in regulating gene expression in a variety of biological processes in physiological and pathological conditions [11] including autoimmune disorders [12]. They can be involved in the development of mature immune cells and in the control of their function [13–15]. MiRNAs are also important in the differentiation and function of the mouse intestinal epithelium [16].

In this study, we evaluated the miRNA expression pattern in the small intestine of children affected by active CD, children with CD on a gluten-free diet (GFD) and control children without CD. Our aim was to look for miRNA-based modulation of gene expression in celiac small intestine, and particularly for genes involved in cell intestinal differentiation/proliferation mechanisms.

## Results

### Clinical features of CD patients and controls

Clinical features of our CD patients and controls are reported in Table 1. Villous atrophy was subtotal or total [TIIIB: n = 3 (15%) and TIIIC: n = 17 (85%)] in all active CD patients. Only minor histological abnormalities were present in GFD patients [T0: n = 5 (56%) and TI: n = 4 (44%)] and in control patients [T0: n = 7 (64%) and TI: n = 4 (36%)].

### CD children and controls have a different miRNA expression levels in small intestine

Figure 1 shows the miRNA expression in the small intestine of children with active CD (panel A) and in children on a GFD (panel B). Ninety of the 365 (25%) miRNAs tested were not expressed in small intestine. Over 50% of miRNAs were expressed at similar levels in the two groups of CD compared to controls. On the contrary, the expression levels of about 20% of miRNAs (22% in active CD and 19% in GFD) differed between CD and controls. In particular, in active CD patients 27 and 55 miRNAs were expressed respectively more (RQ≥2.0) or less (RQ≤0.5) than in controls, whereas in GFD patients 22 and 49 miRNAs were expressed respectively more (RQ≥2.0) or less (RQ≤0.5) than in controls. The miRNAs that were differently expressed in the two CD groups are listed in Table S1.

### Two sets of miRNAs (one down-regulated and one up-regulated compared to controls) show similar expression levels in active and GFD CD patients, being miR-449a the highest expressed miRNA

Among the miRNAs differently expressed between CD children and controls, but with similar expression levels in active and in GFD CD, 9 were up-regulated and 21 were down-regulated (Table 2). Particularly, among the down-regulated miRNAs the set of miR-124a, miR-189, miR-299-5p and miR-379, was previously reported associated with autoimmune disorders [17]. Among the up-regulated miRNAs the miR-449a was expressed at very high levels in all active CD (55.18±16.45 mean RQ±SEM) and GFD children (15.43±7.69 mean RQ±SEM). qRT-PCR confirmed the expression levels both of miR-449a (active CD: 2.8±0.9 mean RQ±SEM) and of 2 other tested miRNAs, the down-regulated miR-124a (active CD:0.6±0.1 mean RQ±SEM) and the similar to control expressed miR-564 (active CD:1.4±0.3 mean RQ±SEM vs 1.2±0.1 at array).

**Table 1.** General characteristics of studied celiac patients (active CD and GFD) and control children (CTRL).

| Characteristics[#] | Subjects | | |
|---|---|---|---|
| | Active CD (n = 20) | GFD[^] (n = 9) | CTRL (n = 11) |
| Sex Female (%) | 55 | 55 | 45 |
| Age (Years) | 4.3±1.3 | 7.6±2.5 | 6.1±1.0 |
| Clinical presentation: | | | |
| Gastrointestinal symptoms (%) | 80 | 22 | 82 |
| Villous atrophy % (Marsh stage)[‡] | TIIIB 15 | T0 56 | T0 64 |
| | TIIIC 85 | TI 44 | TI 36 |
| Positive tTG or EMA (IgA)[§] | 19 | 3 | 0 |
| Familiarity for: | | | |
| CD (%) | 20 | 22 | 0 |
| Other autoimmune diseases (%) | 5 | 11 | 0 |

[#]Data are expressed as percentage (%) or as mean ± standard error of the mean (SEM)

[^]At gluten free diet from at least 2 years.

[‡]According to [41].

[§]Only 1 active CD patient was negative for these antibodies but was positive for both AGA IgG/IgA antibodies. Borderline tTG values in 3/9 GFD patients were attributed to reported sporadic gluten ingestion.

doi:10.1371/journal.pone.0029094.t001

### Bioinformatic prediction of the target genes of miR-449a

Six of the 11 programs [Target Scan 5.1, PicTar, Miranda 1.9, MirTarget2 (v2.0), PITA (Catalog version 3) and RNAhybrid (v2.2)], which we used to predict putative target genes of miR-449a, identified several proteins that are present in relevant biological pathways. The biological pathways predicted to be deregulated by miR-449a and sorted in functional groups are reported in Figure S1 (http://mirecords.biolead.org/interactions.php?species=Homo+sapiens&mirna_acc=hsa-miR449a&targetgene_type=refseq_acc&targetgene_info=&v=yes&search_int=Search (http://www.targetscan.org/cgi-bin/targetscan/vert_50/targetscan.cgi?species=Human&gid=&mir_sc=&mir_c=&mir_nc=&mirg=hsa-miR-449a). Among putative target genes the programs identified NOTCH1, Krueppel-like factor 4 (KLF4), delta-like 1 (DLL1), lymphoid enhancer-binding factor 1 (LEF1) and numb homolog-like (NUMBL) proteins, which are all involved in the Notch pathway. As this pathway plays a relevant role in the control of intestinal cell fate in animal models we further examined the interaction of miR-449a with Notch pathway [18].

**MiR-449a binds to the 3′ UTR of NOTCH1 and KLF4 and inhibits their expression.** We verified the interaction between miR-449a and the 3′ UTR of NOTCH1 and of KLF4 using the luciferase reporter assay. In cells co-transfected with pRL-NOTCH1 vector and pre-miR-449a or with pRL-KLF4 vector, a pre-miR-449a concentration of 100 nmol/L was sufficient to significantly reduce (respectively, p = 0.001 and p = 0.002) *Renilla* luciferase activity versus control values after 48 h (Figure S2A and S2B).This finding confirms the interaction between miR-449a and the 3′ UTR of both NOTCH1 and KLF4.

The direct interaction between miR-449a and the 3′UTRs of both NOTCH1 and KLF4 was further confirmed after mutating the putative target sites in 3′UTR of the two genes (See Materials and Methods S1).

### NOTCH1 and HES1 mRNAs are expressed in the small intestine of CD patients

NOTCH1 and HES1 mRNA levels, tested by qRT-PCR, were expressed in the small intestine of active CD patients (RQ±SEM: 3.4±1.3 and 1.4±0.2, respectively *vs* controls) and of GFD patients (RQ±SEM: 6.5±4.7 and 0.7±0.1, respectively vs controls).

### NOTCH1 and HES1 proteins are underexpressed in the small intestine of CD patients

We next investigated the protein expression of NOTCH1 and of HES1, which is a well known target gene of the Notch receptor family, in small intestinal biopsies from CD patients and controls. Figure 2 shows the results obtained for NOTCH1. NOTCH1 was homogeneously distributed in the intestinal villi and crypts of controls and higher expressed in crypts of controls than in crypts of active and GFD CD patients (panel A, B).

In Figure 2 (panel C) are also the images converted for automated analysis (white: unstained cells, yellow/orange: low/moderately stained cells, brown: intensely stained cells). Significantly more intensely stained and less unstained cells (p = 0.02)

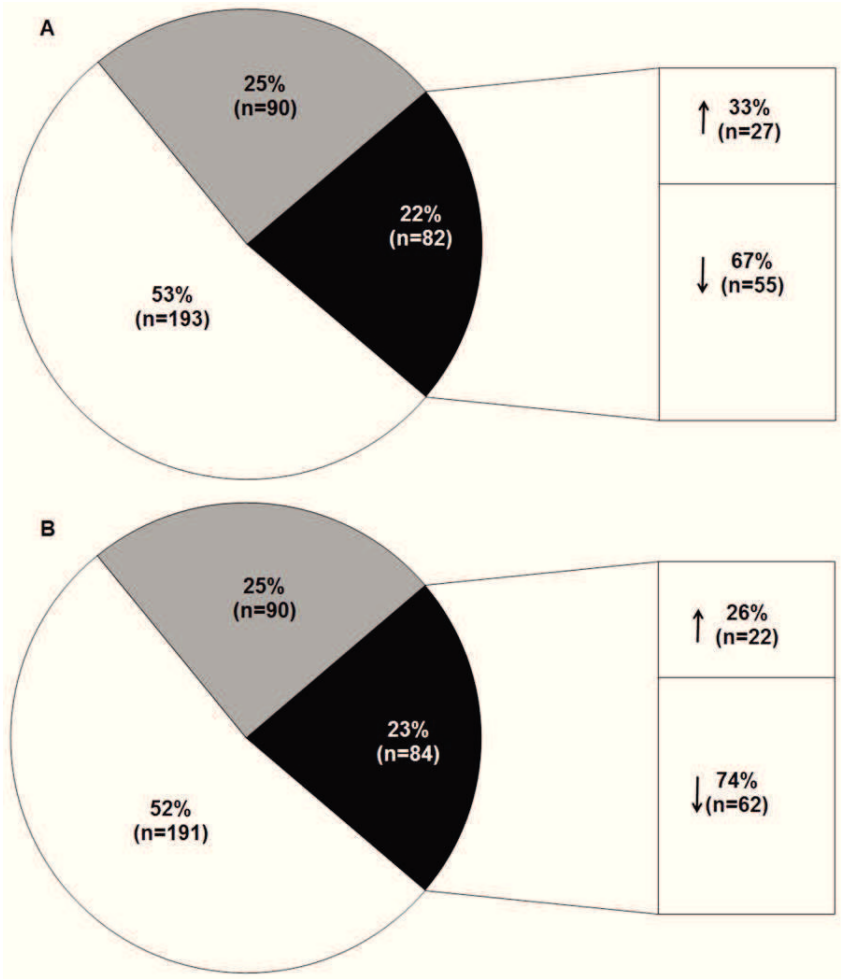


**Figure 1. miRNA expression pattern in small intestine of CD patients.** miRNA expression in the small intestine of patients with active CD (Panel A) and of CD patients on a GFD (Panel B). Data are expressed as percentage of miRNAs tested (n = 365). White areas, miRNAs whose expression levels were similar in the two CD groups and controls; gray areas, miRNAs not expressed; black areas, miRNAs whose expression levels differed between CD patients and controls (up-regulated ↑ (RQ≥2.0) or down-regulated ↓ (RQ≤0.5)).
doi:10.1371/journal.pone.0029094.g001

were detected in controls than in the two groups of CD patients, whereas no statistical significant difference was observed between the two CD groups (Figure S3, panel A and Figure S4). These results indicate that NOTCH1 is less expressed in the small intestine of active and GFD CD patients than in controls. Figure 3 shows the results obtained for HES1. HES1 was homogeneously distributed in the intestinal villi and crypts of controls and higher expressed in crypts of controls than in crypts of active and GFD CD patients (panels A and B). In Figure 3 (panel C) are also the images converted for automated analysis (white: unstained cells, yellow/orange: low/moderately stained cells, brown: intensely stained cells). Significantly more intensely stained cells were detected in controls than in CD patients ($p = 0.02$) and significantly less unstained cells were detected in controls than in active CD patients ($p = 0.03$), whereas no statistical significant difference was observed between the two CD groups (Figure S3, panel B and Figure S5). These results indicate that HES1 is less expressed in the small intestine of active and GFD CD patients with respect to controls. The above findings confirm that NOTCH1 signaling is reduced in patients affected by CD.

## KLF4 protein is reduced and the number of goblet cells is significantly lower in the small intestine of CD patients versus controls

We also investigated the protein expression of KLF4, another selected target gene of miR449a, in small intestinal villi from GFD patients and controls, lacking the villous architecture in active CD patients. We found that the levels of this protein (mean±SEM) were significantly lower in villi from GFD patients vs controls, respectively 29.0±5.0 vs 79.0±3.0 ($p<0.0001$) (Figure S6, panel A). Since KLF4 negatively regulates cellular proliferation, we examined the effect of inhibition of KLF4 on the proliferation of intestinal crypts with the proliferation marker Ki67. The results show that the number of Ki67 positive cells is higher in the crypts of CD patients than in controls (Figure S6, panel B). Because KLF4 is also involved in the differentiation and maturation of secretory goblet cells we examined these cells by immunohistochemistry and using anti-MUC-2 antibodies. We detected statistically fewer MUC-2-stained cells (mean±SEM) in the crypts of active CD patients (18.0±1.6) and GFD patients (15.0±3.0) than in controls (35.0±7.7) ($p = 0.04$) (Figure 4A and B). Moreover, there were fewer goblet cells in the villi of GFD

**Table 2.** List of miRNAs (n = 30) differently expressed in CD patients and controls but with similar expression levels both in active CD and GFD children.

| MiRNA | Active CD | GFD |
|---|---|---|
| **up-regulated miRNAs** | | |
| miR-449a | 55.18±16.45 | 15.43±7.69 |
| miR-492 | 48.88±14.56 | 26.86±9.00 |
| miR-644 | 47.80±8.80 | 37.53±18.85 |
| miR-503 | 19.84±2.36 | 20.55±8.07 |
| miR-196a | 11.06±2.84 | 8.45±1.01 |
| miR-504 | 5.54±0.83 | 8.02±2.86 |
| miR-500 | 5.49±0.70 | 7.88±1.56 |
| miR-330 | 3.84±0.45 | 2.48±0.11 |
| miR-182 | 2.95±0.42 | 2.75±0.13 |
| **down-regulated miRNAs** | | |
| miR-105 | 0.37±0.03 | 0.25±0.03 |
| miR-409-5p | 0.35±0.04 | 0.31±0.05 |
| miR-631 | 0.34±0.03 | 0.27±0.04 |
| miR-659 | 0.33±0.03 | 0.30±0.05 |
| miR-379 | 0.30±0.05 | 0.23±0.10 |
| miR-566 | 0.29±0.02 | 0.23±0.03 |
| miR-512-3p | 0.27±0.03 | 0.26±0.04 |
| miR-614 | 0.26±0.02 | 0.21±0.02 |
| miR-380-5p | 0.25±0.03 | 0.28±0.04 |
| miR-135a | 0.21±0.05 | 0.38±0.05 |
| miR-124a | 0.20±0.02 | 0.21±0.05 |
| miR-600 | 0.19±0.02 | 0.22±0.06 |
| miR-618 | 0.18±0.03 | 0.32±0.07 |
| miR-616 | 0.17±0.04 | 0.11±0.03 |
| miR-189 | 0.15±0.05 | 0.21±0.06 |
| miR-576 | 0.15±0.04 | 0.40±0.10 |
| miR-412 | 0.13±0.03 | 0.18±0.01 |
| miR-202 | 0.12±0.06 | 0.17±0.08 |
| miR-299-5p | 0.11±0.01 | 0.15±0.05 |
| miR-323 | 0.11±0.01 | 0.23±0.08 |
| miR-219 | 0.10±0.01 | 0.27±0.08 |

Data are reported as RQ[#] levels (mean±SEM).
[#]$RQ = 2^{-\text{delta deltaCT}}$ represents miRNA fold change in CD patients vs mean value obtained in control patients.
doi:10.1371/journal.pone.0029094.t002

patients (7.0±1.8) than in controls (20.0±4.9) ($p = 0.04$) (data not shown). This finding demonstrates that the differentiation of the secretory goblet cells is impaired in small intestine of CD patients.

### Expression of beta-catenin

Because NOTCH1 and also KLF4 interact with the WNT pathway to influence the intestinal stem cell fate, we investigated the WNT pathway using beta-catenin antibodies. By counting the beta-catenin positive nuclei/crypt for each patient we observed higher even if not statistical significant mean percentage beta-catenin positive nuclei/crypt in active CD and GFD patients than in controls, respectively 57.0±11.5 and 37.0±4.6 *vs* 27.0±4.6 (Figure S7). This finding suggests that cellular proliferation is increased in the small intestine of CD patients.

## Discussion

A very recent study established the importance of miRNAs in the differentiation and function of the mouse intestinal epithelium [16], whereas there are no data about miRNAs expression in human CD small intestine. Our study reveals that the expression of about 20% of miRNAs tested in the small intestine differed among CD and control children irrespective of whether the disease was active or not. Particularly, the miR-449a showed the highest expression level in CD patients than in controls. The miR-449 (a and b) cluster is embedded into an intronic sequence of the mRNA-encoding gene *CDC20B* on Chr 5q11.2 [17]. MiR-449a seems to be regulated through activation of its host gene, *CDC20B*, and both were induced by the cell cycle regulator E2F1 [19]. The mature miR-449a sequence is evolutionarily conserved across a variety of species (monkey, horse, rodents, and dogs) and therefore it probably exerts an important function [20]. The bioinformatics search for putative target genes of miR-449a revealed about one hundred proteins, among these several belonged to the Notch pathway, i.e., NOTCH1, KLF4 (a NOTCH1 transcription factor) [21], DLL1, LEF1 and NUMBL. Our strategy to choose NOTCH1 gene among the other putative miRNA-target genes was based on many studies highlighting that cellular formation of the villi in small and large intestine is affected by signaling pathways such as Notch, Wnt and BMP [22–25]. Notably, deregulation of the intestinal epithelial formation has been reported in several intestinal diseases such as Crohn, ulcerative colitis and colon cancer [26]. Further, NOTCH1 and KLF4 genes are both involved in the control of mouse intestinal epithelial homeostasis [18,27]. In fact, in mouse intestine, also in cooperation with WNT signals, NOTCH1 guides cell proliferation and differentiation [18] and KLF4 inhibition by NOTCH1 or KLF4 deletion was shown to reduce the differentiation and maturation of goblet cells [21,27–29]. The Notch family is constituted by single transmembrane receptors that, in mammals, after interaction with ligands (DLL1,3,4 and Jagged 1–2) undergo proteolytic cleavage and finally translocate into the nucleus where they activate target gene transcription [30].

After confirmed the interaction between miR-449a and both NOTCH1 and KLF4 mRNA, we measured the NOTCH1 and KLF4 protein levels in small intestinal biopsies of CD children. NOTCH1-positive cells were significantly fewer in biopsies from active and GFD CD patients versus controls. Similar results were also obtained for HES1, a target gene of NOTCH1 [31]. Globally, these data indicate that the NOTCH1 pathway is deregulated in intestinal epithelium of CD children, irrespective of whether the disease is active or not, and that this alteration could be related to the very high miR-449a expression. Accordingly, in a very recent report miR449 by repressing the Delta/Notch pathway was elegantly shown to control the human airway epithelium and vertebrate multilciliogenesis [32]. In our patients we also observed fewer KLF4-positive cells in small intestinal villi from GFD patients than in controls, and, moreover, Ki67 signals were higher in crypts from CD patients versus controls. These two results are in agreement with data very recently reported in a mouse $KLF4^{DELTAIS}$ model [27] and indicate a higher proliferation rate in our CD patients in the presence of reduced KLF4 expression [27]. In parallel the number of goblet cells was significantly lower in the two CD groups than in control children. Ciacci et al [33] previously reported fewer goblet cells/$mm^2$ in untreated (29.1) and in treated CD patients (42.2) than in controls (50.5), although the differences were statistically significant only in untreated patients ($p<0.02$).

The WNT pathway in the small intestine of our CD patients, evaluated based on beta-catenin expression level, did not differ

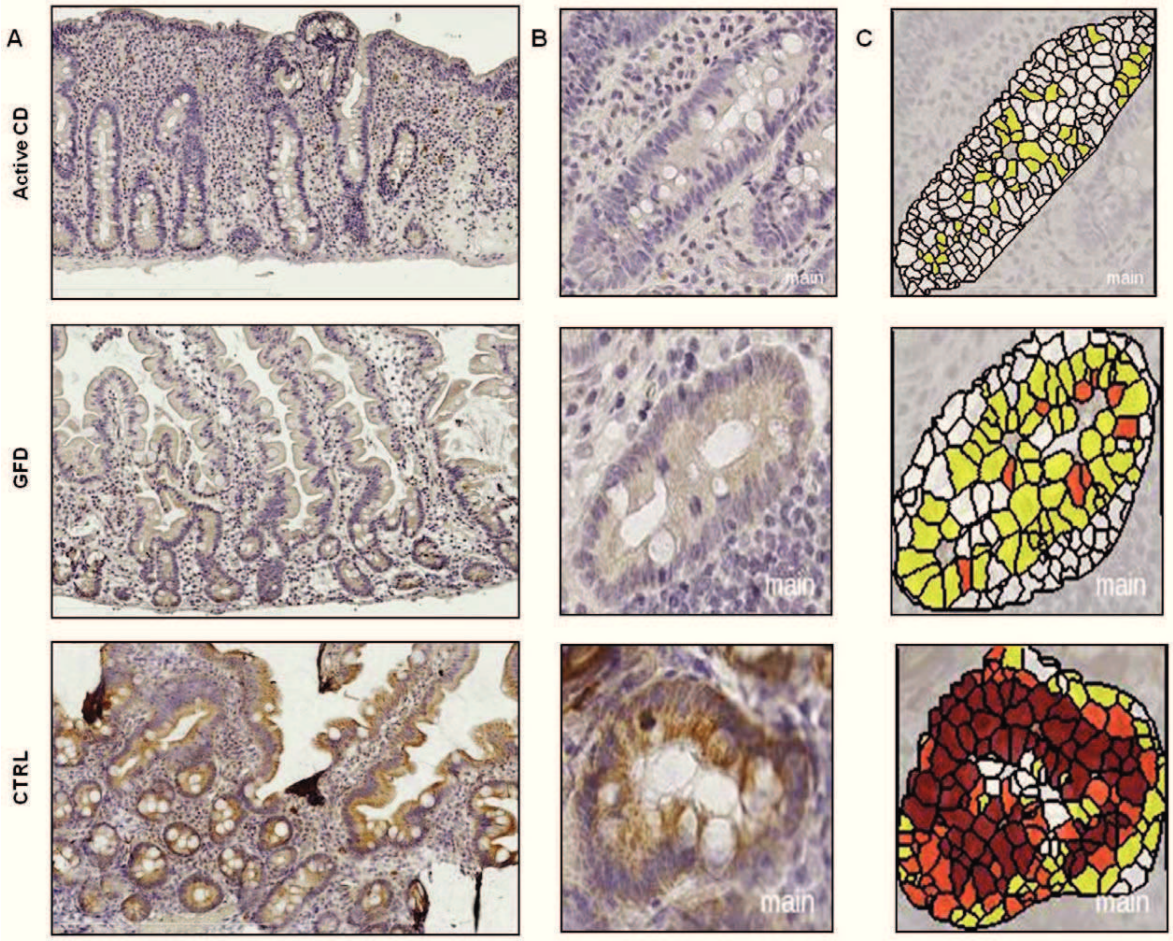


**Figure 2. Decreased expression of NOTCH1 in small intestine of CD patients compared with controls.** An example of NOTCH1 immunohistochemistry in small intestine. **A.** Low magnification picture of the intestinal sections (Original magnification 10×). **B.** Intestinal crypts (Original magnification 40×). Note the homogeneous distribution of NOTCH1 in crypts and along the villi in control sample, whereas in active CD and GFD samples the signals were prevalently detected in the crypts. Higher levels of NOTCH1 were detected in the intestinal crypts of controls than in crypts of active and GFD CD samples. **C.** Images converted for automated analysis (white: unstained cells, yellow/orange: low/moderately stained cells, brown: intensely stained cells). These results indicate that NOTCH1 is less expressed in the small intestine of active and GFD CD samples compared with controls. (CTRL: controls; GFD: gluten free diet; CD: celiac disease).
doi:10.1371/journal.pone.0029094.g002

from that of control children. This result is in agreement with the western blot data reported by Ciccocioppo et al [34] and by Juuti-Uusitalo et al [7]. However, we observed a more evident nuclear localization of beta-catenin, albeit not statistically significant, in the small intestinal crypts from our active and GFD CD patients than in controls, which suggests activation of the WNT pathway. The latter finding is in agreement with a previous study of human CD [7] and with the increased mRNA levels of the genes in the WNT pathway, including beta-catenin, observed in the KLF4$^{DELTAIS}$ mouse [27]. Globally, our data support increased cellular proliferation in the small intestinal epithelium in CD patients. As it is well known, active CD is characterized by an inversion of the differentiation/proliferation program of the intestine with a reduction in the differentiated compartment, up to complete villous atrophy, and an increase of the proliferative compartment, with crypt hyperplasia [7,8]. Furthermore, although GFD intestinal mucosa is characterized by an apparently normal mucosal architecture, it can also be associated with increased crypt cell proliferation (Barone M. V. et al., personal communication). Our data are in contrast with those obtained in mouse models, in which NOTCH1 activation resulted in a reduction of goblet cells consequent to HES-1 dependent repression of Math1 (intestinal secretory cell differentiation factor) [18] and in which NOTCH1 inhibited the expression of KLF4 [35]. However, our data are in agreement with a recent report of increased proliferation, reduced differentiation and goblet cells maturation associated with down-regulation of the expression of components of the Notch pathway (HES1, DLL1, JAG1) in the small intestine of the KLF4$^{DELTAIS}$ mouse [27]. The authors for the latter article hypothesized that KLF4 was involved in a feed-back loop by positively regulating Notch signaling. Our results are suggestive that an altered NOTCH1 and KLF4 expression could lead to the reduction of goblet cells in the small intestine of CD patients. The maintenance of a correct number of functional goblet cells is required for the homeostasis of the intestinal mucosal environment, and deficiencies in the mucin composition renders the mucosa more susceptible to damaging agents in the lumen [36–38]. In fact, loss of goblet cell function leads to spontaneous colitis in mice [39]. Moreover, an altered mucous layer and increased rod-shaped bacteria and interferon-gamma mRNA levels were found in

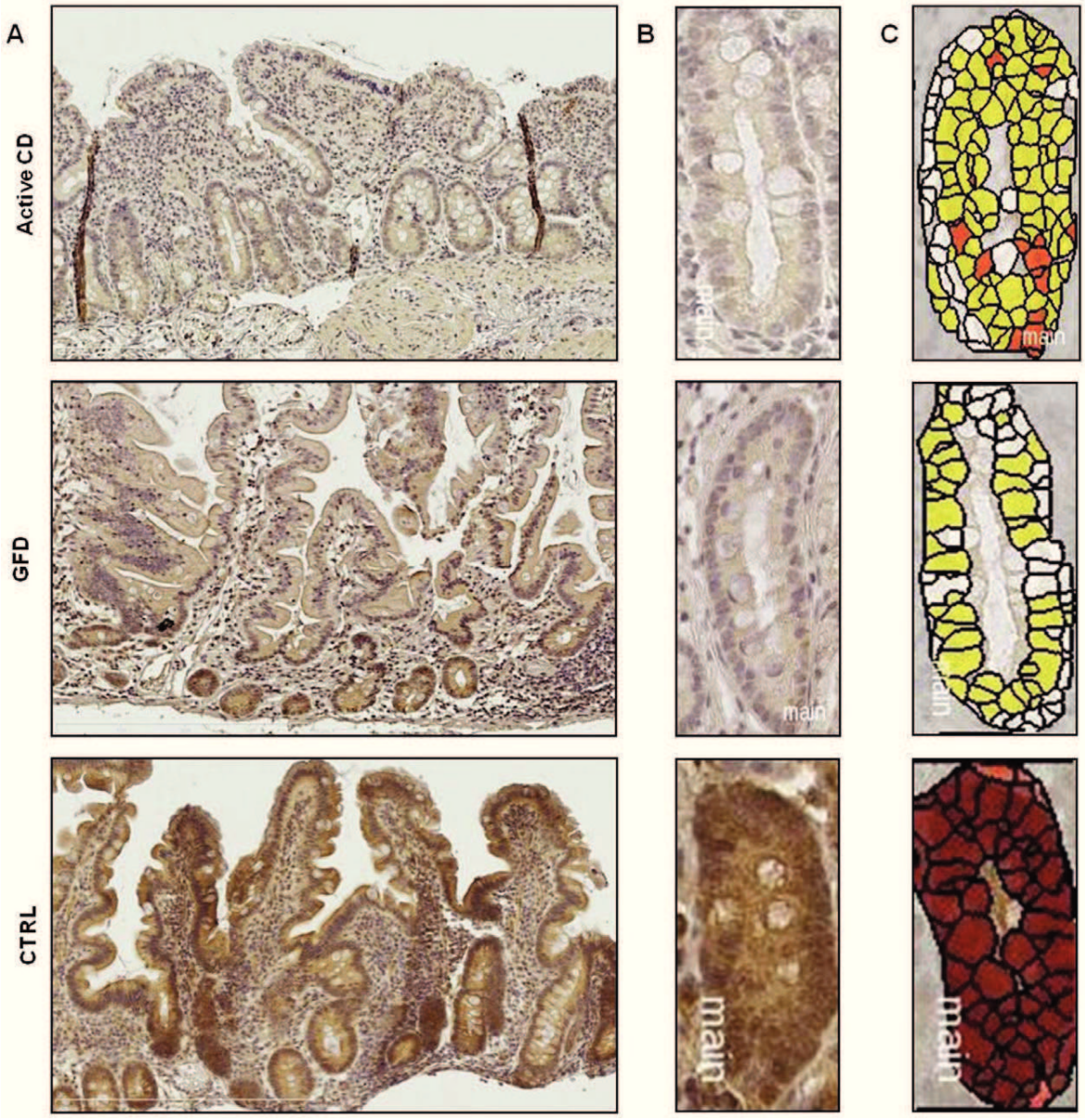


**Figure 3. Decreased expression of HES1 in small intestine of CD patients compared with controls.** An example of HES1 immunohistochemistry in small intestine. **A.** Low magnification picture of the examined intestinal sections (Original magnification 10×). **B.** Intestinal crypts (Original magnification 40×). Note the homogeneous distribution of HES1 in crypts and along the villi in control sample, whereas the signals were prevalently detected in the crypts of active CD and GFD samples. Higher levels of HES1 were detected in the intestinal crypts of controls than in crypts of active and GFD CD samples. **C.** Images converted for automated analysis (white: unstained cells, yellow/orange: low/moderately stained cells, brown: intensely stained cells). These results indicate that HES1 is less expressed in the small intestine of active and GFD CD samples compared with controls. (CTRL: controls; GFD: gluten free diet; CD: celiac disease).
doi:10.1371/journal.pone.0029094.g003

intestine from CD patients [40]. Based on these experimental data, we suggest that the mucus layer in our CD children could be altered so deranging the protective function of the mucosal barrier that interfaces with the environment. In our study, the observed small intestine alterations are not related to inflammation; in fact, they occurred in both the active CD and GFD patients. The major criticism in our work is the gap between the results of the miRNA array with NOTCH1 gene in *a vivo* system, however the lack of a celiac animal model at moment, prevent us from this further validation of our data. Nevertheless, our first description of miRNA pattern in celiac disease and of the correlation of miRNA 449a over expression with NOTCH pathway could pave the way for further research in this field. However, our choice to study Notch pathway doesn't exclude that other relevant biological pathways in addition to it could be miRNA-deregulated in the celiac intestine. Further deeper investigation are necessary to test this hypothesis.

In conclusion we first demonstrate a miRNA mediated gene regulation in small intestine of CD patients. We also highlighted a reduced NOTCH1 pathway in our patients, irrespective of whether

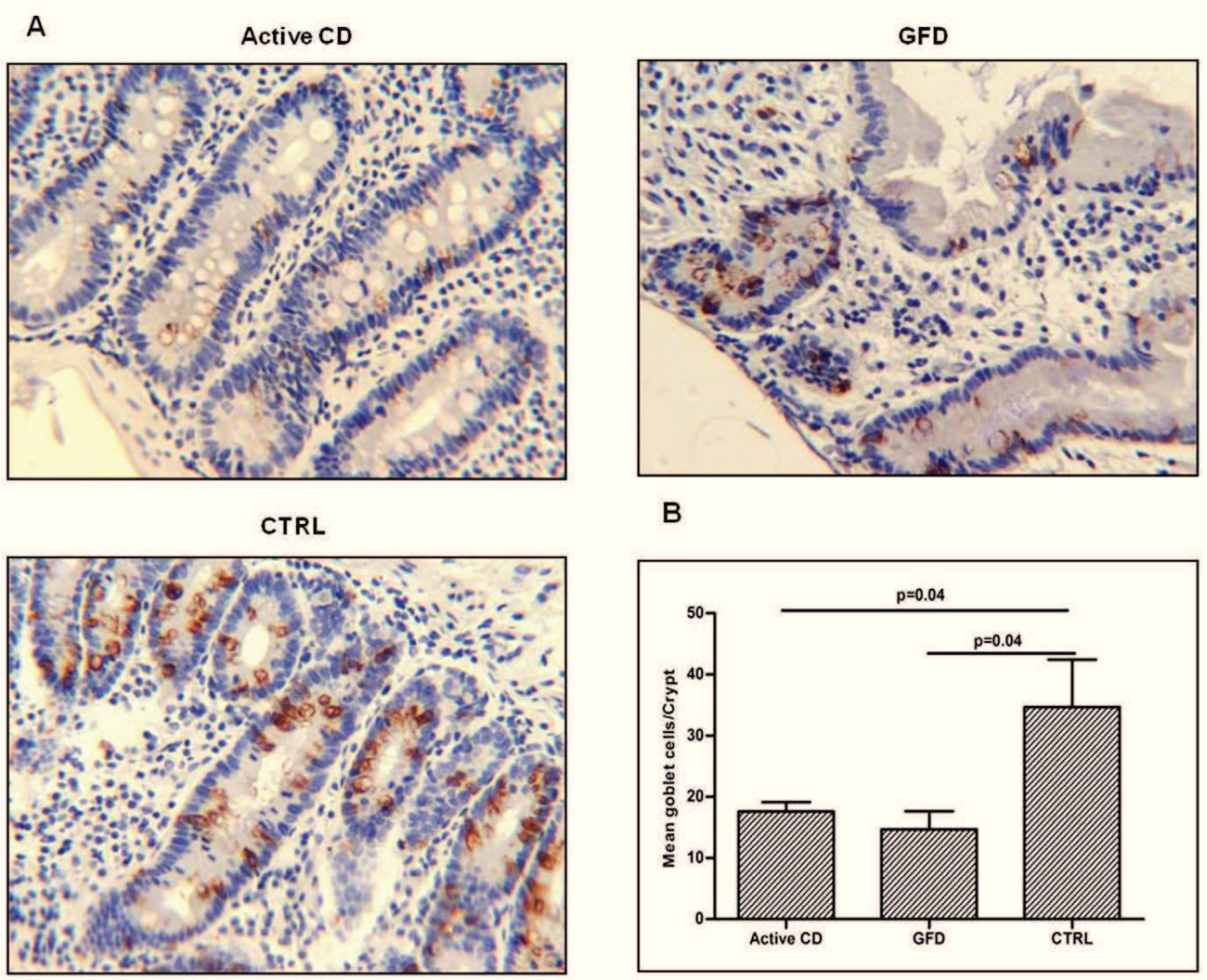


**Figure 4. Decreased expression of MUC2 in small intestine of CD patients compared with controls.** Immunohistochemistry of goblet cells in small intestine. **A.** An example of staining for MUC-2 shows fewer MUC-2 stained cells in active and in GFD CD samples than in controls. (Original magnification 20×). **B.** MUC2 stained cells evaluated in CD patients (6 active CD and 6 GFD patients) and in controls (n = 4). Data are expressed as mean of the number of goblet cells/crypt measured in 10 crypts/children. Significantly fewer stained cells were detected in active and GFD CD samples than in controls (p = 0.04). These results indicate that MUC2 is less expressed in small intestine of active and GFD CD patients compared with controls. (CTRL: controls; GFD: gluten free diet; CD: celiac disease).
doi:10.1371/journal.pone.0029094.g004

the disease was active or not. We suggest that NOTCH pathway could be constitutively altered in the celiac small intestine and could drive the increased proliferation and the decreased differentiation of intestinal cells towards the secretory goblet cell lineage.

## Materials and Methods

### Ethics approval

The study was conducted according to the Helsinki II declaration and it was approved by the Ethics Committee of the School of Medicine Federico II, Naples, Italy.

Written informed consent was obtained from the parent/guardian of all children involved in our study before their enrollment.

### Patients and controls

Forty-four children were recruited, in a two months period, among patients attending the Department of Paediatrics of the University of Naples Federico II where the European Laboratory for the Investigation of Food-Induced Diseases (ELFID) is also present. In our center about 40 biopsies are monthly performed and about 50% of them are usually indicative of CD. Twenty/44 children were diagnosed celiacs according to the criteria established by the European Society for Paediatric Gastroenterology, Hepatology and Nutrition (ESPGHAN) [41]; the CD was excluded based on both absence of CD antibodies and slight or no abnormalities in the mucosal architecture in 15/44 children. In four of these latter children (4/15) the final diagnoses were IgA deficiency (2 cases), De George syndrome (1 case) and autoimmune thyroiditis (1 case), these subjects were excluded from the study to avoid potentially confounding diseases. In the other 11/15 CD-negative children the final diagnoses were: *Helicobacter pylori* infection, recurrent vomiting, food refusal or reflux esophagitis, they were our enrolled controls. Nine out 44 children were CD patients on gluten free diet for at least 2 years undergoing CD

follow-up in the same study period of the active CD patients and controls. There was no statistically significant difference in mean age at diagnosis among the groups evaluated (4.3±1.3 years old in active CD subjects, 7.6±2.5 in GFD subjects, and 6.1±1.0 in controls [mean±SEM]). About 50% of each group was girls. From all participants, we collected a fasting serum sample, a blood sample with EDTA, and a small intestine biopsy sample.

## Biochemical parameters

Anti-Endomysium IgA were detected by indirect immunofluorescence on rhesus monkey esophagus substrate (Eurospital, Trieste, Italy); tTG IgA, anti-gliadin (AGA) IgA/IgG were analyzed by ELISA with human recombinant tTG as antigen (DIA Medix Corp., Miami, FL, USA).

## Histopathological analysis

Architectural abnormalities were classified according to the modified Marsh classification: normal mucosa (T0), intraepithelial lymphocytosis (TI), intraepithelial lymphocytosis and crypt hyperplasia (TII), intraepithelial lymphocytosis, crypt hyperplasia and villous atrophy (partial TIIIA, subtotal TIIIB, total TIIIC) [42].

## DNA and RNA extraction

Genomic DNA was extracted using the Nucleon BACC 2 kit (Amersham Biosciences Europe, Milan, Italy). Total RNA, including miRNAs, was extracted from small intestinal biopsy samples using the Mirvana extraction kit (Applied Biosystems, Foster City, CA, USA).

## HLA typing

DQ2/DQ8 HLA CD-associated molecules were identified by using primers and the PCR conditions of a commercial kit (BAG Health care GmbH, Lich, Germany), which allows to identify the HLA-alleles coding DQ2/DQ8 molecules.

## MiRNAs evaluation

TaqMan low density arrays (TLDA), micro fluidic cards were used to detect and quantify mature miRNAs (Applied Biosystems' 7900HT) according to manufacturer's instructions (see Materials and Methods S1 for details). We considered differently expressed in CD vs controls, the miRNAs whose mean RQ levels were $\leq 0.5$ (down-regulated) or $\geq 2.0$ (up-regulated).

## Bioinformatic approach

The prediction of putative target genes of miRNAs was determined using miRecords (http://mirecords.biolead.org/), which is an integration of 11 established miRNA target prediction programs. The lists of target genes that were predicted by two or more programs were then combined and analyzed using the Gene Ontology Tree Machine (GOTM) (http://bioinfo.vanderbilt.edu/gotm/) and KEGG database (http://www.genome.ad.jp/kegg/). Finally, we identified the biological pathways that contained at least two up- or down-regulated genes with a statistically significant probability ($p<0.01$).

## Quantitative real-time polymerase chain reaction (qRT-PCR) of miRNAs and mRNAs

The levels of a group of deregulated miRNAs (up-regulated miR-449a, down-regulated miR-124a, and similar to controls expressed miR-564) were also evaluated with TaqMan miRNA assays (Applied Biosystems) to validate the array results.

mRNA expression levels of neurogenic locus notch homolog protein 1 (NOTCH1) and of hairy and enhancer of split 1 (HES1) were measured in small intestinal tissues by qRT-PCR using single TaqMan mRNA assays (Applied Biosystems) according to the manufacturer's instructions and using the housekeeping gene beta-actin as control. Reverse transcription reactions were performed with the High Capacity cDNA Reverse Transcription Kit (Applied Biosystems). The expression levels of miRNAs and mRNAs were quantified using the ABI Prism 7900HT Sequence Detection System 2.3 software.

## Transfection and inhibition experiments

The oligonucleotides, plasmids (pGL3-control, pRL-NOTCH1-encoding, pRL-KLF4-encoding and mutated pR-KLF4-encoding, firefly luciferase and Renilla luciferase, respectively) and human embryonic kidney cell lines (HEK293 cell line, ATCC number CRL-1573, supplied by the Centre for Applied Microbiology and Research, Salisbury, Wiltshire, UK) used for cell transfection experiments are described in detail in the online Materials and Methods S1.

Forty-eight hours after transfection, we measured firefly and *Renilla* luciferase activities using a dual luciferase assay according to the manufacturer's instructions (Promega, Naples, Italy).

## Protein evaluation by immunohistochemistry

Given the small amount of sample available for each patient (1–2 mg of intestinal tissue/patient) we tested the expression of selected proteins by immunohistochemistry instead of by western blotting. The NOTCH1, HES1, MUC-2, KLF4, Ki67 and beta-catenin proteins were identified on formalin-fixed paraffin-embedded small intestinal tissue blocks in CD patients and in controls. We randomly selected six active CD, six GFD and four controls (see Materials and Methods S1 for details). We also tested the specificity of our NOTCH1 and HES1 signals evaluating two different human tissue samples where it is known NOTCH1 and HES1 be present or absent respectively, that are colon cancer and endothelial wall (Figure S8).

## Scanning and automated image analysis of NOTCH1 and HES1

To increase precision, we automated the quantification of the immunohistochemical signals. Sections of the small intestine were scanned with the NanoZoomer 2.0 system (Hamamatsu, Japan), equipped with a 20×, 0.7 Numerical Aperture Plan-Apochromat lens, using a lens of 0.23 mm pixel size. The compressed jpeg files were transferred to the Definiens Analyst LS5.0 system (Definiens AG, Germany) that counted the NOTCH1, HES1 and beta-catenin -positive and -negative cells and quantified the staining signal (see materials and methods S1 for Definiens Analyst software details). The Definiens Analyst software (Definiens AG, Germany) is based on cognition network technology that is a semantic network of objects and their mutual relationships. Two rule sets, using cognition network language, were specifically written for this evaluation to automatically detect and measure the small intestinal area and to count positive and negative crypt cells. The signal was classified as intensely stained, low/moderate stained and unstained. Thus, both the percentage and intensity of labeled cells were taken into account. The detection and exclusion of areas not belonging to crypt were visually checked for all image files. Ten crypts/patient were counted.

## Immunohistochemical analysis of MUC-2, KLF4 and beta-catenin

Because the MUC-2 staining of goblet cells was patchy, we picked ten crypts from each slide and manually counted the

number of goblet cells stained in each crypt. We also evaluated MUC-2 staining of villi, when possible, i.e., in GFD patients and controls. We also evaluated KLF4-positive villi (in GFD patients) and both beta-catenin- and Ki67-positive nuclei/crypt in each subject. Two independent observers evaluated the immunohistochemical slides.

### Statistics

All variables were expressed as mean±standard error of the mean (SEM). Student t's test and ANOVA were used to compare group means and p values<0.05 were considered significant. Statistically significant ($p<0.01$) miRNA-regulated pathways were selected by the GOTM program.

## Supporting Information

**Materials and Methods S1**
(DOC)

**Figure S1 Bioinformatics analysis of miR-449a putative target genes.** miR-449a putative target genes with most favorable context score, selected by bioinformatics, were sorted into pathways using GOTM(http://bioinfo.vanderbilt.edu/webgestalt/) and then combined into functional groups. (http://mirecords.biolead.org/interactions.php?species=Homo+sapiens&mirna_acc=hsa-miR-449a&targetgene_type=refseq_acc&targetgene_info=&v=yes&search_int=Search) (http://www.targetscan.org/cgibin/targetscan/vert_50/targetscan.cgi?species=Human&gid=&mir_sc=&mir_c=&mir_nc=&mirg=hsa-miR-449a). In each functional group are reported the genes belonging to NOTCH pathway/total gene number.
(TIF)

**Figure S2 The luciferase assay confirms that miR-449a inhibits the expression of NOTCH1 and KLF4.** In HEK293 cells co-transfected or with pRL-NOTCH1 vector (panel A) or with pRL-KLF4 vector (panel B), a pre-miR-449a concentration of 100 nmol/L was sufficient to significantly reduce (respectively, $p = 0.001$ and $p = 0.002$) *Renilla* luciferase activity versus control values. No inhibition of the *Renilla* luciferase expression was observed in mutant 3′UTR of KLF4-mRNA with miR-449a, so confirming the miR-449a/3′UTR KLF4-mRNA direct interaction (panel B). We didn't verify the interaction miR-449a/3′UTR NOTCH1 being this latter recently validated by Marcet B et al [32].
(TIF)

**Figure S3 Automated Counts of NOTCH1 and HES1 stained/unstained cells. A.** Automated counts of NOTCH1 stained/unstained cells (reported in Figure 2) in small intestine from CD patients (6 active CD and 6 GFD patients) and from controls ($n = 4$). Data are expressed as mean percent of intensely stained, low-moderately stained and unstained cells of the total intraepithelial cells (IECs) counted in ten crypts. The numbers of intensely stained and unstained cells were significantly ($p = 0.02$) higher and lower, respectively, in CTRL than in active CD and in GFD patients. **B.** Automated counts of HES1 stained/unstained cells (reported in Figure 3) in small intestine from CD patients (6 active CD and 6 GFD patients) and from controls ($n = 4$). Data are expressed as mean percent of intensely stained, low-moderately stained and unstained cells of the total intraepithelial cells (IECs) counted in ten crypts. The number of intensely stained cells was significantly higher in controls versus CD and GFD patients ($p = 0.02$) and the number of unstained cells was significantly lower in CTRL than in active CD patients ($p = 0.03$). (CTRL: controls; GFD: gluten free diet; CD: celiac disease).
(TIF)

**Figure S4 Other examples of NOTCH1 immunohistochemistry in CD patients.** Examples of NOTCH1 immunohistochemistry in 4 CD patients (2 active CD: TIII Marsh stage and 2 GFD: TI and T0 Marsh stage) and 2 controls (T0 Marsh stage). The images show that the low expression levels of NOTCH1 in intestinal mucosa from CD patients were always present from TIII to T0 Marsh stage. (CTRL: controls; GFD: gluten free diet; CD: celiac disease).
(TIF)

**Figure S5 Other examples of HES1 immunohistochemistry in CD patients.** Examples of HES1 immunohistochemistry in 4 CD patients (2 active CD: TIII Marsh stage and 2 GFD: TI and T0 Marsh stage) and 2 controls (T0 Marsh stage). The images show that the low expression levels of HES1 in intestinal mucosa from CD patients were always present from TIII to T0 Marsh stage. (CTRL: controls; GFD: gluten free diet; CD: celiac disease).
(TIF)

**Figure S6 Decreased KLF4 and increased Ki67 expression in small intestine from CD patients compared with controls. A.** KLF4 staining of small intestinal villi in GFD patients and Controls (Original magnification 20×). A statistically significant reduced KLF4-positive cells/villi were counted in GFD patients than in controls, respectively 29.0±5.0 vs 79.0±3.0 (mean±SEM) ($p<0.0001$). **B.** Increased Ki67 signal is present in small intestinal crypts of active CD, GFD patients than in controls (Original magnification 20×). (CTRL: controls; GFD: gluten free diet; CD: celiac disease).
(TIF)

**Figure S7 Increased expression of beta-catenin in small intestine from CD patients compared with controls.** Immunostaining with beta-catenin in small intestinal crypts from active CD, GFD and controls. We counted the beta-catenin labeled nuclei. Similar counts of beta-catenin labelled nuclei were detected in the crypts of the small intestine in all groups. However, higher even if not statistical significant mean percentage counts (beta-catenin positive nuclei/crypt) were obtained in active CD and GFD than in controls, respectively 57.0±11.5 and 37.0±4.6 vs 27.0±4.6 (Original magnification 63×). (CTRL: controls; GFD: gluten free diet; CD: celiac disease).
(TIF)

**Figure S8 Specificity of NOTCH1 and HES1 signals by immunohistochemistry.** Specificity controls of NOTCH1 and HES1 antibodies. Positive NOTCH1 (**A**) and HES1 (**B**) immunostaining signals obtained in human colon cancer and negative NOTCH1 (**C**) and HES1 (**D**) immunostaining signals obtained in human endothelial wall.
(TIF)

**Table S1 MiRNAs differently expressed in active and GFD CD patients.**
(DOC)

## Acknowledgments

Jean Ann Gilder (Scientific Communication srl) provided writing assistance.

Provenance and peer review not commissioned; externally peer reviewed.

This paper is dedicated to Prof. Salvatore Auricchio. He has promoted research in celiac disease in Naples for 40 years and kindly read and commented on this study. We are grateful to M. V. Barone for helpful discussion and to Carolina Tarantino for skilled technical assistance.

## Author Contributions

Conceived and designed the experiments: LS. Performed the experiments: MC LI NT LS. Analyzed the data: LS MC LI NT VC GT DM. Contributed reagents/materials/analysis tools: LG VI FT DM. Wrote the paper: LS MC LI.

## References


1. Nisticò L, Fagnani C, Coto I, Percopo S, Cotichini R, et al. (2006) Concordance, disease progression, and heritability of coeliac disease in Italian twins. Gut 55: 803–808.
2. Greco L, Romino R, Coto I, Di Cosmo N, Percopo S, et al. (2002) The first large population based twin study of coeliac disease. Gut 50: 624–628.
3. Schuppan D, Junker Y, Barisani D (2009) Celiac disease: from pathogenesis to novel therapies. Gastroenterology 137: 1912–1933.
4. Hunt KA, van Hell DA (2009) Recent advances in celiac disease genetics. Gut 58: 473–476.
5. Sacchetti L, Calcagno G, Ferrajolo A, Sarrantonio C, Troncone R, et al. (1998) Discrimination between celiac and other gastrointestinal disorders in childhood by rapid human lymphocyte antigen typing. Clin Chem 44: 1755–1757.
6. Van Heel DA, Franke L, Hunt KA, Gwilliam R, Zhernakova A, et al. (2007) A genome-wide association study for celiac disease identifies risk variants in the region harboring IL2 and IL21. Nat Genet 39: 827–829.
7. Juuti-Uusitalo K, Mäki M, Kainulainen H, Isola J, Kaukinen K (2007) Gluten affects epithelial differentiation-associated genes in small intestinal mucosa of coeliac patients. Clin Exp Immunol 150: 294–305.
8. Diosdado B, Wapenaar MC, Franke L, Duran KJ, Goerres MJ, et al. (2004) A microarray screen for novel candidate genes in coeliac disease pathogenesis. Gut 53: 944–951.
9. Inui M, Martello G, Piccolo S (2010) MicroRNA control of signal transduction. Nature review 11: 252–263.
10. Lee RC, Feinbaum RL, Ambros V (1993) The C. elegans heterochronic gene lin-4 encodes small RNAs with antisense complementarity to lin-14. Cell 75: 843–854.
11. Pauley KM, Chan EKL (2008) MicroRNAs and their emerging roles in immunology. Ann NY Acad Sci 1143: 226–239.
12. Pauley KM, Cha S, Chan EKL (2009) MicroRNA in autoimmunity and autoimmune diseases. J Autoimmun 32: 189–194.
13. Neilson JR, Zheng GXY, Burge CB, Sharp PA (2007) Dynamic regulation of miRNA expression in ordered stages of cellular development. Genes Dev 21: 578–589.
14. Wu H, Neilson JR, Kumar P, Manocha M, Shankar P, et al. (2007) miRNA profiling of naïve, effector and memory CD8 T cells. PLoS One 10;2(10): e1020.
15. Zhou B, Wang S, Mayr C, Bartel DP, Lodish HF (2007) miR-150, a microRNA expressed in mature B and T cells, blocks early B cell development when expressed prematurely. Proc Natl Acad Sci U S A 104: 7080–7085.
16. McKenna LB, Schug J, Vourekas A, McKenna JB, Bramswig NC, et al. (2010) MicroRNAs control intestinal epithelial differentiation, architecture, and barrier function. Gastroenterology 139: 1654–1664.
17. Iborra M, Bernuzzi F, Invernizzi P, Danese S (2010) MicroRNAs in autoimmunity and inflammatory bowel disease: Crucial regulators in immune response. Autoimmun Rev;doi:10.1016/j.autrev.2010.07.002.
18. Fre S, Pallavi SK, Huyghe M, Laé M, Janssen KP, et al. (2009) Notch and Wnt signals cooperatively control cell proliferation and tumorigenesis in the intestine. Proc Natl Acad Sci 106: 6309–6314.
19. Lizé M, Pilarski S, Dobbelstein M (2010) E2F1-inducible microRNA 449a/b suppresses cell proliferation and promotes apoptosis. Cell Death Differ 17: 452–458.
20. Noonan EJ, Place RF, Pookot D, Basak S, Whitson JM, et al. (2009) miR-449a targets HDAC-1 and induces growth arrest in prostate cancer. Oncogene 28: 1714–1724.
21. McConnell BB, Ghaleb AM, Nandan MO, Yang VW (2007) The diverse functions of Krüppel-like factors 4 and 5 in epithelial biology and pathobiology. Bioessays 29: 549–557.
22. Clevers H (2006) Wnt/beta-catenin signaling in development and disease. Cell 127(3): 469–480.
23. Fre S, Huyghe M, Mourikis P, Robine S, Louvard D, et al. (2005) Notch signals control the fate of immature progenitor cells in the intestine. Nature 435(7044): 964–968.
24. Oshima S, Nakamura T, Namiki S, Okada E, Tsuchiya K, et al. (2004) Interferon regulatory factor 1 (IRF-1) and IRF-2 distinctively up-regulate gene expression and production of interleukin-7 in human intestinal epithelial cells. Mol Cell Biol 24(14): 6298–6310.
25. Crosnier C, Stamataki D, Lewis J (2006) Organizing cell renewal in the intestine: stem cells, signals and combinatorial control. Nat Rev Genet 7(5): 349–359.
26. Okamoto R, Tsuchiya K, Nemoto Y, Akiyama J, Nakamura T, et al. (2009) Requirement of Notch activation during regeneration of the intestinal epithelia. Am J Physiol Gastrointest Liver Physiol 296(1): G23–G35.
27. Ghaleb AM, McConnell BB, Kaestner KH, Yang VW (2011) Altered intestinal epithelial homeostasis in mice with intestine-specific deletion of the Krüppel-like factor 4 gene. Developmental Biology 349: 310–320.
28. Zheng H, Pritchard DM, Yang X, Bennett E, Liu G, et al. (2009) KLF4 gene expression is inhibited by the notch signaling pathway that controls goblet cell differentiation in mouse gastrointestinal tract. Am J Physiol Gastrointest Liver Physiol 296(3): G490–G498.
29. Katz JP, Perreault N, Goldstein BG, Lee CS, Labosky PA, et al. (2002) The zinc-finger transcription factor Klf4 is required for terminal differentiation of goblet cells in the colon. Development 129: 2619–2628.
30. Kopan R, Ilagan MXG (2009) The canonical Notch signaling pathway: unfolding the activation mechanism. Cell 137: 216–233.
31. Yin L, Velazquez OC, Liu ZJ (2010) Notch signaling: emerging molecular targets for cancer therapy. Biochem Pharmacol 80: 690–701.
32. Marcet B, Chevalier B, Luxardi G, Curaux C, Zaragosi LE, et al. (2011) Control of vertebrate multiciliogenesis by miR-449 through direct repression of the Delta/Notch pathway. Nat Cell Biol 6: 693–699.
33. Ciacci C, Di Vizio D, Seth R, Insabato G, Mazzacca G, et al. (2002) Selective reduction of intestinal trefoil factor in untreated coeliac disease. Clin Exp Immunol 130: 526–531.
34. Ciccocioppo R, Finamore A, Ara C, Di Sabatino A, Mengheri E, et al. (2006) Altered Expression, Localization, and Phosphorylation of Epithelial Junctional Proteins in Celiac Disease. Am J Clin Pathol 125: 502–511.
35. Ghaleb AM, Aggarwal G, Bialkowska AB, Nandan MO, Yang VW, et al. (2008) Notch inhibits expression of the Krüppel-like factor 4 tumor suppressor in the intestinal epithelium. Mol Cancer Res 6(12): 1920–1927.
36. McAuley JL, Linden SK, Png CW, King RM, Pennington HL, et al. (2007) MUC1 cell surface mucin is a critical element of the mucosal barrier to infection. J Clin Invest 2007;117: 2313–2324.
37. Corfield AP, Myerscough N, Longman R, Sylvester P, Arul S, et al. (2000) Mucins and mucosal protection in the gastrointestinal tract: new prospects for mucins in the pathology of gastrointestinal disease. Gut 2000;47: 589–594.
38. Festen EA, Szperl AM, Weersma RK, Wijmenga C, Wapenaar MC, et al. (2009) Inflammatory bowel disease and celiac disease: overlaps in the pathology and genetics, and their potential drug targets. Endocr Metab Immune Disord Drug Targets 9: 199–218.
39. Van der Sluis M, De Koning BA, De Bruijn AC, Velcich A, Meijerink JP, et al. (2006) Muc2-deficient mice spontaneously develop colitis, indicating that MUC2 is critical for colonic protection. Gastroenterology 131: 117–129.
40. Forsberg G, Fahlgren A, Hörstedt P, Hammarström S, Hernell O, et al. (2004) Presence of bacteria and innate immunity of intestinal epithelium in childhood celiac disease. Am J Gastroenterol 99(5): 894–890.
41. Report of Working Group of European Society of Paediatric Gastroenterology and Nutrition (1990) Revised criteria for diagnosis of coeliac disease. Arch disease child 65: 909–911.
42. Marsh MN, Crowe PT (1995) Morphology of the mucosal lesion in gluten sensitivity. Baillieres Clin Gastroenterol 9(2): 273–293.

Journal of proteome research

Article

pubs.acs.org/jpr

# miRNA and Protein Expression Profiles of Visceral Adipose Tissue Reveal miR-141/YWHAG and miR-520e/RAB11A as Two Potential miRNA/Protein Target Pairs Associated with Severe Obesity

Valentina Capobianco,[†] Carmela Nardelli,[‡,§] Maddalena Ferrigno,[§] Laura Iaffaldano,[‡,§] Vincenzo Pilone,[∥] Pietro Forestieri,[∥] Nicola Zambrano,[‡,§] and Lucia Sacchetti*[,‡,§]

[†]Fondazione IRCCS SDN, Istituto di Ricerca Diagnostica e Nucleare, Via Gianturco 113, 80143 Naples, Italy

[‡]Dipartimento di Biochimica e Biotecnologie Mediche, Università degli Studi di Napoli Federico II, Via Pansini 5, 80131 Naples, Italy

[§]CEINGE Biotecnologie Avanzate S.C. a R.L., Via Gaetano Salvatore 486, 80145, Naples, Italy

[∥]Dipartimento di Chirurgia Generale, Geriatrica, Oncologica e Tecnologie Avanzate, Università degli Studi di Napoli Federico II, Via Pansini 5, 80131 Naples, Italy

Supporting Information

**ABSTRACT:** Adipose tissues show selective gene expression patterns, to whom microRNAs (miRNAs) may contribute. We evaluated in visceral adipose tissue (VAT) from obese and nonobese females, both miRNA and protein expression profiles, to identify miRNA/protein target pairs associated with obesity (metabolic pathways miRNA-deregulated during obesity). Obese and nonobese females [BMI 42.2 ± 1.6 and 23.7 ± 1.2 kg/m$^2$ (mean ± SEM), respectively] were enrolled in this study. Notably, most miRNAs were down-expressed in obese tissues, whereas most of the proteins from the investigated spots were up-expressed. Bioinformatics integration of miRNA expression and proteomic data highlighted two potential miRNA/protein target pairs: miR-141/YWHAG (tyrosine 3-monooxygenase/tryptophan 5-monooxygenase activation protein, gamma polypeptide) and miR-520e/RAB11A (Ras-related protein RAB-11A); the functional interaction between these miRNAs and their target sequences on the corresponding mRNAs was confirmed by luciferase assays. Both RAB11A and YWHAG proteins are involved in glucose homeostasis; YWHAG is also involved in lipid metabolism. Hence, the identified miRNA/protein target pairs are potential players in the obese phenotype.

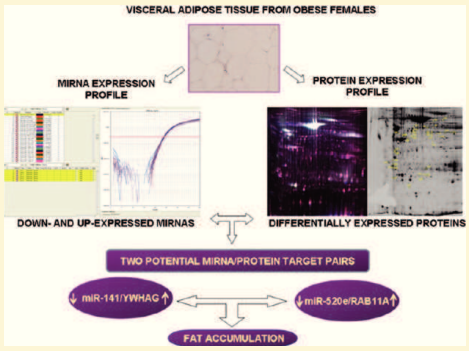


**KEYWORDS:** *obesity, visceral adipose tissue, miRNAs, 2D-DIGE*

## INTRODUCTION

Obesity is an epidemic health problem worldwide that causes morbidity and mortality associated with increased risk of cardiovascular disease, metabolic syndrome, and cancer.[1,2] In particular, central obesity, i.e., fat accumulated in visceral adipose tissue (VAT), is the major risk factor for obesity-related disorders.[3,4] VAT represents up to 10−20% of total fat in men and 5−8% in females. It is anatomically present in the mesentery and omentum, and it drains directly to the liver through the portal vein. This characteristic allows the direct access of the free fatty acids and of adipokines released from fat to the liver.[4] In addition, adipose tissues show selective gene expression patterns,[2,3,5,6] to whom microRNAs (miRNAs) may contribute.[7] miRNAs are small noncoding RNAs ∼21 nucleotides long that bind specific regions of mRNA targets to mediate their cleavage or translational repression, and they regulate about 50% of human genes.[8] In mammals, miRNAs have been also shown to modulate adipocyte differentiation.[9] Previous work from our laboratory showed that up-expression of miR-519d in subcutaneous adipose tissue (SAT) from obese patients was associated with down-expression of the PPARA protein.[10] There are biological differences between VAT and SAT. In fact, compared with SAT, VAT contains more large and insulin-resistant adipocytes and inflammatory cells such as macrophages that secrete pro-inflammatory cytokines (TNF-$\alpha$, IL-6, and CRP).[4]

In the present study, we evaluated miRNA and protein signatures using transcriptomic and proteomic approaches, respectively, in VAT from the women studied previously. Our aim was to investigate for metabolic pathways miRNA-regulated in VAT that could be altered during obesity. Our results indeed show that VAT from obese females is characterized by peculiar miRNA and protein expression signatures. Most of the tested miRNAs are down-expressed in VAT from obese females. Accordingly, most of proteins in VAT from the obese group showed increased levels by proteomic profile. Finally, the functional association of the transcriptomic and proteomic profiles revealed two potential miRNA/protein

**Received:** February 15, 2012
**Published:** April 27, 2012





dx.doi.org/10.1021/pr300152z | J. Proteome Res. 2012, 11, 3358−3369

target pairs in VAT, namely, miR-141/YWHAG (tyrosine 3-monooxygenase/tryptophan 5-monooxygenase activation protein, gamma polypeptide) and miR-520e/RAB11A (Ras-related protein RAB-11A), which may contribute to altered gene expression in obesity.

## EXPERIMENTAL SECTION

### Subjects and Experimental Design

Fifteen obese females (age range: 19−65 years, BMI [mean ± SEM] 42.2 ± 1.6 kg/m$^2$) and 10 nonobese females (age range: 19−57 years, BMI [mean ± SEM] 23.7 ± 1.2 kg/m$^2$) were enrolled in the study. During surgery (gastric banding or laparoscopic cholecystectomy for obese and nonobese females, respectively), a bioptic sample of VAT was collected and frozen in liquid nitrogen. The main anamnestic, clinical, and general characteristics of the enrolled subjects were recorded at admission. The day before surgery, a fasted blood sample was collected from all subjects and tested for the main biochemical parameters (glucose, cholesterol, triglycerides, AST, ALT, ALP, GGT) by routine methods (Table 1). Written informed consent was obtained from all recruited subjects, and the study was approved by the Ethics Committee of our Faculty of Medicine.

**Table 1. General Characteristics of the Obese ($n$ = 15) and Nonobese ($n$ = 10) Females Enrolled in the Study[a]**

| | females | |
|---|---|---|
| | obese | nonobese |
| subjects ($n$) | 15 | 10 |
| age (years) | 41.6 (4.4) | 38.0 (3.5) |
| weight (kg)†[b] | 115.2 (6.3) | 62.5 (2.6) |
| height (m) | 1.7 (0.04) | 1.6 (0.01) |
| BMI (kg/m$^2$)‡[b] | 42.2 (1.6) | 23.7 (1.2) |
| systolic blood pressure (mmHg) | 133.6 (6.7) | 115 (4.5) |
| diastolic blood pressure (mmHg)[c] | 80.0 (80.0−90.0) | 80.0 (70.0−80.0) |
| cardiac frequency[d] | 80.0 (2.2) | 67.6 (3.7) |
| glucose (mmol/L)[e] | 4.9 (0.2) | 4.3 (0.2) |
| cholesterol (mmol/L) | 5.9 (0.5) | 5.8 (0.6) |
| triglycerides (mmol/L) | 1.4 (0.1) | 0.9 (0.1) |
| AST (U/L)[c] | 18.5 (16.0−21.0) | 18.0 (13.5−19.0) |
| ALT (U/L)[c] | 17.0 (13.0−28.5) | 14.0 (12.0−21.0) |
| ALP (U/L) | 79.3 (5.8) | 89.2 (19.3) |
| GGT (U/L) | 28.5 (4.7) | 17.3 (3.5) |

[a]Data are expressed as mean (SEM) value (unless specified otherwise) and interquartile range (nonparametric distributions). [b]Statistically significant differences (designated by † and ‡) at Student's $t$ test $p < 0.0001$. [c]Data are expressed as median value. [d]$p = 0.01$. [e]$p = 0.03$.

### RNA Isolation

Total RNA (including miRNAs) was isolated from the VAT of all subjects using the mirVana miRNA isolation kit (Ambion, Austin, TX, USA) according to the manufacturer's instructions. RNA concentration was evaluated using the NanoDrop ND-1000 UV−vis spectrophotometer (NanoDrop Technologies, Wilmington, DE, USA).

The total RNA isolated from nonobese females was pooled to serve as control in the comparison of the miRNA expression profiles of the obese females.

### miRNA Expression Profile

We used the commercially available TaqMan Array Human MicroRNA Panel v1.0 (Applied Biosystems Inc., Foster City, CA, USA) to measure miRNA expression profile in 10/15 obese and 4/10 nonobese females. The panel contains 365 different human miRNA assays in addition to two small nucleolar RNAs (snoRNAs) that function as endogenous controls for data normalization. We used 80 ng of total RNA for reverse transcription. RT-PCR was performed using the 7900 HT real-time PCR system (Applied Biosystems). The miRNA expression values were normalized to RNU48 (endogenous control), and relative expression values were obtained using the ΔΔCT method (relative quantification, RQ = $2^{-\Delta\Delta CT}$) with sequence detection system (SDS) v2.3 and RQ Manager 1.2 software (Applied Biosystems). To further normalize our miRNA data and to minimize interindividual variability, we considered differently expressed the miRNAs whose mean RQ levels were <0.5 (down-expressed) or >2.0 (up-expressed) in at least 6/10 obese females.

### Quantitative Real-Time Polymerase Chain Reaction (qRT-PCR) of miRNAs and mRNAs

The expression levels of some selected miRNAs (miR-141, miR-200c, miR-520e, and miR-520d) were also validated by TaqMan miRNA assays (Applied Biosystems) in accordance with the manufacturer's instructions on the 7900 HT real-time PCR system (Applied Biosystems). The expression of one of these selected miRNAs, namely, miR-141, was preliminarily tested in each nonobese control, and after ensuring that the expression was comparable among these individuals, we pooled their RNAs to obtain a control against which to compare miRNA levels in obese females.

The expression levels of the selected miRNAs (miR-141, miR-200c, miR-520e, and miR-520d) were first normalized to the endogenous control (RNU48), and then the relative expression values were obtained versus the nonobese control pool using the ΔΔCT method (relative quantification, RQ = $2^{-\Delta\Delta CT}$) with SDS v2.3 and RQ Manager 1.2 software (Applied Biosystems).

Real-time RT-PCR of RAB11A and YWHAG mRNAs was performed using gene- specific primers (**RAB11a**, forward: AACATCAGCATATTATCGTGGA and reverse: GATCACTCTTATTGCCCACA; **YWHAG**, forward: AGACCCAGCCCCGCGAAGAT and reverse: TCTGTCACGTTCTTCATGGCCGC), the Power SYBR Green PCR Master Mix (Applied Biosystems) and the PRISM 7900HT sequence detection system (Applied Biosystems).

### Bioinformatic Analysis

Biological targets of miRNAs differently expressed in obese vs nonobese females were predicted using the TargetScan Release 5.0 algorithm (http://www.targetscan.org). This algorithm assigns a "total context score" for each predicted target. Target genes with a "total context score" < −0.30 were further analyzed using the KEGG database (http://www.genome.ad.jp/kegg/) to identify the pathways that involve the target genes of miRNAs and then using the Gene Ontology (GO) database (http://www.geneontology.org/ontologies) to identify the biological processes in which the proteins identified by DIGE participate. Gene ontology classification of the differentially expressed proteins revealed by 2D-DIGE analysis was performed in the web-accessible DAVID (v 6.7) annotation system (http://david.abcc.ncifcrf.gov/home.jsp).[11,12]


dx.doi.org/10.1021/pr300152z | J. Proteome Res. 2012, 11, 3358−3369

### Preparation of Protein Extracts and Two-Dimensional Fluorescence Difference Gel Electrophoresis (2D-DIGE) Analysis

Protein extracts from VAT samples of 6/15 obese and 3/10 nonobese females were prepared using a lysis buffer containing 2% SDS, 10% glycerol, 6.25 mM Tris-HCl pH 6.8, 0.5 mM EDTA, 20 mM NaF, 1 mM $Na_3VO_4$ (Santa Cruz Biotechnology, Santa Cruz, CA), and the Sigma-Aldrich cocktail of protease inhibitors. The suspensions were shaken in Tissue Lyser II (Qiagen) for 4 min at maximum frequency. After 30 min on ice, samples were centrifuged at 15000*g* for 10 min at 4 °C. The clear interface of each sample was recovered and was transferred to a clean tube. Protein concentrations were determined by the Bradford method using BioRad protein reagent (Bio-Rad Laboratories, Hercules, CA). For 2D-DIGE analysis, proteins extracted from VAT were precipitated for 16 h at −20 °C with 9 volumes of a mix composed of acetone and methanol (9:1) and then centrifuged at 15000*g* for 30 min at 4 °C; protein pellets were solubilized in a buffer, UTC, containing 7 M urea, 2 M thiourea, 4% CHAPS (3-[(3-cholamidopropyl)dimethylammonium]-1-propane sulfonate) in 30 mM Tris-HCl. Protein concentrations were redetermined after precipitation by using BioRad protein reagent. Thirty micrograms of each protein extract were labeled with 240 pmol of Cy3 or Cy5 fluorescent dye on ice, in the dark for 30 min. To exclude preferential binding of a label to a set of proteins, we dye-swapped the samples. The internal standard containing equal amounts of proteins from each sample was labeled with Cy2. The same internal standard was run in all gels to normalize the experiments and to reduce gel-to-gel variations. Labeling reactions were stopped by adding 1 mM lysine. Sample pairs labeled with Cy3 and Cy5 and the internal standard were combined and used to hydrate passively individual strips as follows: each mix of labeled samples was diluted in UTC solution containing 130 mM DTT, 2% IPG Buffer pH 3−10 NL (GE Healthcare, Buckinghamshire, UK), 2.8% DeStreak reagent (GE Healthcare) in a final volume of 400 μL. The mixtures were used to hydrate 24 cm IPG strips pH 3−10NL required for protein separation in the first dimension. Isoelectric focusing (IEF) was run in an IPGphor II apparatus (GE Healthcare) according to this voltage protocol: 300 V for 3 h, linear gradient to 600 V in 3 h, linear gradient to 1000 V in 3 h, linear gradient to 8000 V in 5 h, 8000 V for 6 h. After the first dimension, the strips were equilibrated in equilibration buffer (100 mM Tris-HCl, 6 M urea, 30% (v/v) glycerol, 2% (w/v) SDS, and trace of bromophenol blue, pH 8.0) containing 0.5% (w/v) DTT for 15 min and thereafter in equilibration buffer containing 4.5% (w/v) iodoacetamide for a further 15 min. The equilibrated strips were transferred onto 12% polyacrylamide gels for the second dimension (Ettan Dalt six electrophoresis system, GE Healthcare). The SDS-PAGE electrophoresis was run using a Peltier-cooled DALT II Electrophoresis unit (GE Healthcare) at 30W. After the electrophoresis, the gels were scanned with a Typhoon 9400 variable mode imager (GE Healthcare) at 100 μm resolution, using appropriated individual excitation/emission wavelengths: 488/520 for Cy2, 532/580 for Cy3 and 633/670 for Cy5. The images were captured with Image Quant software and were analyzed with DeCyder software (GE Healthcare). We chose the most representative gel as master gel to compare results obtained from other samples. Globally we analyzed VAT samples from 6 randomly selected obese (mean BMI 38.7) and 3 nonobese females (mean BMI 23.5). We used the Student's *t* test to determine the fold change between obese and nonobese females. Only protein spots with a $p < 0.05$ were investigated further.

### Protein Identification with Liquid Chromatography−Tandem Mass Spectrometry (LC−MS/MS)

We used 250 μg of protein sample for the preparative gel. After 2D-electrophoresis, performed under the conditions reported for the analytical experiment, the gel was stained with SYPRO Ruby ready-to-use formula (BIORAD), and the spot map so obtained was matched with the analytical reference gel. The spots differentially expressed in obese and nonobese females were excised from the preparative gel using the Ettan Spot Picker robotic system (GE Healthcare). The excised spots were analyzed with LC−MS/MS (Functional and Structural Proteomics Facility, CEINGE−Biotecnologie Avanzate, Italy).

The excised spots were washed in 50 mM ammonium bicarbonate pH 8.0 in 50% acetonitrile to a complete destaining. The gel pieces were resuspended in 50 mM ammonium bicarbonate pH 8.0 containing 100 ng of trypsin and incubated for 2 h at 4 °C and overnight at 37 °C. The supernatant containing the resulting peptide mixtures was removed, and the gel pieces were re-extracted with acetonitrile. The two fractions were then collected and freeze-dried. The peptide mixtures were further analyzed by LC−MS/MS using the LC−MSD Trap XCT Ultra apparatus (Agilent Technologies, Palo Alto, CA, USA) equipped with a 1100 HPLC system and a chip cube (Agilent Technologies). After loading, the peptide mixture (8 μL in 0.5% TFA) was first concentrated at 4 μL/min in 40 nL enrichment column (Agilent Technologies chip), with 0.1% formic acid as eluent. The sample was then fractionated on a C18 reverse-phase capillary column (75 μm × 43 mm in the Agilent Technologies chip) at a flow rate of 300 nL/min, with a linear gradient of eluent B (0.1% formic acid in acetonitrile) in eluent A (0.1% formic acid) from 7 to 50% in 35 min. Elution was monitored on the mass spectrometer without a splitting device. Peptide analysis was performed using data-dependent acquisition of one MS scan ($m/z$ range from 400 to 2000 Da/e) followed by MS/MS scans of the three most abundant ions in each MS scan. Dynamic exclusion was used to acquire a more complete survey of the peptides by automatic recognition and temporary exclusion (2 min) of ions from which definitive mass spectral data had previously been acquired. A permanent exclusion list of the most frequent peptide contaminants (keratins and trypsin peptides) was included in the acquisition method in order to focus on significant data. Mass spectral data obtained from the LC−MS/MS analyses were used to search a nonredundant protein database using an in-house version of the Mascot v. 2.1 (Matrix Science, Boston, MA, USA) software and NCBI database (221,338 human sequences, timestamp: March and April, 2009). Peptide mass values and sequence information from the LC−MS/MS experiments were used in the MS/MS ion search taking into account the Carbamidomethyl-Cys as fixed modification, Met oxidized, Pyro-Carbamidomethyl-Cys (with N-term Carbamidomethyl-Cys) and Pyro-Glu (with N-term E) as variable modifications. The maximum missed cleavage of 1, and a precursor ion and fragment ion mass tolerance of ±600 ppm and 0.6 Da, respectively, were used. In agreement with the proposed Guidelines for the Analysis and Documentations of Peptide and Protein Identifications (Paris Consensus), we report the number of identified peptides whose individual ion

score (as provided by Mascot) was higher than the designated confidence level (95%)/protein sequence coverage (%). The sequences and charge state of the peptides used for protein identification of each DIGE spot obtained by LC−MS/MS are reported in Supporting Information Table S1.

### Western Blot

Protein evaluation by Western blot was performed in 8/15 obese and 7/10 nonobese females with 35 μg of total proteins separated by SDS-PAGE (13% polyacrylamide gel) and electroblotted onto hydrophobic polyvinylidene difluoride (PVDF) membranes (Amersham) for 19 h at 33 V. Blots were blocked with 5% BSA in TBS buffer with 0.1% Tween 20 for 2 h at room temperature. Immunoblotting was performed with the specific polyclonal antibody: rabbit anti-14-3-3γ (dilution 1:800), rabbit anti-RAB11A (1 μg/mL), and rabbit antiactin (dilution 1:800) (Abcam, Cambridge, UK) for 4 h. For the following incubation with primary antibody, membrane was washed in TBS buffer with 0.1% Tween 20 and incubated for 45 min IgG-HRP-conjugated secondary antibody (dilution 1:10000 for anti-14-3-3γ and antiactin; 1:50000 for anti-RAB11A). Immunoreactive bands were visualized with the chemiluminescence reagent kit (ECL Western blotting detection reagents, GE Healthcare). We used the same membrane for each immunoblot, washing it in TBS buffer with 0.1% Tween 20 for 10 min after each experiment.

After each immunoblot, the membrane was exposed to X-ray film (Amersham) for different times. The images of three different exposures were captured by Gel Doc XR (Bio-Rad) and quantitated with the Quantity One software (Bio-Rad). Each protein band was contained within a rectangular area, identical for each sample, and background values were subtracted from each band. The triplicate sample values were normalized to the corresponding triplicate actin values. Then, the mean values from the different ratio calculations were calculated for each sample. The data were expressed as percent relative expression, the sample with the highest expression of either RAB11A or YWHAG having been set as 100%. The data obtained were used to obtain the corresponding box plots and *p*-values (Student's *t* test) in the Microsoft Excel software.

### Oligonucleotides and Plasmids

Chemically modified double-stranded RNA molecules (microRNA precursor molecules: pre-miR-520e and pre-miR-141) and pre-miR-negative control were purchased from Ambion (Austin, TX, USA). The final concentration of pre-miR molecules and the corresponding pre-miR negative control were 100 nM each. The plasmids used were pGL3-control (Promega Corp., Madison, WI, USA) encoding for firefly luciferase and pRL-CMV encoding for *Renilla* luciferase (Promega Corp., Madison, WI, USA). The 3′UTRs of RAB11A (1258−1264 bp 3′UTR) and of YWHAG (2489−2495 bp 3′UTR) genes, containing respectively the miR-520e and miR-141 binding sites, as well as the mutated 3′UTRs of these two genes (three bases of each seed region were changed by complementary bases), were obtained from genomic DNA by PCR with a sense and antisense primers carrying a XbaI restriction site and cloned downstream to *Renilla* luciferase gene in pRL-CMV vector in XbaI site.

### Cell Culture, Transfection, and Luciferase Assay

Human embryonic kidney (HEK) 293 cells were cultured in DMEM (Invitrogen) supplemented with 2 mM glutamine (Invitrogen), 100 U/mL penicillin/streptomycin (Invitrogen), and 10% FBS (Invitrogen). The day before transfection, cells were plated in 24-well plates to allow adherence and to reach 70−90% confluence at the time of transfection. Transfection of plasmids, carrying wild-type or mutant 3′UTRs, with pGL3-control and each pre-miRNAs or pre-miR negative control (Ambion, Austin, TX, USA) in HEK293 was performed using Lipofectamine 2000 following the manufacturer's instructions. Firefly and *Renilla* luciferase activities were measured 48 h after transfection, with the dual-luciferase reporter system (Promega) in a Sirius Luminometer (Berthold Detection Systems, Huntsville, AL, USA). All transfection experiments were done in triplicate.

### Statistical Analysis

The investigated parameters were expressed as mean ± standard error of the mean (SEM) (parametric distribution) or as median value and interquartile range (nonparametric distributions). Student's *t* test was used to compare group means, and a *p*-level < 0.05 was considered statistically significant. Statistical analyses were carried out with the PASW package for Windows (Ver.18; SPSS Inc. Headquarters, Chicago, Ill).

## RESULTS

### miRNA Expression Signature in Visceral Adipose Tissue from Obese Females

Expression profile showed that a large set of the tested miRNAs was expressed in VAT from both obese and nonobese females (243/365, 66%). A small set (50/365, 14%) was not expressed, whereas 72/365 (20%) miRNAs were expressed only in VAT from one or more obese females. On the basis of the normalization criteria reported above (see the Experimental Section), namely, miRNAs whose expression levels versus controls were up- or down-expressed (respectively, RQ > 2 or < 0.5) in at least 6/10 obese females, we found that 61/243 (25%) miRNAs were down-expressed, and 10/243 (4.1%) miRNAs were up-expressed (Table 2). The search for gene targets of these differentially expressed miRNAs was performed by TargetScan 5.0 algorithm and their assembly in metabolic pathways by Kegg database. The main significant ($p < 0.01$) pathways predicted to be affected by miRNAs in VAT samples during obesity are reported in Supplementary Figure 1.

### Protein Expression Signature in VAT from Obese Females

We studied the protein expression signature of VAT samples from obese and nonobese subjects using 2D-DIGE analysis. Figure 1A shows the master gel used to match the whole set of the 2-DE profiles obtained. The analysis performed with DeCyder Software detected approximately 2700 protein spots per gel in a 3−10 pH range, with a molecular mass of 10−120 kDa. Approximately 1500 spots were matched throughout the gels. The DeCyder statistical analysis revealed 172 spots differentially expressed in obese vs nonobese VAT samples with average ratio ≥ 1.50 for up-expressed protein spots and ≤ −1.50 for down-expressed spots ($p < 0.05$). Some spots were excluded from further evaluation, i.e., those at the extreme right and left sides of the gel and those (30 spots) representing contaminating serum proteins. Furthermore, many spots were not objected to further investigation, because of their low abundance on the analytical gel or on the preparative gel. As a result, we focused on 33 spots with optimal features.

Figure 1B shows the position of the 33 selected spots on the preparative gel. The latter was stained with SYPRO Ruby protein stain and used for automated spot picking. The isolated


dx.doi.org/10.1021/pr300152z | J. Proteome Res. 2012, 11, 3358−3369

**Table 2. Differentially Expressed miRNAs in Visceral Adipose Tissue from Obese Vs Nonobese Females Identified with the TaqMan Array Human MicroRNA Panel v1.0[a]**

| | RQ value | |
|---|---|---|
| down-expressed miRNAs | mean | SEM |
| hsa-miR-514-4373240 | 0.007 | 0.002 |
| hsa-miR-520e-4373255 | 0.014 | 0.005 |
| hsa-miR-520f-4373256 | 0.029 | 0.010 |
| hsa-miR-184-4373113 | 0.030 | 0.010 |
| hsa-miR-518d-4373248 | 0.057 | 0.021 |
| hsa-miR-196a-4373104 | 0.059 | 0.019 |
| hsa-miR-337-4373044 | 0.065 | 0.025 |
| hsa-miR-520d-4373254 | 0.066 | 0.022 |
| hsa-miR-490-4373215 | 0.067 | 0.025 |
| hsa-miR-508-4373233 | 0.069 | 0.022 |
| hsa-miR-519c-4373251 | 0.073 | 0.026 |
| hsa-miR-369-3p-4373032 | 0.075 | 0.025 |
| hsa-miR-202-4378075 | 0.078 | 0.027 |
| hsa-miR-141-4373137 | 0.079 | 0.025 |
| hsa-miR-562-4380939 | 0.080 | 0.030 |
| hsa-miR-591-4380955 | 0.085 | 0.028 |
| hsa-miR-580-4381024 | 0.086 | 0.029 |
| hsa-miR-380-5p-4373021 | 0.086 | 0.029 |
| hsa-miR-518a-4373186 | 0.092 | 0.035 |
| hsa-miR-618-4380996 | 0.096 | 0.034 |
| hsa-miR-494-4373219 | 0.097 | 0.037 |
| hsa-miR-624-4380964 | 0.099 | 0.035 |
| hsa-miR-519b-4373250 | 0.102 | 0.032 |
| hsa-miR-185-4373181 | 0.113 | 0.043 |
| hsa-miR-219-4373080 | 0.120 | 0.042 |
| hsa-miR-509-4373234 | 0.124 | 0.039 |
| hsa-miR-548d-4381008 | 0.125 | 0.047 |
| hsa-miR-206-4373092 | 0.126 | 0.042 |
| hsa-miR-200c-4373096 | 0.130 | 0.041 |
| hsa-miR-196b-4373103 | 0.166 | 0.055 |
| hsa-miR-653-4381012 | 0.168 | 0.068 |
| hsa-miR-493-4373218 | 0.178 | 0.059 |
| hsa-miR-629-4380969 | 0.181 | 0.074 |
| hsa-miR-198-4373101 | 0.187 | 0.062 |
| hsa-miR-450-4373208 | 0.199 | 0.070 |
| hsa-miR-375-4373027 | 0.202 | 0.071 |
| hsa-miR-518b-4373246 | 0.208 | 0.069 |
| hsa-miR-137-4373174 | 0.222 | 0.091 |
| hsa-miR-649-4381005 | 0.224 | 0.079 |
| hsa-miR-189-4378067 | 0.226 | 0.080 |
| hsa-miR-489-4373214 | 0.240 | 0.085 |
| hsa-miR-451-4373209 | 0.242 | 0.099 |
| hsa-miR-615-4380991 | 0.248 | 0.083 |
| hsa-miR-335-4373045 | 0.250 | 0.088 |
| hsa-miR-215-4373084 | 0.264 | 0.088 |
| hsa-miR-422b-4373016 | 0.271 | 0.090 |
| hsa-miR-500-4373225 | 0.271 | 0.111 |
| hsa-miR-601-4380965 | 0.285 | 0.108 |
| hsa-miR-203-4373095 | 0.298 | 0.122 |
| hsa-miR-410-4378093 | 0.298 | 0.122 |
| hsa-miR-330-4373047 | 0.320 | 0.121 |
| hsa-miR-30a-5p-4373061 | 0.324 | 0.122 |
| hsa-miR-486-4378096 | 0.327 | 0.133 |
| hsa-miR-22-4373079 | 0.332 | 0.125 |
| hsa-miR-181c-4373115 | 0.332 | 0.117 |
| hsa-miR-30d-4373059 | 0.334 | 0.126 |
| hsa-miR-101-4373159 | 0.346 | 0.141 |
| hsa-miR-376a-4373026 | 0.372 | 0.152 |
| hsa-miR-191-4373109 | 0.386 | 0.146 |
| hsa-miR-99a-4373008 | 0.393 | 0.161 |
| hsa-miR-7-4373014 | 0.396 | 0.162 |
| | RQ value | |
| up-expressed miRNAs | mean | SEM |
| hsa-miR-433-4373205 | 21.563 | 7.624 |
| hsa-miR-520 h-4373258 | 13.617 | 5.559 |
| hsa-miR-153-4373125 | 12.447 | 4.705 |
| hsa-miR-579-4381023 | 12.047 | 4.553 |
| hsa-miR-520b-4373252 | 9.400 | 3.553 |
| hsa-miR-616-4380992 | 3.954 | 1.495 |
| hsa-miR-296-4373066 | 3.872 | 1.463 |
| hsa-miR-517c-4373264 | 3.342 | 1.365 |
| hsa-miR-501-4373226 | 3.068 | 1.160 |
| hsa-miR-594-4380958 | 2.714 | 1.108 |

[a]The normalization criteria are detailed in the Experimental Section. Data are expressed as RQ. RQ value was calculated as $2^{-\Delta\Delta Ct}$ (see the Experimental Section for details), and it is reported as mean and SEM.

spots were digested with trypsin and then analyzed by LC–MS/MS, followed by database search. The relative expression ratios (in obese vs nonobese VAT) for each of the 33 spots and their statistical values are listed in Table 3. Interestingly, most (32/33) of the spots were increased, and only 1 spot (number 2312) was decreased.

Globally, a total of 67 proteins, after the exclusion of very abundant proteins that we considered not informative, were identified in these spots (http://pubs.acs.org/paragonplus/submission/jprobs/jprobs_proteomics_guidelines.pdf) (Table 3). Most of these proteins were bioinformatically predicted by DAVID database to be functionally annotated in two main clusters (Figure 2). Annotation cluster 1 (Figure 2A) was constituted by the following: (i) 5 members of the 14.3.3 family of proteins, namely, YWHAB, YWHAE, YWHAG, YWHAH, and YWHAZ; (ii) 9 proteins (YWHAB, YWHAE, YWHAZ, RAB11A, RAB7A, ANXA7, ARCN1, FLOT1, and SERPINF1) involved in the GOTERM_CC_FAT *vesicle* pathway, on the basis of their subcellular localization; and (iii) 7 regulated proteins involved in *intracellular protein transport* (YWHAB, YWHAE, YWHAH, YWHAG, YWHAZ, RAB11A, and ARCN1). Annotation cluster 2 (Figure 2B) was constituted by a predominance of metabolic enzymes clustered in the KEGG pathways: *valine*, *leucine*, and *isoleucine* degradation (6 members, ACAT2, ACADS, ALDH2, BCKDHA, ECHS1, and HADHB), *butanoate metabolism* (5 members, ACAT2, ACADS, ALDH2, ECHS1, and PDHAD1) and *fatty acid metabolism* (5 members, ACAT2, ACADS, ALDH2, ECHS1, and HADHB).

## miRNA/Protein Target Pairs in VAT from Obese Females

To find potential miRNA/protein target pairs, we integrated miRNA expression and proteomic data. Specifically, we combined the list of the identified protein spots with the miRNAs predicted to possess the ability to target the proteins we identified. The last column of Table 3 shows the potential miRNA counterparts of the identified proteins, as revealed by bioinformatics tools (TargetScan). Among the potential miRNA/protein target pairs deriving from this analysis, we

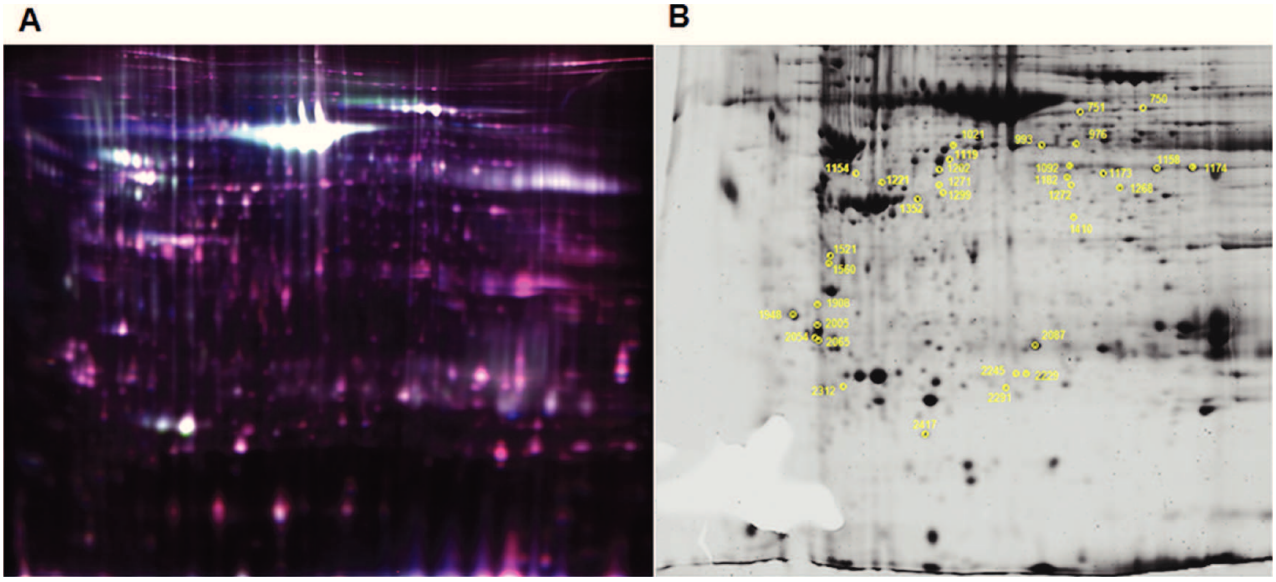


**Figure 1.** 2D-DIGE of visceral adipose tissue (VAT) proteins. (A) Scan of master gel used to match protein spots from the different gels used for the analysis. This gel is constituted by three overlapped images: (1) VAT proteins of a nonobese female labeled with Cy3 (green), (2) VAT proteins of an obese female labeled with Cy5 (red), and (3) VAT proteins from a mixture of the random selected samples (used for normalization) labeled with Cy2 (blue). (B) Scan of preparative gel of VAT proteins from a mixture of samples stained with SYPRO Ruby protein stain. Numbers correspond to differentially expressed protein spots as indicated in Table 3.

selected those including miRNAs down-expressed in almost all VAT samples (9/10 or 10/10): miR-206/ARCN1 (spot 751); miR-141/YWHAG and miR-200c/YWHAG (spot 2005); miR-206/YWHAZ (spot 2054); miR-520d/RAB11A and miR-520e/RAB11A (spot 2229) (bold characters in Table 3).

The expression levels of the above miRNAs (miR-206, miR-141, miR-200c, miR-520e, and -520d) were further validated by qRT-PCR. The qRT-PCR results, except slight differences due to the two different methodologies, were in close agreement with those obtained by TaqMan array (respectively, mean RQ ± SEM): miR-206 (0.209 ± 0.066 vs 0.126 ± 0.042), miR-141 (0.099 ± 0.032 vs 0.079 ± 0.025), miR-200c (0.138 ± 0.044 vs 0.130 ± 0.041), miR-520e (0.554 ± 0.175 vs 0.014 ± 0.005), except for miR-520d, whose results did not differ from controls in the qRT-PCR validation (0.944 ± 0.299 vs 0.066 ± 0.022). Consequently the miR-520d was discarded in our following evaluations.

All the miRNA/protein target pairs reported above warrant further investigation. However, functional annotation clustering in the DAVID database revealed that ARCN1, YWHAG, YWHAZ, and RAB11A are present in the annotation cluster *intracellular protein transport* (Figure 2A), which may be involved in the physiopathology of the adipose tissue. Among the miRNAs associated to these targets, miR-141 and miR-520e were accordingly regulated in the complete set of RNA samples (10/10) from obese VAT. Thus, we selected the functional pairs miR-141/YWHAG and miR-520e/RAB11A for further analysis.

Since the effects of miRNA down-regulations may result in increased mRNA stability and/or mRNA translation, we tested the transcript levels for RAB11A and YWHAG by qRT-PCR. We indeed observed that both mRNAs were more abundantly expressed in VAT of obese women (RQ ± SEM: 6.1 ± 2.6 and 4.8 ± 0.7, respectively) compared to control VAT mRNA samples (data not shown). Next, we tested YWHAG and RAB11A protein expression by Western blot in VAT from a subset of obese (8/15) and nonobese (7/10) females whose samples were available. These samples were also probed with an actin antibody for protein normalization. As shown in Figure 3, both YWHAG and RAB11A proteins were significantly ($p$ = 0.001 and $p$ = 0.00001, respectively) up-expressed in obese than in nonobese VAT tissues.

Taken together, our data suggest that in VAT from obese females, there is a functional interplay between the mRNAs of two up-expressed proteins (YWHAG and RAB11A, as emerged from 2D-DIGE analysis, qRT-PCR, and Western blot validations) and two down-expressed miRNAs (miR-141 and miR-520e, respectively, as revealed by the transcriptomic screening and qRT-PCR analysis). Thus, to determine whether the mRNAs of YWHAG and RAB11A are targets of miR-141 and miR-520e, respectively, we cloned the regions encompassing the 3′UTRs of the two mRNAs downstream the *Renilla* luciferase gene, under the transcriptional control of the cytomegalovirus promoter. The constructs were cotransfected with the pre-miRNAs for miR-141 or miR-520e, and as a transfection control, we used a pGL3-control that expresses firefly luciferase. As shown in Figure 4, both pre-miR-520e (A) and pre-miR-141 (B) significantly reduced the normalized *Renilla* luciferase activities of the constructs containing respectively the RAB11A ($p$ = 0.004) and the YWHAG 3′UTRs ($p$ = 0.02). No inhibition was observed in mutant 3′UTR of RAB11A (A) and YWHAG (B) constructs. These data are consistent with a functional interaction between the selected miRNAs and the 3′UTRs of their mRNA targets, thereby suggesting that changes in the levels of these two miRNAs may modulate the expression of RAB11A and YWHAG.

## ■ DISCUSSION

Understanding the molecular mechanisms underpinning obesity could pave the way for new therapeutic strategies to contrast obesity-related metabolic disorders. miRNAs, which


dx.doi.org/10.1021/pr300152z | *J. Proteome Res.* 2012, 11, 3358−3369

**Table 3. Identification and Characterization of Proteins Differently Expressed in Visceral Adipose Tissue from Obese Vs Nonobese Females by 2D-DIGE Analysis Followed by LC−MS/MS**

| spot no.[a] | DIGE ($p$-value)[b] | DIGE obese/ control[c] | accession no.[d] | protein name | MW (Da)[e] | pI[f] | no. of qualified peptides/ coverage (%)[g] | score[h] | gene symbol[i] | miRNA[j] |
|---|---|---|---|---|---|---|---|---|---|---|
| B1_750 | 0.035 | 1.7 | gi/5031875 | Lamin A/C isoform 2 | 65153 | 6.40 | 13/25 | 743 | LMNA | |
| | | | gi/20127454 | 5-aminoimidazole-4-carboxamide ribonucleotide formyltransferase/IMP cyclohydrolase | 65089 | 6.27 | 7/16.5 | 440 | ATIC | |
| | | | gi/5803181 | Stress induced phosphoprotein 1 | 63227 | 6.40 | 4/9 | 228 | STIP1 | |
| C1_751 | 0.023 | 1.73 | gi/55960506 | Chaperonin containing TCP1, subunit 3 (gamma) | 58505 | 6.46 | 17/43 | 1043 | CCT3 | |
| | | | gi/4503377 | Dihydropyrimidinase −like 2 | 62711 | 5.95 | 7/19 | 465 | DPYSL2 | |
| | | | gi/11863154 | **Archain isoform 1** | 57630 | 5.89 | 9/19 | 503 | **ARCN1*** | **mir-206** |
| | | | gi/189926 | Phosphoglucomutase 1 | 61674 | 6.35 | 4/9 | 208 | PGM1* | mir-30a, -30d |
| | | | gi/6009626 | Brain carboxylesterase hBr1 | 47100 | 6.02 | 3/8 | 189 | CES1 | |
| D1_ 976 | 0.004 | 1.67 | gi/5453603 | Chaperonin containing TCP1, subunit 2 | 57794 | 6.01 | 17/50 | 1271 | CCT2 | |
| | | | gi/178390 | Aldehyde dehydrogenase | 56858 | 7.00 | 6/15 | 387 | ALDH2 | |
| | | | gi/2183299 | Aldehyde dehydrogenase 1 | 55427 | 6.30 | 5/12 | 319 | ALDH1 | |
| | | | gi/5771523 | 3-phosphoglycerate dehydrogenase | 57370 | 6.29 | 4/9 | 225 | PHGDH | |
| E1_993 | 0.011 | 1.78 | gi/16306550 | Selenium binding protein 1 | 52928 | 5.93 | 13/37 | 711 | SELENBP1 | |
| F1_1021 | 0.008 | 2.01 | gi/15620780 | Glutamate carboxypeptidase | 53161 | 5.71 | 3/7 | 143 | CNDP2 | |
| G1_1092 | 0.039 | 1.88 | gi/5174529 | Methionine adenosyltransferase II, alpha | 43975 | 6.05 | 2/7 | 143 | MAT2A* | mir-30a, -30d,-22 |
| H1_1119 | 0.007 | 1.43 | gi/4504169 | Glutathione synthetase | 52523 | 5.67 | 7/23 | 458 | GSS | |
| | | | gi/1049219 | Gamma-aminobutyraldehyde dehydrogenase | 54410 | 6.01 | 5/11 | 306 | E3 | |
| | | | gi/21410323 | Perilipin | 56216 | 5.82 | 2/5 | 112 | PLIN | |
| A2_1154 | 0.003 | 1.61 | gi/21361144 | Proteasome 26S ATPase subunit 3 | 49458 | 5.13 | 15/50 | 843 | PSMC3 | |
| | | | gi/340219 | Vimentin | 53738 | 5.03 | 4/9 | 273 | VIM | |
| | | | gi/7106299 | Ataxin 10 | 54196 | 5.12 | 4/4 | 241 | ATXN10 | |
| B2_1158 | 0.011 | 1.48 | gi/4503571 | Enolase 1 | 47481 | 7.01 | 13/46 | 906 | ENOI | |
| | | | gi/40068518 | Phosphogluconate dehydrogenase | 53619 | 6.8 | 6/17 | 427 | PGD | |
| C2_1173 | 0.003 | 1.87 | gi/4503481 | Eukaryotic translation elongation factor 1 gamma | 50429 | 6.25 | 10/34 | 576 | EEF1G | |
| | | | gi/496902 | Translation initiation factor | 47088 | 6.08 | 5/7 | 297 | E2F1 | |
| | | | gi/4504327 | Mitochondrial trifunctional protein, beta subunit precursor | 51547 | 9.45 | 4/9 | 207 | HADHB* | mir-203 |
| D2_1174 | 0.006 | 2.08 | gi/5031699 | Flotillin 1 | 47554 | 7.08 | 4/12 | 265 | FLOT1 | |
| E2_1182 | 0.002 | 2.01 | gi/4502111 | Annexin VII isoform 1 | 50569 | 6.25 | 9/24 | 526 | ANXA7 | |
| | | | gi/7546384 | Chain A, Human branched- chain Alpha-Keto Acid Dehydrogenase | 45770 | 6.32 | 4/11 | 213 | BCKDHA | |
| | | | gi/4099506 | ErbB3 binding protein EBP1 | 38321 | 7.15 | 4/15 | 211 | PA2G4 | |
| | | | gi/18379349 | Vesicle amine transport protein 1 | 42122 | 5.88 | 2/8 | 121 | VAT1 | |
| F2_1202 | 0.012 | 1.85 | gi/39725934 | Serine (or cysteine) proteinase inhibitor, clade F member 1 | 46454 | 5.97 | 11/38 | 695 | SERPINF1 | |
| | | | gi/9836652 | BSCv | 47887 | 5.78 | 5/13 | 305 | C20ORF3 | |
| | | | gi/285975 | Human rab GDI | 51088 | 5.94 | 2/5 | 116 | GDI | |
| | | | gi/515634 | Ubiquinol-cytochrome C reductase core I protein | 53270 | 5.94 | 2/4 | 122 | UQCRC1 | |
| | | | gi/338695 | Beta-tubulin | 50240 | 4.75 | 2/5 | 121 | TUBB | |
| G2_1221 | 0.045 | 2.61 | gi/4503529 | Eukaryotic translation initiation factor 4A isoform 1 | 46353 | 5.32 | 8/27 | 487 | EIF4A1 | |
| H2_1268 | 0.013 | 1.6 | gi/181914 | DNA-binding protein | 36086 | 9.20 | 2/7 | 122 | | |
| A3_1271 | 0.002 | 1.54 | gi/33415057 | Transformation-related protein 14 | 43248 | 5.49 | 5/19 | 309 | TRG14 | |
| B3_1272 | 0.010 | 1.99 | gi/4557809 | Ornithine aminotransferase precursor | 48846 | 6.57 | 7/23 | 435 | OAT | |
| | | | gi/387011 | Pyruvate dehydrogenase E1-alpha precursor | 47098 | 8.79 | 4/9 | 265 | PDHA1* | mir-203 |
| | | | gi/3641398 | NADP-dependent isocitrate dehydrogenase | 46944 | 6.34 | 2/7 | 86 | IDH1* | mir-30a, -30d |
| C3_1299 | 0.004 | 1.81 | gi/24308406 | Secernin 2 | 46989 | 5.44 | 4/16 | 231 | SCRN2 | |
| | | | gi/6678271 | TAR DNA binding protein | 45053 | 5.85 | 2/7 | 162 | TARDBP* | mir-137, -203 |
| D3_1352 | 0.006 | 1.67 | | not identified | | | | | | |
| E3_1410 | 0.023 | 1.59 | gi/4557233 | Acyl-Coenzyme A dehydrogenase, C-2 to C-3 short chain precursor | 44611 | 8.13 | 8/30 | 436 | ACADS | |
| | | | gi/148539872 | Acetyl-Coenzyme A acetyltransferase 2 | 41783 | 6.47 | 2/8 | 99 | ACAT2 | |
| F3_1521 | 0.006 | 1.64 | gi/7661704 | Osteoglycin preprotein | 34243 | 5.46 | 5/18 | 307 | OGN* | mir-22 |


dx.doi.org/10.1021/pr300152z | J. Proteome Res. 2012, 11, 3358−3369

Table 3. continued

| spot no.[a] | DIGE ($p$-value)[b] | DIGE obese/ control[c] | accession no.[d] | protein name | MW (Da)[e] | pI[f] | no. of qualified peptides/ coverage (%)[g] | score[h] | gene symbol[i] | miRNA[j] |
|---|---|---|---|---|---|---|---|---|---|---|
| | | | gi/25453472 | Eukaryotic translation elongation factor 1delta | 31217 | 4.90 | 4/17 | 277 | EFF1D | |
| G3_1560 | 0.033 | 1.69 | gi/194373515 | Unnamed protein product (Corrisp. in Sprot a P68363 Tubulin alpha-1B chain) | 33856 | 4.88 | 2/8 | 151 | DNAJB2 | |
| | | | gi/157833780 | Chain A, human Annexin V with Proline substitution by thioproline | 36041 | 4.94 | 3/11 | 153 | ANXA5 | |
| H3_1908 | 0.001 | 1.67 | gi/24119203 | Tropomyosin 3 isoform 2 | 29243 | 4.75 | 11/40 | 598 | TPM3 | |
| | | | gi/4507651 | Tropomyosin 4 | 28619 | 4.67 | 2/9 | 104 | TPM4 | |
| | | | gi/13236577 | Thiamine triphosphatase | 25721 | 4.75 | 3/15 | 165 | THTPA | |
| A4_1948 | 0.001 | 1.68 | gi/5803225 | Tyrosine 3/tryptophan 5-monooxygenase activation protein, epsilon polypeptide | 29326 | 4.63 | 15/65 | 943 | YWHAE | |
| B4_2005 | 0.001 | 1.91 | gi/21464101 | **Tyrosine 3-monooxygenase/tryptophan 5-monooxygenase activation protein, gamma polypeptide** | 28456 | 4.80 | 5/21 | 329 | **YWHAG*** | **mir-141, -200c,** |
| | | | gi/119598039 | Tropomyosin 1 (alpha), isoform Cra_m | 28730 | 4.78 | 4/17 | 215 | TPM1 | |
| C4_2054 | 0.010 | 1.64 | gi/4507953 | **Tyrosine 3/tryptophan 5-monooxygenase activation protein, zeta polypeptide** | 27899 | 4.73 | 9/52 | 629 | **YWHAZ*** | **mir-206,** -30a, -30d, -22 |
| D4_2065 | 0.001 | 1.72 | gi/4507949 | Tyrosine 3/tryptophan 5-monooxygenase activation protein, beta polypeptide | 28179 | 4.76 | 5/29 | 310 | YWHAB | |
| | | | gi/4507951 | Tyrosine 3/tryptophan 5-monooxygenase activation protein, eta polypeptide | 28372 | 4.76 | 3/15 | 225 | YWHAH | |
| E4_2087 | 0.038 | 1.7 | gi/4504517 | Heat shock protein beta-1 | 22826 | 5.98 | 6/27 | 330 | HSPB1 | |
| | | | gi/1922287 | EnoylCoA hydratase | 31807 | 8.34 | 5/23 | 330 | ECHS1 | |
| F4_ 2229 | 0.007 | 1.64 | gi/4758984 | **Ras-related protein Rab-11A** | 24492 | 6.12 | 2/11 | 99 | **RAB11A*** | **mir-520e, -520d,** |
| G4_2245 | 0.039 | 1.51 | gi/2204207 | Glutathione S-transferase | 23595 | 5.43 | 6/38 | 372 | GSTP1 | |
| | | | gi/1174149 | Small GTP binding protein Rab 7 | 23732 | 6.40 | 2/12 | 101 | RAB7A* | mir-30a, -30d |
| H4_2291 | 0.008 | 1.65 | gi/14249382 | Abhydrolase domain containing 14B | 22446 | 5.94 | 5/32 | 264 | ABHD14B | |
| A5_2312 | >0.001 | −2.12 | gi/5020074 | Glyoxalase-I | 20934 | 5.24 | 3/16 | 166 | GLO I | |
| | | | gi/17986273 | Fast skeletal myosin alkali light chain 1 isoform 1f | 21189 | 4.97 | 3/18 | 215 | MYL1 | |
| B5_2417 | 0.024 | 2.27 | | not identified | | | | | | |

[a]Spot numbering as shown in 2-DE gel in Figure 1. [b]$p$-value at Student's $t$ test. [c]Average abundance ratio (obeses/controls) as calculated by DeCyder Analysis. [d]Protein accession number from NCBI. [e]Theoretical molecular weight (Da). [f]Theoretical p$I$. [g]According to the Proposed Guidelines for the Analysis and Documentation of Peptide and Protein Identifications (Paris consensus), we included in this table the complete figures of merit regarding the MS identification as the number of identified peptides whose individual ion score (as provided by Mascot) was higher than the designated confidence level (95%)/protein sequence coverage (%). [h]Identification score indicating a probabilistic measure of the goodness of the MS protein identification. [i]Gene symbol from NCBI. [j]Down-expressed miRNAs in at least 6/10 obese females, which targeted 3′UTR-mRNA regions of asterisk genes. In bold are indicated down-expressed miRNAs in VAT from 9 or 10/10 obese females and their targeted proteins.

have been involved in the regulation of a variety of biological processes, including appetite regulation, adipocyte differentiation, and insulin secretion,[13] are interesting candidate molecules to be investigated in adipose tissues as potential mediators of metabolic pathway alterations in obesity. We previously reported that miRNA expression was altered in SAT from morbidly obese patients, and that up-expressed miR-519d plays a role in adipocyte lipid metabolism.[10] We now describe the miRNA and proteome VAT signatures in morbidly obese females and show several miRNAs and proteins differentially expressed between obese and nonobese females.

Globally, our miRNA expression profile revealed that 71 miRNAs were deregulated in the VAT from obese females. Interestingly, most of these miRNAs (61/71) were down-expressed. This latter finding coincides with a report of a similar global down-expression of miRNAs in VAT from obese individuals with nonalcoholic steatohepatitis than those with nonalcoholic fatty liver disease that, moreover, was correlated with enhanced expression of inflammatory adipocytokines.[14] Eleven of the 61 largely down-expressed miRNAs in the VAT of our obese females were also found in the above report;[14] in particular, we previously reported 7/11 of these miRNAs (miR-200c, miR-519b, miR-206, miR-618, miR-30a, miR-181c, and miR-7) down-expressed in SAT from the same obese females.[10]

In a mouse model, Xie et al.[15] reported an inverse correlation of miRNA expression between adipogenesis and obesity.[15] In fact, they observed that up-expressed miRNAs during adipogenesis tended to be down-expressed in the mouse epididymal fat pads, and vice versa, and suggested that these changes could be linked to the chronic local inflammation environment in the fat mouse obese tissue. Lastly, Kloting et al.[7] reported that miR-198, one of our down-expressed miRNAs, was inversely correlated with omental adipocyte diameter during obesity.[7]

Our 2D-DIGE analysis showed that 172 protein spots were differentially expressed in VAT from obese vs nonobese females. Analysis of 33 of these protein spots, those with optimal features, led to the identification of 67 proteins because most spots were related to more than one protein. Our data confirm, and also integrate, proteomic data previously obtained in VAT.[3,16,17] In particular, we detected high levels of EIF4A1, CES1, SELENBP1, ALDH1, ALDH2, GSTP1, HSPB1 proteins that were previously reported to be increased in the omental vs

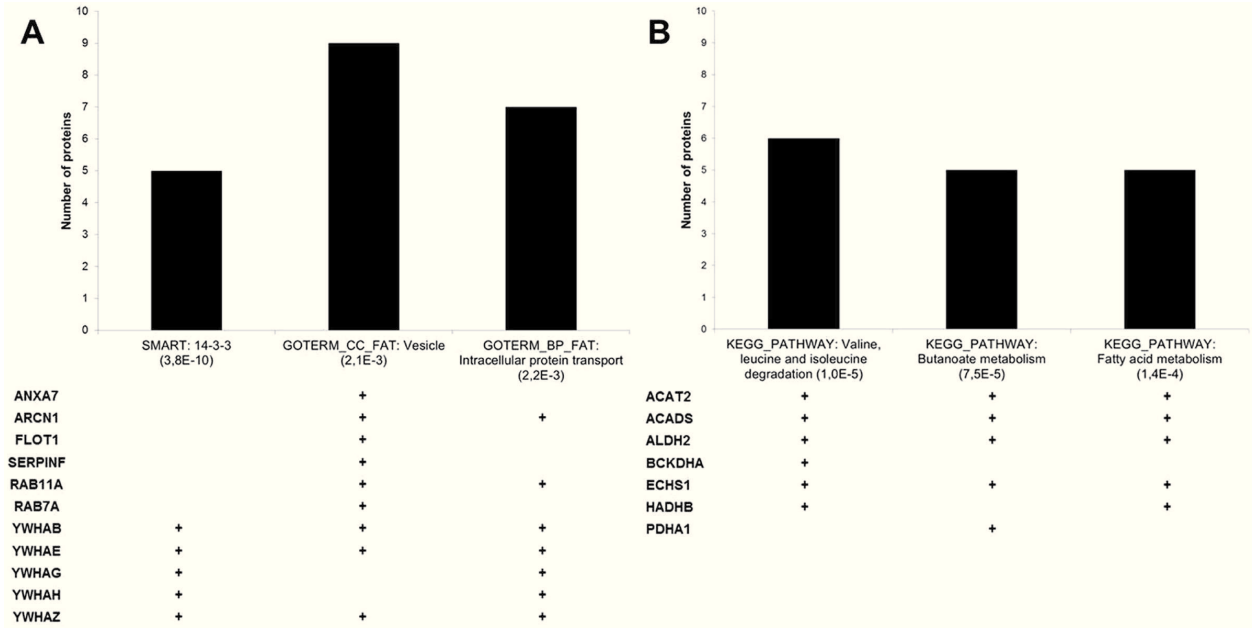


**Figure 2.** VAT proteins, overexpressed in obese females and identified by LC−MS/MS, were bioinformatically predicted by DAVID database to be functionally annotated in two main clusters: (A) annotation cluster 1 and (B) annotation cluster 2.

SAT in an obese population, or proteins that were differently expressed in VAT from obese vs nonobese females, such as ACADS, LMNA, VIM,[17] which indicates that VAT is not only a lipid storage site, but also a highly active metabolic tissue.[3] Furthermore, Pérez-Pérez et al.[3] suggested that EIF4A1 could be involved in the altered protein synthesis pathways preceding insulin resistance and/or type 2 diabetes.[3] In agreement with another study,[18] we detected high levels of E2F1, which could play a role in glucose metabolism.[18] We also identified proteins involved in intracellular trafficking, i.e., ARCN1 (or COPI), PLIN, RAB11A, and RAB14, in agreement with earlier reports.[19,20] Furthermore, we observed an up-expression of proteins involved in antioxidant activity and in apoptosis, namely, GSS, ANXA5, ANXA7, PRDX3, and GSTP1, some of which were reported by Córton et al.[16] in a proteomic study of VAT from obese females with or without polycystic ovary syndrome.[16]

A novelty of our study is that we evaluated simultaneously the miRNome and the proteome of VAT in obese and nonobese women to identify potential biological mechanisms, based on the concerted action of miRNA and protein targets, associated with obesity. To this aim, we intersected the list of the bioinformatically predicted protein targets of the deregulated miRNAs with the whole set of identified proteins from the experimental comparison of the VAT proteomes. This screening enabled us to identify in the obese VAT samples a potential miRNA-based mechanism for the up-expression of some proteins, in particular YWHAG and RAB11A, which was associated with down-expression of miR-141 and miR-520e, respectively. The functional luciferase assay confirmed the binding of these miRNAs to the 3′UTRs of the YWHAG and RAB11A transcripts. We investigated YWHAG and RAB11A because they are involved in glucose homeostasis,[21−23] and YWHAG also in lipid metabolism,[24,25] and hence are potential actors in the obese phenotype.

Rab proteins are a large family of small GTPases that are involved in vesicular trafficking, in cytoskeleton organization, and in the control of cell proliferation and differentiation.[20] Members of the Rab family, which includes about 70 proteins in humans, continuously cycle between the cytosol and different membranes as inactive GDP-bound or active GTP-bound forms, assisted by different Rab-associated proteins.[26] Defects in Rab-associated proteins lead to abnormal intracellular trafficking and have been associated with several monogenic inherited disorders and multigenic conditions such as type 2 diabetes.[26,27] Several Rab GTPases have been implicated in GLUT4 trafficking in relation to the cell type studied; among these, RAB10, RAB11, and RAB14 have been identified in adipocytes.[28] An additional player in GLUT4 trafficking is the GTPase-activating protein AS160. The latter, under basal conditions contributes to cytosolic retention of GLUT4, whereas, upon insulin stimulation, it is phosphorylated at Thr642 by AKT kinase and inactivated, so that AS160 dissociates from GLUT4 vesicles to favor an increase in the GTP-bound form of RAB. This event facilitates the transport of GLUT4 from storage vesicles toward cell surface.[21]

YWHAG (14-3-3$\gamma$) protein belongs to a seven-member protein family in mammals. These proteins, by interacting with target proteins, typically at phospho-residues, regulate a variety of functions, including subcellular redistribution.[22] Studies conducted in animal models and/or in cellular systems have shown that 14-3-3 plays a relevant role in both cellular insulin-mediated glucose transport and lipid metabolism. In fact, in mice, insulin-stimulated YWHAG binding to AS160 at phospho-Thr649 (equivalent to Thr642 in human AS160) normally regulates GLUT4 trafficking from storage vesicles to plasma membrane, thereby influencing glucose uptake.[23] AS160-Thr649Ala knock-in mice (Ala: nonphosphorylable residue) display impaired glucosal and insulin sensitivity.[23] Furthermore, in 3T3-L1 adipocytes, the up-expression of 14-3-3 promotes the cytoplasmic localization of Lipin1, a bifunctional protein involved in lipid metabolism.[24] The subcellular localization of this protein is relevant to its activities; in fact, its nuclear isoform promotes the activation

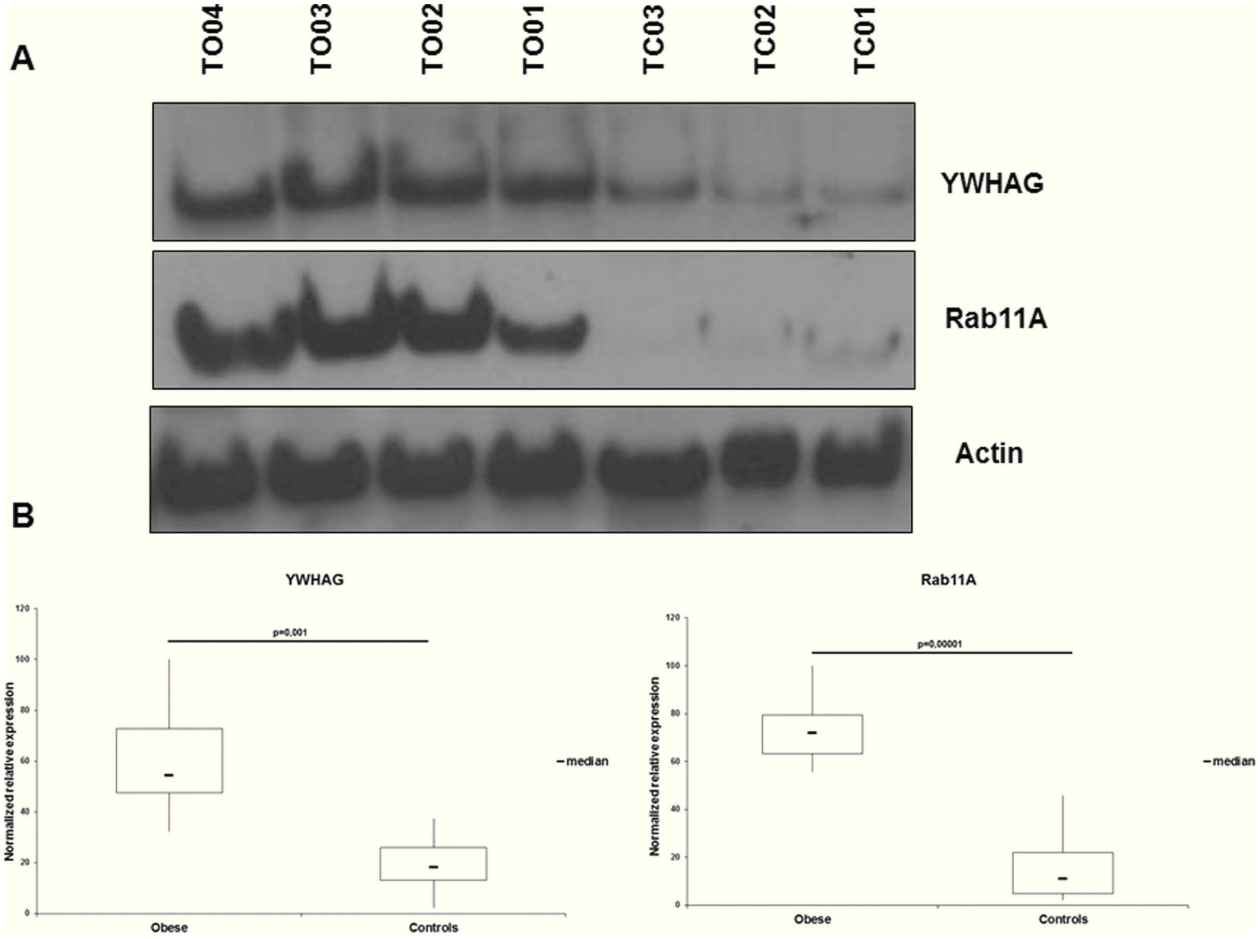


**Figure 3.** (A) An example of the Western blot evaluation of YWHAG and RAB11A proteins from VAT of randomly selected obese females (TO01, TO02, TO03, TO04) and controls (TC01, TC02, TC03). (B) The box plots of the data normalized to actin content, after densitometric analysis of YWHAG and RAB11A immunoblots. The data are expressed as percent relative expression, the sample with the highest expression of either RAB11A ($p$ = 0.00001) or YWHAG ($p$ = 0.001) having been set as 100%. The bottom and top of each box represent the 25th and 75th percentile, respectively; the thick band inside each box shows the 50th percentile (the median). The ends of the whiskers represent the minimum and maximum values of each group of data.

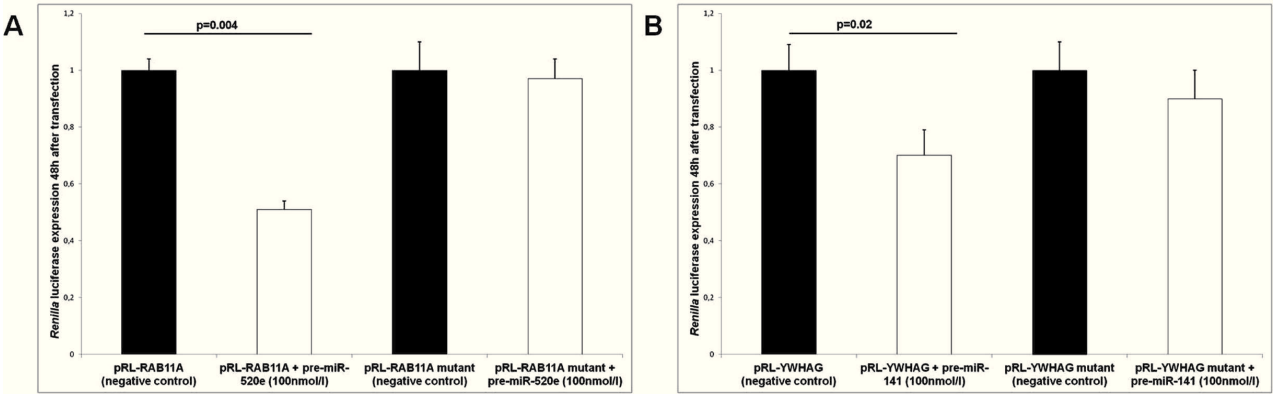


**Figure 4.** Validation of interaction between miR-520e and miR-141 with respectively wild-type or mutant 3′UTR of RAB11A or YWHAG. HEK-293 cells were transfected with wild-type or mutant 3′UTR of RAB11A, pGL3-control, pre-miR-520e, or pre-miR-negative control (A) and with wild-type or mutant 3′UTR of YWHAG, pGL3-control, pre-miR-141, or pre-miR-negative control (B). Pre-miR-520e and the pre-miR-141 significantly inhibited the expression of a *Renilla* luciferase-expressing construct that contains the 3′UTR region of the RAB11A ($p$ = 0.004) and YWHAG ($p$ = 0.02), respectively. No inhibition was observed in mutant 3′UTR of RAB11A (A) and YWHAG (B) constructs. All experiments were done in triplicate. Error bars denote SEM.

of genes involved in oxidative metabolism. In the cytosol, its insulin-mediated phosphorylation leads to the conversion of phosphatidate (PA) to diacylglycerol (DAG), a precursor of triacylglycerol (TAG).[25]


dx.doi.org/10.1021/pr300152z | J. Proteome Res. 2012, 11, 3358−3369

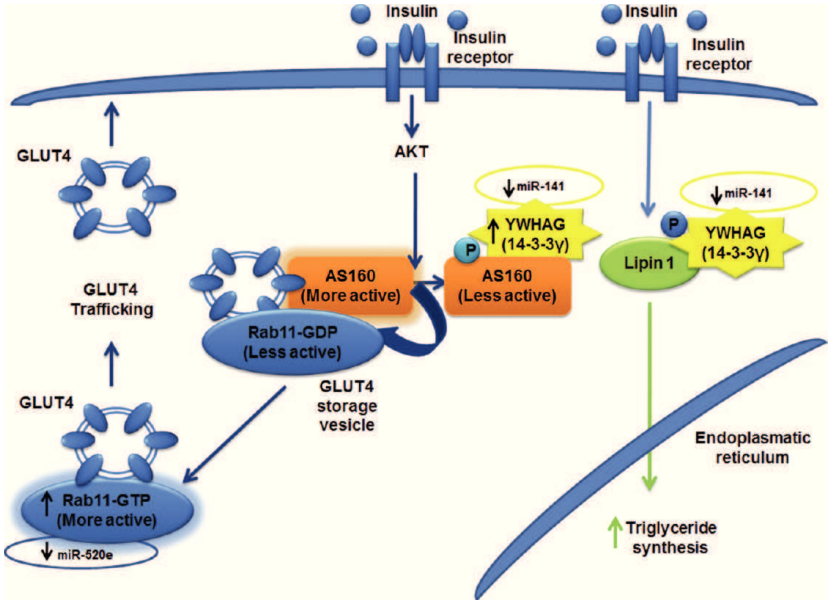


**Figure 5.** Proposed model of visceral adipose tissue (VAT) accumulation based on miR-141/YWHAG and miR-520e/RAB11A interaction. Under basal conditions, the Akt substrate of 160 kDa (AS160) binds RAB11-bound guanosine diphosphate (GDP) that retains glucose transporter protein (GLUT4) vesicles in the cytosol. After insulin stimulation, Akt phosphorylates AS160 that binds YWHAG (14-3-3$\gamma$) and catalyzes the phosphorylation of RAB11-GDP in RAB11-bound guanosine triphosphate (GTP). This process results in GLUT4 translocation toward the cell surface. In response to insulin, lipin1 is phosphorylated and interacts with YWHAG (14-3-3$\gamma$). The interaction between these two proteins induces increased synthesis of triglycerides in the endoplasmic reticulum. The figure also shows the down-expressed miRNAs that target RAB11A and YWHAG (14-3-3$\gamma$).

On the basis of above-mentioned mechanisms, we hypothesize (Figure 5) that in VAT from obese subjects, low expression levels of some miRNAs, including miR-520e and miR-141, by modulating the up-expression of RAB11A and YWHAG proteins, respectively, may lead to increased glucose uptake and to increased triglyceride synthesis. This could then contribute to worsening the obese phenotype by increasing the accumulation of adipose tissue. Obviously, the analysis of suitable cellular systems is required to provide mechanistic details for the proposed model and clarify the role of insulin as an independent, or co-operative model, linked to the observed miRNA down-expression and protein target up-expression in obesity.

Furthermore, studies on larger cohorts of obese and nonobese subjects are necessary to verify our results on the expression of miR-520e and miR-141, as well as of YWHAG and RAB11A proteins, in obesity risk assessment.

Lastly, we did not study the 72/365 miRNAs that were expressed only in VAT from obese females. Further investigations are necessary to test if these miRNAs may play a role in obesity insurgence and/or in the metabolic-associated alterations.

In conclusion, our study provides an integrated view of both miRNAs and protein expression profiles in VAT during obesity and gives clues as to the metabolic pathways that may be involved in adipose tissue accumulation.

## ■ ASSOCIATED CONTENT

### Supporting Information

Figure S1: Main bioinformatically predicted pathways that are deregulated by miRNAs in VAT from obese females. Putative target genes of deregulated miRNAs in VAT from obese patients were sorted into pathways using the Kegg database. In parentheses are the number of genes targeted by miRNAs. Table S1: The sequences and charge states of each peptide used for identification of the proteins by LC–MS/MS. This material is available free of charge via the Internet at http://pubs.acs.org.

## ■ AUTHOR INFORMATION

### Corresponding Author

*Fax: 0039-081-7462404. Tel.: 0039-081-7463541. E-mail: sacchett@unina.it.

### Notes

The authors declare no competing financial interest.

## ■ ACKNOWLEDGMENTS

The present work was supported by grants from CEINGE Regione Campania (DGRC 1901/2009) and by MIUR-PRIN 2008. We thank the Genomics for Applied Research Consortium (GEAR) for granting full access to the 2D-DIGE platform. We thank Jean Ann Gilder (Scientific Communication srl) for revising and editing the manuscript. We thank Piero Pucci's group at the Proteomic Facility of CEINGE–Biotecnologies Avanzate for support and guidance in the production and interpretation of LC–MS/MS data.

## ■ REFERENCES

(1) Maury, E.; Brichard, S. M. Adipokine dysregulation, adipose tissue inflammation and metabolic syndrome. *Mol. Cell. Endocrinol.* **2010**, *314* (1), 1–16.

(2) Gesta, S.; Blüher, M.; Yamamoto, Y.; Norris, A. W.; Berndt, J.; Kralisch, S.; Boucher, J.; Lewis, C.; Kahn, C. R. Evidence for a role of developmental genes in the origin of obesity and body fat distribution. *Proc. Natl. Acad. Sci. U. S. A.* **2006**, *103* (17), 6676–6681.

(3) Pérez-Pérez, R.; Ortega-Delgado, F. J.; García-Santos, E.; López, J. A.; Camafeita, E.; Ricart, W.; Fernández-Real, J. M.; Peral, B. Differential proteomics of omental and subcutaneous adipose tissue

reflects their unalike biochemical and metabolic properties. *J. Proteome Res.* **2009**, *8* (4), 1682−1693.
(4) Ibrahim, M. M. Subcutaneous and visceral adipose tissue: structural and functional differences. *Obes. Rev.* **2010**, *11* (1), 11−18.
(5) Linder, K.; Arner, P.; Flores-Morales, A.; Tollet-Egnell, P.; Norstedt, G. Differentially expressed genes in visceral or subcutaneous adipose tissue of obese men and females. *J. Lipid Res.* **2004**, *45* (1), 148−154.
(6) van Beek, E. A.; Bakker, A. H.; Kruyt, P. M.; Hofker, M. H.; Saris, W. H.; Keijer, J. Intra- and interindividual variation in gene expression in human adipose tissue. *Pfluegers Arch.* **2007**, *453* (6), 851−861.
(7) Klöting, N.; Berthold, S.; Kovacs, P.; Schön, M. R.; Fasshauer, M.; Ruschke, K.; Stumvoll, M.; Blüher, M. MicroRNA expression in human omental and subcutaneous adipose tissue. *PLoS One* **2009**, *4* (3), e4699.
(8) Krol, J.; Loedige, I.; Filipowicz, W. The widespread regulation of microRNA biogenesis, function and decay. *Nat. Rev. Genet.* **2010**, *11* (9), 597−610.
(9) Ortega, F. J.; Moreno-Navarrete, J. M.; Pardo, G.; Sabater, M.; Hummel, M.; Ferrer, A.; Rodriguez-Hermosa, J. I.; Ruiz, B.; Ricart, W.; Peral, B.; Fernández-Real, J. M. MiRNA expression profile of human subcutaneous adipose and during adipocyte differentiation. *PLoS One* **2010**, *5* (2), e9022.
(10) Martinelli, R.; Nardelli, C.; Pilone, V.; Buonomo, T.; Liguori, R.; Castanò, I.; Buono, P.; Masone, S.; Persico, G.; Forestieri, P.; Pastore, L.; Sacchetti, L. miR-519d overexpression is associated with human obesity. *Obesity* **2010**, *18* (11), 2170−2176.
(11) Huang, D. W.; Sherman, B. T.; Lempicki, R. A. Systematic and integrative analysis of large gene lists using DAVID Bioinformatics Resources. *Nat. Protoc.* **2009**, *4* (1), 44−57.
(12) Huang, D. W.; Sherman, B. T.; Lempicki, R. A. Bioinformatics enrichment tools: paths toward the comprehensive functional analysis of large gene lists. *Nucleic Acids Res.* **2009**, *37* (1), 1−13.
(13) Heneghan, H. M.; Miller, N.; Kerin, M. J. Role of microRNAs in obesity and the metabolic syndrome. *Obes. Rev.* **2010**, *11* (5), 354−361.
(14) Estep, M.; Armistead, D.; Hossain, N.; Elarainy, H.; Goodman, Z.; Baranova, A.; Chandhoke, V.; Younossi, Z. M. Differential expression of miRNAs in the visceral adipose tissue of patients with non-alcoholic fatty liver disease. *Aliment. Pharmacol. Ther.* **2010**, *32* (3), 487−497.
(15) Xie, H.; Lim, B.; Lodish, H. F. MicroRNAs induced during adipogenesis that accelerate fat cell development are downregulated in obesity. *Diabetes* **2009**, *58* (5), 1050−1057.
(16) Cortón, M.; Botella-Carretero, J. I.; López, J. A.; Camafeita, E.; San Millán, J. L.; Escobar-Morreale, H. F.; Peral, B. Proteomic analysis of human omental adipose tissue in the polycystic ovary syndrome using two-dimensional difference gel electrophoresis and mass spectrometry. *Hum. Reprod.* **2008**, *23* (3), 651−661.
(17) Pérez-Pérez, R.; García-Santos, E.; Ortega-Delgado, F. J.; López, J. A.; Camafeita, E.; Ricart, W.; Fernández-Real, J. M.; Peral, B. Attenuated metabolism is a hallmark of obesity as revealed by comparative proteomic analysis of human omental adipose tissue. *J. Proteomics* **2012**, *75* (3), 783−795.
(18) Fajas, L.; Blanchet, E.; Annicotte, J. S. The CDK4-pRB-E2F1 pathway: A new modulator of insulin secretion. *Islets* **2010**, *2* (1), 51−53.
(19) Beller, M.; Thiel, K.; Thul, P. J.; Jäckle, H. Lipid droplets: a dynamic organelle moves into focus. *FEBS Lett.* **2010**, *584* (11), 2176−2182.
(20) Stenmark, H. Rab GTPases as coordinators of vesicle traffic. *Nat. Rev. Mol. Cell Biol.* **2009**, *10* (8), 513−525.
(21) Cartee, G. D.; Funai, K. Exercise and insulin: Convergence or divergence at AS160 and TBC1D1? *Exercise Sport Sci. Rev.* **2009**, *37* (4), 188−195.
(22) Ramm, G.; Larance, M.; Guilhaus, M.; James, D. E. A role for 14-3-3 in insulin-stimulated GLUT4 translocation through its interaction with the RabGAP AS160. *J. Biol. Chem.* **2006**, *281* (39), 29174−29180.
(23) Chen, S.; Wasserman, D. H.; MacKintosh, C.; Sakamoto, K. Mice with AS160/TBC1D4-Thr649Ala knockin mutation are glucose intolerant with reduced insulin sensitivity and altered GLUT4 trafficking. *Cell Metab.* **2011**, *13* (1), 68−79.
(24) Péterfy, M.; Harris, T. E.; Fujita, N.; Reue, K. Insulin-stimulated interaction with 14-3-3 promotes cytoplasmic localization of lipin-1 in adipocytes. *J. Biol. Chem.* **2010**, *285* (6), 3857−3864.
(25) Reue, K.; Brindley, D. N. Thematic Review Series: Glycerolipids. Multiple roles for lipins/phosphatidate phosphatase enzymes in lipid metabolism. *J. Lipid Res.* **2008**, *49* (12), 2493−2503.
(26) Mitra, S.; Cheng, K. W.; Mills, G. B. Rab GTPases implicated in inherited and acquired disorders. *Semin. Cell Dev. Biol.* **2011**, *22* (1), 57−68.
(27) Kaddai, V.; Gonzalez, T.; Keslair, F.; Grémeaux, T.; Bonnafous, S.; Gugenheim, J.; Tran, A.; Gual, P.; Le Marchand-Brustel, Y.; Cormont, M. Rab4b is a small GTPase involved in the control of the glucose transporter GLUT4 localization in adipocyte. *PLoS One* **2009**, *4* (4), e5257.
(28) Larance, M.; Ramm, G.; Stöckli, J.; van Dam, E. M.; Winata, S.; Wasinger, V.; Simpson, F.; Graham, M.; Junutula, J. R.; Guilhaus, M.; James, D. E. Characterization of the role of the Rab GTPase-activating protein AS160 in insulin-regulated GLUT4 trafficking. *J. Biol. Chem.* **2005**, *280* (45), 37803−37813.

# High Aminopeptidase N/CD13 Levels Characterize Human Amniotic Mesenchymal Stem Cells and Drive Their Increased Adipogenic Potential in Obese Women

**Running Title**

**Increased expression of CD13 in obese hA-MSCs**

**Laura Iaffaldano,[1,2*] Carmela Nardelli,[1,2*] Maddalena Raia,[1] Elisabetta Mariotti,[1] Maddalena Ferrigno,[1] Filomena Quaglia,[3] Giuseppe Labruna,[4] Valentina Capobianco,[1,2] Angela Capone,[3] Giuseppe Maria Maruotti,[3] Lucio Pastore,[1,2] Rosa Di Noto,[1,2] Pasquale Martinelli,[3] Lucia Sacchetti,[1,2†] Luigi Del Vecchio.[1,2]**

[1]CEINGE-Biotecnologie Avanzate S.C.a R.L., Naples, Italy.

[2]Dipartimento di Medicina Molecolare e Biotecnologie Mediche, Università degli Studi di Napoli Federico II, Naples, Italy.

[3]Dipartimento di Neuroscienze e Scienze Riproduttive ed Odontostomatologiche, Naples, Italy.

[4]Fondazione IRCCS SDN–Istituto di Ricerca Diagnostica e Nucleare, Naples, Italy.

*These two authors contributed equally to this work.

†**Corresponding author:** Lucia Sacchetti, CEINGE-Biotecnologie Avanzate S.C.a R.L.

Via G. Salvatore 486 - 80145 Naples, Italy.

Fax 0039-081-7462404

Tel. 0039-081-7463541

e-mail: sacchett@unina.it

**Abstract**

Maternal obesity is associated to increased fetal risk of obesity and other metabolic diseases. Human amniotic mesenchymal stem cells (hA-MSC) have not been characterized in obese women. The aim of this study was to isolate and compare hA-MSC immunophenotypes from obese (Ob-) and normal weight control (Co-) women to identify alterations possibly predisposing the fetus to obesity. We enrolled 16 Ob- and 7 Co-women at delivery (mean/SEM pre-pregnancy BMI: 40.3/1.8 kg/m$^2$ and 22.4/1.0 kg/m$^2$, respectively) and 32 not pregnant women. hA-MSCs were phenotyped by flow cytometry; several maternal and newborn clinical and biochemical parameters were also measured. The expression of membrane antigen CD13 was higher on Ob-hA-MSCs than on Co-hA-MSCs (P=0.0043). Also serum levels of CD13 at delivery were higher in Ob- versus Co-pregnant women and correlated with CD13 antigen expression on Ob-hA-MSCs ($r^2$=0.84, P<0.0001). Adipogenesis induction experiments revealed that Ob-hA-MSCs had a higher adipogenic potential than Co-hA-MSCs as witnessed by higher PPARγ and aP2 mRNA levels (P=0.02 and P=0.03, respectively) at post-induction day 14 associated with increased CD13 mRNA levels from baseline to day 4 post-induction (P<0.05). Adipogenesis was similar in the two sets of hA-MSCs after CD13 silencing, whereas it was increased in Co-hA-MSCs after CD13 overexpression. CD13 expression was high also in Ob-h-MSCs from umbilical cords or visceral adipose tissue of not pregnant women. In conclusion, antigen CD13, by influencing the adipogenic potential of hA-MSCs could be an *in-utero* risk factor for obesity. Our data strengthen the hypothesis that high levels of serum and MSC CD13 are obesity markers.

## Introduction

The increase in the incidence of obesity in pregnant women in the last two decades has paralleled that observed in the general population [1-3]. Although maternal fat stores increase in all pregnant women, irrespective of pre-pregnancy weight [4], the storage capacity of subcutaneous adipose tissue (SAT) is impaired, and fat predominantly accumulates in visceral adipose tissue (VAT) [5]. VAT is an important risk factor for metabolic imbalance in human subjects, also during pregnancy [6-8]. In fact, maternal obesity is related to offspring obesity [9], and there is an increased risk of adverse outcomes for both mother and child [10-13]. Moreover, the risk of childhood obesity was quadrupled if the mother was obese before pregnancy [14], which suggests that the *in utero* environment is obesogenic. In mammals, the placenta is the main interface between fetus and mother; it regulates intrauterine development and modulates adaptive responses to suboptimal *in utero* conditions [15,16].

Placenta is also an important source of stem/progenitor cells [17-19]. In particular, human amniotic mesenchymal stem cells (hA-MSCs) have been shown to differentiate into cell types of mesenchymal origin such as chondrocytes, adipocytes and osteocytes [20-22]. The phenotype of hA-MSCs from normal pregnant women has been characterized and found to differ in terms of cytokine expression from that of pregnant women affected by preeclampsia [23]. Thus far, little is known about hA-MSCs from obese women.

The aim of this study was to characterize hA-MSCs from term placenta of obese (Ob-) women and to test their adipogenic potential with respect to that of normal weight control (Co-) women. We also measured several maternal and newborn clinical and biochemical parameters, and looked for correlations between these parameters with the hA-MSC immunophenotype. We found that the Ob-hA-MSC immunophenotype was characterized by increased expression levels of the CD13 surface antigen that correlated with maternal CD13 serum levels. Adipogenesis was higher in Ob-hA-MSCs than in Co-hA-MSCs, and returned to the control value after CD13 silencing. On the other hand, CD13

overexpression increased the adipogenic potential of Co-hA-MSCs. Our findings suggest that CD13 could contribute to obesity programming in the fetus and indicates that maternal serum CD13 is an obesity risk marker.

## Materials and methods

### *Patients and controls*

Sixteen Ob- (age range: 26–39 years) and seven Co-pregnant women, (age range: 26–38 years), pre-pregnancy BMI (mean/SEM) 40.3/1.8 kg/m$^2$ and 22.4/1.0 kg/m$^2$, respectively and thirty-two not pregnant women (16 obese and 16 normal weight, BMI >30 kg/m$^2$ and <25 kg/m$^2$, respectively) were recruited at the Dipartimento di Neuroscienze e Scienze Riproduttive ed Odontostomatologiche, University of Naples "Federico II". The clinical, personal and family history of the 23 women was recorded during a medical interview conducted by an expert upon hospitalization. Data relative to each pregnancy follow-up and delivery were also recorded. The general characteristics of the newborn and clinical data (birth weight, length, head circumference, Apgar score) were recorded at birth.

### *Sample collection*

Two fasting peripheral blood samples were collected in the morning from not pregnant women and from Ob- and Co-pregnant women, immediately before delivery. One sample was used for DNA extraction, whereas the other was centrifuged at 2,500 rpm for 15 min and serum was stored at -80°C until further processing. At delivery, placentas were collected by C-section from each enrolled women and immediately processed. Bioptic samples of visceral adipose tissue (VAT) were also collected from not pregnant obese and control women during obstetric surgery (ovarian cysts). All patients and controls gave their informed consent to the study and both parents gave consent for their newborns.

The study was performed according to the Helsinki II Declaration and was approved by the Ethics Committee of our Faculty.

***Biochemical evaluations***

The main serum biochemical parameters were evaluated by routine assays. Leptin and adiponectin were measured in maternal serum with Luminex xMAP Technology on a BioRad Multiplex Suspension Array System (Bio-Rad, Hemel Hempstead, Herts., UK), according to the manufacturer's instructions. The ratio leptin/adiponectin (L/A) was also calculated.

***Aminopeptidase N/CD13 ELISA assay***

Aminopeptidase N (APN)/CD13 serum levels were measured by ELISA (Life Science, Houston). Briefly, the microtiter plate was pre-coated with a specific anti-CD13 antibody. Standards or samples were then added to the appropriate microtiter plate wells with a biotin-conjugated polyclonal antibody preparation specific for CD13. Next, avidin conjugated to horseradish peroxidase was added to each microplate well and incubated for 15 min at room temperature. A TMB substrate solution (3,3′,5,5′-tetramethylbenzidine) was then added to each well. The enzyme-substrate reaction was terminated by the addition of a sulphuric acid solution and the color change was measured spectrophotometrically at a wavelength of 450 nm. The amount of CD13 in each sample was determined by comparing the absorbance of the sample to a standard curve.

***Cell isolation from placenta tissue***

Placentas were collected and immediately processed, according to Parolini et al. [24]. After removal of the maternal decidua, the amnion was manually separated from the chorion and extensively washed 5 times in 40 mL of phosphate-buffered saline (PBS) containing 100 U/mL penicillin, 100 µg/mL

streptomycin and 250 µg/mL amphotericin B (all from Sigma-Aldrich, Missouri) after which it was mechanically minced into small pieces [24]. Amnion fragments were digested overnight at 4°C in ACCUMAX® reagent (Innovative Cell Technology, San Diego), a combination of DNase, protease and collagenolytic enzymes [25], containing 100 U/mL penicillin, 100 µg/mL streptomycin and 250 µg/mL amphotericin B. The next day, digestion enzymes were inactivated with complete culture medium constituted by low glucose D-MEM (Sigma-Aldrich) supplemented with 10% of heat-inactivated bovine serum (FBS), 1% of non-essential amino acids and 2% of Ultraglutamine (all from Lonza, Basel, Switzerland). After centrifugation at 300g for 10 min, cell pellets and digested tissue fragments were seeded in a cell culture dish (BD Falcon, New York) in complete culture medium and incubated at 37°C in 5% $CO_2$. One week later, digested tissue pieces were removed from the dish and discarded, and isolated cells formed distinct fibroblast colony-forming units. When the colonies reached 70% confluence, they were washed with PBS and detached with trypsin/EDTA (Sigma-Aldrich), counted and reseeded in complete medium for expansion at a concentration of about 5,000/$cm^2$ [24].

***Cell preparation***

hA-MSCs were expanded for several passages. Absence of mycoplasma contamination was assessed as described previously [26]. The population-doubling level was calculated for each subcultivation with the following equation: population doubling= $[\log_{10}(N_H) - \log_{10}(N_I)]/\log_{10}(2)$, where $N_I$ is the cell inoculum number and $N_H$ is cell harvest number [27]. The increase in population doubling was added to the population doubling levels of the previous passages to yield the cumulative population doubling level. When 70%-80% confluent cultures reached about 4 population doublings they were detached with trypsin/EDTA, resuspended in PBS with 10% FBS, and processed for flow cytometry, DNA and RNA extraction. Cellular viability was assessed by both Trypan blue dye exclusion and the analysis of light scatter proprieties in flow cytometry, and it was never lower than 90%.

Using the above cell isolation and preparation procedures, h-MSCs were also isolated from umbilical cord (hUC-MSCs) of one obese and one control pregnant woman.

***Isolation of visceral adipose tissue mesenchymal stem cells (hVAT-MSCs)***

Briefly, VAT bioptic samples were washed with phosphate buffered saline (PBS) containing 100 U/mL penicillin, 100 µg/mL streptomycin and 250 µg/mL amphotericin B (all from Sigma-Aldrich), minced into small pieces and digested with 1.5 mg/ml collagenase type I (GIBCO, USA) at 37C°. The digestion enzymes were inactivated with FBS. After centrifugation at 1500*g* for 5 min, cell pellets and digested tissue fragments were washed and seeded in a cell culture dish (BD Falcon, New York) in complete culture medium and incubated at 37°C in 5% $CO_2$. When the colonies reached 60-70% confluence, they were washed with PBS and detached with trypsin/EDTA (Sigma-Aldrich), counted and reseeded in complete medium for expansion at a concentration of about 5,000/$cm^2$ [28].

***DNA typing***

The fetal origin of both amnion and hA-MSCs was verified by DNA typing. Genomic DNA was extracted from the mother's peripheral blood, from amnion samples and from hA-MSCs using the Nucleon BACC2 extraction kit (Illustra DNA Extraction Kit BACC2, GE Healthcare, Calfont St. Giles, Bucks., UK). DNA concentration was evaluated using the NanoDrop® ND-1000 UV-Vis spectrophotometer (NanoDrop Technologies, Wilmington, DE). Genomic DNA (1 ng) was amplified in a final volume of 25 µL using the AmpFlSTR® Identifiler™ PCR Amplification Kit (Applied Biosystems, Foster City). The AmpFlSTR® Identifiler™ PCR Amplification Kit is a short tandem repeat (STR) multiplex assay that amplifies 15 repeat loci and the Amelogenin gender determining marker in a single PCR amplification using a primer set labeled with four fluorescent molecules. The amplification was performed with the GeneAmp PCR System 9700 (Applied Biosystems) instrument.

PCR products were then analyzed by capillary electrophoresis on the ABI Prism 3130 Genetic Analyzer (Applied Biosystems) together with an allelic ladder that contained all the most common alleles for the analyzed loci that were present in Caucasian populations and both a negative- and a positive-quality control sample. Typically, 1μL of each sample was diluted in 18.7μL of deionized formamide; each sample was supplemented with 0.3μL of an internal size standard (LIZ 500 Applied Biosystems) labeled with an additional fluorophore. The samples were denatured at 95 °C for 4 min and then placed in the auto sampler tray (maximum of 96 samples) on the ABI Prism 3130 for automatic injection in the capillaries. The data were analyzed by Gene Mapper Software (Applied Biosystems).

***Immunophenotyping of h-MSCs by flow cytometry***

We analyzed the expression of 38 hematopoietic, mesenchymal, endothelial, epithelial and no-lineage membrane antigens on the surface of hA-MSCs, hUC-MSCs and hVAT-MSCs by four-color flow cytometry (Table 1). The antibody cocktails contained in each tube are detailed in Supplementary Table 1. All monoclonal antibodies (MoAbs) were from Becton Dickinson (San Jose) except anti-CD338-APC, which was from R&D (Minneapolis), anti-CD-133-PE and anti-CD271-APC MoAbs, which were from Milenyi Biotec (Bergisch Gladbach, Germany). For all antibody staining experiments, at least $1x10^5$ hA-MSCs isolated from each placenta sample were incubated at 4°C for 20 min with the appropriate amount of MoAbs, washed twice with PBS and finally analyzed with an unmodified Becton-Dickinson FACSCanto II flow cytometer (Becton-Dickinson, San Jose), that was set up according to published guidelines [29]. For each sample the respective control was prepared in order to determine the level of background cellular autofluorescence without antibody staining.

CaliBRITE beads (Becton-Dickinson, catalog no. 340486) were used as quality controls across the study as described elsewhere [30, 31], according to the manufacturer's instructions. Daily control of

CaliBRITE intensity showed no change in instrument sensitivity throughout the study. The relative voltage range for each detector was assessed *una tantum* using the "eight-peak" technology (Rainbow Calibration Particles, Becton-Dickinson, catalog no. 559123) at the beginning of the study.

Compensation was set in the FACS-DiVa (Becton-Dickinson) software, and compensated samples were analyzed. Samples were acquired immediately after staining using the FACSCanto II instrument, and at least 10,000 events were recorded for each monoclonal combination. Levels of CD antigen expression were displayed as median fluorescence intensity (MFI). The FACS-DiVa software (Becton-Dickinson) was used for cytometric analysis.

***Differentiation potential towards the adipogenic lineage***

hA-MSCs and hVAT-MSCs were cultured in low glucose D-MEM (Sigma-Aldrich) supplemented with 10% of FBS, 2% of ultraglutamine and 1% of non-essential amino acids at 37°C in 5% $CO_2$ (all from Lonza, Basel, Switzerland). The cells were passaged twice before the addition of differentiation medium composed of DMEM with the addition of 10% FBS, 1 µM dexamethasone, 0.5 mM 3-isobutyl-1-methylxhantine, 200 µM indomethacin and 10 µg/mL insulin. Media were changed every two days and cells were either stained or collected for RNA extraction.

***CD13 RNA interference and overexpression***

hA-MSCs plated at a density of 5,000 cells/$cm^2$ were transfected using 20 µL Lipofectamine 2000 according to the manufacturer's instructions (Invitrogen, Paisley, UK) with 8 µg short hairpin RNAs (shRNAs)-expressing plasmids (Open Biosystem, Huntsville) or with 8 µg pCMV-Sport 6 Vector (Invitrogen, Paisley, UK), to silence or to overexpress CD13 mRNA, respectively. Transfected cells were induced to differentiate towards the adipogenic lineage up to 4 days.

***Effect of IFN-γ on the expression of CD13 on the surface of h-MSCs***

The expression of CD13 on the surface of Co- and of Ob-h-MSCs isolated from amnion, umbilical cord and VAT was measured after exposure of cells to 0.8 and 12.5 ng/mL IFN-γ at 37° C for 24 h, using untreated Co- and Ob-h-MSCs as controls. At the end of incubation, the cells were harvested by trypsin, washed in PBS, counted, and adjusted to the same concentrations of $1x10^5$ h-MSCs. Subsequently, their immunophenotype was examined by flow cytometry.

**Adipocyte staining**

After 14 days of differentiation, the adipocyte cultures were stained for lipid droplets, which are an index of differentiation. The cells were washed in PBS and fixed in 10% formalin for 1 h. Then they were washed in PBS and the lipids were stained for 15 min with Oil-red-O prepared by mixing vigorously three parts of stock solution (0.5% Oil-red-O in 98% isopropanol) with two parts of water and then eliminating undissolved particles with a 0.4-μm filter. Cells were then washed with water and the number of adipocytes was evaluated with a microscope. Relative lipid levels were assessed by redissolving the Oil-Red-O present in stained cells in 98% isopropanol and then determining absorbance at 550 nm.

**RNA isolation**

Total RNA was purified from hA-MSCs isolated from term placentas of Co- and of Ob-pregnant women using the mirVana™ miRNA isolation kit (Ambion, Austin) and its concentration was evaluated with the NanoDrop® ND-1000 UV-Vis spectrophotometer (NanoDrop Technologies, Wilmington).

***Quantitative real-time polymerase chain reaction (qRT-PCR) of mRNAs***

Real-time quantitative PCR was carried out on the Applied Biosystems 7900HT Sequence Detection system (Applied Biosystems). cDNAs were synthesized from 2 μg of total RNA using hexamer random primers and M-MuLV Reverse Transcriptase (New England BioLabs, Beverly). The PCR reaction was performed in a 20 μL final volume containing cDNA, 1X SYBR Green PCR mix, 10 μM of each specific primer. Supplementary Table 2 lists the oligonucleotide primers used for PCR of selected genes: peroxisome proliferator-activated receptor gamma (PPARγ), CD13, protein homologous to myelin P2 (aP2), and glyceraldehyde-3-phosphate dehydrogenase (GAPDH). The PCR conditions for reverse transcription were: stage 1: 50°C, 2 min; stage 2: 95°C, 10 min; stage 3: 95°C, 15 s; 60°C, 1 min/40 cycles; and stage 4: 95°C, 15 s; 60°C, 1 min. Levels of target genes were quantified using specific oligonucleotide primers and normalized for GAPDH expression.

***Statistical analysis***

The parameters investigated were expressed as mean and standard error of the mean (SEM) (parametric distributions) or as median value and $25^{th}$ and $75^{th}$ percentiles (non parametric distributions). Student's "t" and Mann-Whitney tests were used to compare parametric and nonparametric data, respectively. P values $<0.05$ were considered statistically significant. Correlation analysis was performed with the SPSS package for Windows (ver. 18; SPSS Inc., Headquarters, Chicago).

**Results**

The clinical and biochemical characteristics of the mothers and their newborns are reported in Table 2 (A and B, respectively). Weight gain was lower (P=0.025) and diastolic blood pressure was higher (P=0.039) in Ob- than in Co-pregnant women. Both leptin concentration (P<0.0001) and the L/A ratio (P<0.0001) were higher in Ob- than in Co-pregnant women at delivery. Biometric characteristics did not differ significantly between Ob- and Co-newborns.

***Isolation of hA-MSCs***

We isolated hA-MSCs from the mesenchymal layer of amniotic membranes obtained from our Ob- and Co-pregnant women at delivery. The fetal origin of all isolated hA-MSCs was confirmed by STR typing of DNA of the mother and of the hA-MSCs. Mycoplasma contamination of cultures was checked and excluded (data not shown). All isolated hA-MSCs were characterized by a high proliferation potential and collected after 4 population doublings. Morphologically, cultured Ob- and Co-hA-MSCs showed a similar fibroblastic-like morphology after 4 population doublings (Supplementary Fig. 1).

***Immunophenotyping of h-MSCs***

The antigenic mosaic displayed by Ob- and Co-hA-MSCs is shown in Table 3. Seventeen of the 38 antigens investigated were not expressed on the surface of hA-MSCs (hematopoietic antigens: CD14, CD15, CD16, CD19, CD28, CD33, CD34, CD45 and CD117; the endothelial marker PECAM-1/CD31; and no-lineage markers: thrombospondin receptor/CD36, Bp50/CD40, Prominin-1/CD133, MDR-1/CD243, NGFR/CD271, ABCG-2/CD338 and HLA-DR). Both Ob- and Co-hA-MSCs were positive for the following mesenchymal markers: CD9, CD10, CD13, CD26, CD29, CD44, CD47, CD49d, CD54, CD56, CD58, CD71, CD81, CD90, CD99, CD105, CD151, CD166, CD200 and HLA-ABC. A

very weak positivity for the epithelial antigen E-cadherin/CD324 was also observed. Interestingly, CD13 expression was significantly higher in Ob-hA-MSCs than in Co-hA-MSCs, i.e., MFI: 9,802.0 and 3,950.0, respectively (P=0.0043) (Table 3 and Fig. 1A). The immunophenotype characterization confirmed the mesenchymal origin and the higher CD13 expression in hVAT-MSCs and hUC-MSCs from Ob- than from Co-women (hVAT-MSCs - MFI: 8,200.0 *vs* 1,100.0 and hUC-MSCs - MFI: 4,965.0 *vs* 3,155.0, respectively).

***APN/CD13 serum levels***

We first measured baseline serum levels of CD13 in a small group of not pregnant obese and normal weight women and found significantly higher values in the obese subset (medians: 6.00 U/L and 1.00 U/L, P=0.02, respectively) (Fig. 1B). The serum levels of CD13 were also significantly higher in Ob- than in Co-pregnant women at delivery (medians: 24.00 U/L and 7 U/L, P=0.002, respectively), (Fig. 1B). CD13 levels were significantly higher in Ob- and Co-pregnant women than in not pregnant Ob- and Co-women: 4 (P=0.0003) and 7 times (P=0.003), respectively. Furthermore, in Ob-pregnant women, serum CD13 levels were significantly correlated to the levels of CD13 on the surface of hA-MSCs ($r^2$=0.84; P<0.0001) (Fig. 1C).

***CD13 h-MSC expression and adipogenic differentiation***

To investigate whether CD13 is involved in adipogenesis, we cultured Ob- and Co-hA-MSCs for 14 days in adipogenic induction medium. At the end of incubation, the adipogenic potential, as measured by PPARγ and aP2 mRNA levels, was higher in Ob- than in Co-hA-MSCs. In fact, as shown in Fig. 2A and 2B, the mean RQs at day 14 were 0.04 and 0.02, respectively for PPARγ (P=0.02), and 0.02 and 0.01, respectively for aP2 (P=0.03). The same results were obtained with Oil-Red staining; in fact, staining was more intense in Ob- than in Co-hA-MSCs at day 14 of differentiation [Abs (550 nm) = 0.6

and 0.4, P=0.02, respectively] (Fig. 2C). During adipogenesis, CD13 mRNA levels remained higher in Ob- than in Co-hA-MSCs. CD13 silencing by shRNA in Ob-hA-MSCs resulted in a switch-off of CD13 mRNA expression, as evaluated by RT-PCR (Fig. 3A), and, at the same time, the adipogenic potential of these cells did not differ from that observed in Co-hA-MSCs, as shown by similar PPARγ mRNA levels measured in silenced Ob-hA-MSCs and in Co-hA-MSCs (P=0.71) (Fig. 3B). In agreement to CD13 involvement in adipogenesis, we overexpressed CD13 in Co-hA-MSCs (mRNA CD13 mean RQ=7.23) and observed at day 4 of differentiation that PPARγ mRNA levels were higher in treated (mean RQ=0.015) than in untreated (mean RQ=0.001) Co-hA-MSCs. The adipogenic potential at day 14 was also higher in Ob- than in Co-hVAT-MSCs isolated from not pregnant women [aP2: RQs were 0.050 and 0.036; Oil-red-O Abs (550 nm): 0.559 and 0.437, respectively].

***Upregulation of CD13 h-MSC expression by IFN-γ***

We next evaluated if CD13 expression could be upregulated in h-MSCs by IFN-γ as occurs in murine cellular models [32]. To this aim, we treated the Co- and Ob-hA-MSCs with 0.8 ng/mL or 12.5 ng/mL IFN-γ for 24 h. We found that CD13 expression was significantly higher on membranes of Co-hA-MSCs treated with 12.5 ng/mL IFN-γ (P=0.04) than in untreated cells, whereas there was a slight, not significant, increase in treated Ob-hA-MSCs (Supplementary Fig. 2) versus the untreated counterpart cells. In addition, IFN-γ treatment (12.5 ng/mL at 37° C for 24 h) induced the increase of CD13 membrane expression in hVAT-MSCs (Ob- and Co-MSCs: 39% and 8%, respectively) and in Co-hUC-MSCs (4%) versus the untreated counterpart cells, but not in Ob-hUC-MSCs. Our results suggest that high levels of INF-γ drive the up-regulation of CD13 expression in Co-h-MSCs, irrespective of their source and of pregnancy, whereas its effect on Ob-h-MSCs CD13 expression during obesity is ambiguous.

**Discussion**

Human amniotic membrane is a readily available source of abundant fetal MSCs that are free from ethical concerns [33]. hA-MSCs isolated from normal weight healthy women at delivery have been characterized [24, 34, 35], but, to our knowledge, the features of hA-MSCs from obese women are largely unknown. In this study, we used flow cytometry to characterize hA-MSCs isolated at delivery from two groups of women: pre-pregnancy normal weight and pre-pregnancy severely obese women. The immunophenotypic characterization confirmed the mesenchymal origin of the isolated cells [36]. In particular, the distribution of CD56 was in agreement with the placental origin of the isolated hA-MSCs. In fact, this marker is absent from bone marrow [34] and from adipose tissue-derived mesenchymal stem cells [37]. Similarly, the endothelial marker PECAM-1/CD31, and the hematopoietic antigens CD14, CD15, CD16, CD19, CD28, CD33, CD34, CD45 and CD117 were absent from isolated Ob- and Co-hA-MSCs. Staining for the E-cadherin/CD324 epithelial antigen was very weak in our Ob- and Co-hA-MSC preparations; the co-expression of epithelial, albeit at a low intensity, and mesenchymal markers on our h-AMSCs was in agreement with previous findings [38, 39]. Overall, our results are similar to those reported by Parolini et al. [24] and/or Roubelakis [35] regarding the expressed (CD49d, CD90, HLA-ABC, CD13, CD56, CD105, CD166, CD10, CD29, CD44 and CD54) and not expressed (PECAM-1/CD31, HLA-DR, CD14, Prominin-1/CD133, NGFR/CD271, CD34 and CD45) membrane-bound antigens in hA-MSCs. We found that the Ob-hA-MSC immunophenotype is characterized by a significantly higher expression of the APN/CD13 antigen with respect to the Co-hA-MSC phenotype. Besides amnion, CD13 was overexpressed in h-MSCs isolated from umbilical cord in obese womenand in those isolated from VAT in not pregnant women.

Type II metalloprotease APN/CD13 (EC. 3.4.11.2) is a heavily glycosylated membrane-bound protein (~ 960aa, ~ 150 kDA) that is encoded by the human ANPEP gene located on chromosome 15 (q25-q26) [40]. This protein exists also in a soluble form. APN/CD13 is a ubiquitous enzyme present in

a wide variety of human organs, tissues and cell types including placenta, human umbilical vein endothelial cells, monocytes, lymphocytes T, hypothalamus, and epithelial intestinal cells [41]. It has various mechanisms of action: enzymatic cleavage of peptides, endocytosis and signal transduction [42]. APN/CD13 is involved in inflammation, cellular differentiation and proliferation, apoptosis, cell adhesion and motility [42]. Dysregulated expression of membrane and/or soluble forms of APN/CD13 has been observed in many diseases [43], but until now it has never been associated with obesity. Here, we provide the first demonstration that the CD13 antigen is increased on hA-MSCs during obesity and could play a role in adipogenesis. In fact, we first detected a higher adipogenic potential in Ob- than in Co-hA-MSCs after 14 days of adipogenic differentiation and then observed that the adipogenic potential of Ob-hA-MSCs was comparable to that of Co-hA-MSCs after CD13 silencing. Conversely, the adipogenic potential increased in Co-hA-MSCs after CD13 overexpression. Furthermore, we provide evidence that INFγ upregulated CD13 expression in Co-hA-MSCs.

Intriguingly, in Ob-pregnant women APN/CD13 serum levels at delivery were higher than in Co-pregnant women and correlated with CD13 surface Ob-hA-MSC expression ($r^2$=0.89, P<0.0001), which support the hypothesis that the placenta is the major source of the high CD13 levels measured in maternal serum [44]. We also found that leptin concentration and the L/A ratio were increased in Ob-maternal serum at delivery. This finding confirms the concept that these two parameters are obesity risk markers [45, 46].

In conclusion, this characterization of Ob-hA-MSCs shows that antigen CD13, by influencing the adipogenic potential of these cells, could be an *in-utero* risk factor for obesity. Our data strengthen the hypothesis that high serum CD13 and mesenchymal stem cell CD13 are markers of obesity.

**Acknowledgments**

The present work was supported by grants from CEINGE Regione Campania (DGRC 1901/2009) and by MIUR-PRIN 2008. We thank Jean Ann Gilder (Scientific Communication srl, Naples, Italy) for revising and editing the manuscript.

**Author Disclosure Statement**

The authors declare no financial conflicts of interest.

**References**

1. Guelinckx I, Devlieger R, Beckers K, Vansant G. (2008). Maternal obesity: pregnancy complications, gestational weight gain and nutrition. Obes Rev 9:140-50.
2. Heslehurst N, Ells LJ, Simpson H, Batterham A, Wilkinson J, Summerbell CD. (2007). Trends in maternal obesity incidence rates, demographic predictors, and health inequalities in 36,821 women over a 15-year period. BJOG 114:187-94.
3. Kim SY, Dietz PM, England L, Morrow B, Callaghan WM. (2007). Trends in pre-pregnancy obesity in nine states, 1993-2003. Obesity (Silver Spring) 15:986-93.
4. Pipe NG, Smith T, Halliday D, Edmonds CJ, Williams C, Coltart TM. (1979). Changes in fat, fat-free mass and body water in human normal pregnancy. Br J Obstet Gynaecol 86:929-40.
5. Ehrenberg HM, Huston-Presley L, Catalano PM. (2003). The influence of obesity and gestational diabetes mellitus on accretion and the distribution of adipose tissue in pregnancy. Am J Obstet Gynecol 189:944-8.
6. Capobianco V, Nardelli C, Ferrigno M, Iaffaldano L, Pilone V, Forestieri P, Zambrano N, Sacchetti L. (2012). miRNA and Protein Expression Profiles of Visceral Adipose Tissue Reveal miR-141/YWHAG and miR-520e/RAB11A as Two Potential miRNA/Protein Target Pairs Associated with Severe Obesity. J Proteome Res. 11:3358−3369.
7. Drolet R, Richard C, Sniderman AD, Mailloux J, Fortier M, Huot C, Rhéaume C, Tchernof A. (2008). Hypertrophy and hyperplasia of abdominal adipose tissues in women. Int J Obes (Lond) 32:283-91.
8. Bartha JL, Marín-Segura P, González-González NL, Wagner F, Aguilar-Diosdado M, Hervias-Vivancos B. (2007). Ultrasound evaluation of visceral fat and metabolic risk factors during early pregnancy. Obesity (Silver Spring) 15:2233-9.

9. Harvey NC, Poole JR, Javaid MK, Dennison EM, Robinson S, Inskip HM, Godfrey KM, Cooper C, Sayer AA; SWS Study Group. (2007). Parental determinants of neonatal body composition. J Clin Endocrinol Metab 92:523-6.
10. Chu SY, Callaghan WM, Kim SY, Schmid CH, Lau J, England LJ, Dietz PM. (2007). Maternal obesity and risk of gestational diabetes mellitus. Diabetes Care 30:2070-6.
11. O'Brien TE, Ray JG, Chan WS. (2003). Maternal body mass index and the risk of preeclampsia: a systematic overview. Epidemiology 14:368-74.
12. Metwally M, Ong KJ, Ledger WL, Li TC. (2008). Does high body mass index increase the risk of miscarriage after spontaneous and assisted conception? A meta-analysis of the evidence. Fertil Steril 90:714-26.
13. Sattar N, Clark P, Holmes A, Lean ME, Walker I, Greer IA. (2001). Antenatal waist circumference and hypertension risk. Obstet Gynecol 97:268-71.
14. Li C, Kaur H, Choi WS, Huang TT, Lee RE, Ahluwalia JS. (2005). Additive interactions of maternal prepregnancy BMI and breast-feeding on childhood overweight. Obes Res 13:362-71.
15. Fowden AL, Forhead AJ. (2004). Endocrine mechanisms of intrauterine programming. Reproduction 127:515-26.
16. Fowden AL, Forhead AJ, Coan PM, Burton GJ. (2008). The placenta and intrauterine programming. J Neuroendocrinol 20:439-50.
17. Okawa H, Okuda O, Arai H, Sakuragawa N, Sato K. (2001). Amniotic epithelial cells transform into neuron-like cells in the ischemic brain. Neuroreport 12:4003-7.
18. Zeigler BM, Sugiyama D, Chen M, Guo Y, Downs KM, Speck NA. (2006). The allantois and chorion, when isolated before circulation or chorio-allantoic fusion, have hematopoietic potential. Development 133:4183-92.

19. Fukuchi Y, Nakajima H, Sugiyama D, Hirose I, Kitamura T, Tsuji K. (2004). Human placenta-derived cells have mesenchymal stem/progenitor cell potential. Stem Cells 22:649-58.
20. Pittenger MF, Mackay AM, Beck SC, Jaiswal RK, Douglas R, Mosca JD, Moorman MA, Simonetti DW, Craig S, Marshak DR. (1999). Multilineage potential of adult human mesenchymal stem cells. Science 284:143–7.
21. In 't Anker PS, Scherjon SA, Kleijburg-van der Keur C, de Groot-Swings GM, Claas FH, Fibbe WE, Kanhai HH. (2004). Isolation of mesenchymal stem cells of fetal or maternal origin from human placenta. Stem Cells 22:1338–45.
22. Katz AJ, Tholpady A, Tholpady SS, Shang H, Ogle RC. (2005). Cell surface and transcriptional characterization of human adipose-derived adherent stromal (hADAS) cells. Stem Cells 23:412–23.
23. Hwang JH, Lee MJ, Seok OS, Paek YC, Cho GJ, Seol HJ, Lee JK, Oh MJ. (2010). Cytokine expression in placenta-derived mesenchymal stem cells in patients with pre-eclampsia and normal pregnancies. Cytokine 49:95-101.
24. Parolini O, Alviano F, Bagnara GP, Bilic G, Bühring HJ, Evangelista M, Hennerbichler S, Liu B, Magatti M, Mao N, Miki T, Marongiu F, Nakajima H, Nikaido T, Portmann-Lanz CB, Sankar V, Soncini M, Stadler G, Surbek D, Takahashi TA, Redl H, Sakuragawa N, Wolbank S, Zeisberger S, Zisch A, Strom SC. (2008). Concise review: isolation and characterization of cells from human term placenta: outcome of the first international Workshop on Placenta Derived Stem Cells. Stem Cells 26:300-11.
25. Grant A, Palzer S, Hartnett C, Bailey T, Tsang M, Kalyuzhny AE. (2005). A cell-detachment solution can reduce background staining in the ELISPOT assay. Methods Mol Biol 302:87-94.
26. Mariotti E, Mirabelli P, Di Noto R, Fortunato G, Salvatore F. (2008). Rapid detection of mycoplasma in continuous cell lines using a selective biochemical test. Leuk Res 32:323-6.

27. Bieback K, Kern S, Klüter H, Eichler H. (2004). Critical parameters for the isolation of mesenchymal stem cells from umbilical cord blood. Stem Cells 22:625-34.

28. Schäffler A, Büchler C. (2007). Concise review: adipose tissue-derived stromal cells--basic and clinical implications for novel cell-based therapies. Stem Cells. 25:818-27.

29. Perfetto SP, Ambrozak D, Nguyen R, Chattopadhyay P, Roederer M. (2006). Quality assurance for polychromatic flow cytometry. Nat Protocols 1:1522–1530.

30. Lamoreaux L, Roederer M, Koup R. (2006). Intracellular cytokine optimization and standard operating procedure. Nat Protocols 1:1507–1516.

31. Maeker HT, Trotter J. (2006). Flow cytometry controls, instrument setup, and the determination of positivity. Cytometry Part A 69A:1037–1042.

32. Gabrilovac J, Cupić B, Zivković E, Horvat L, Majhen D. (2011). Expression, regulation and functional activities of aminopeptidase N (EC 3.4.11.2; APN; CD13) on murine macrophage J774 cell line. Immunobiology 216:132-44.

33. Miki T, Lehmann T, Cai H, Stolz DB and Stromk SC. (2005). Stem cell characteristics of amniotic epithelial cells. Stem Cells 23:1549-1559.

34. Mariotti E, Mirabelli P, Abate G, Schiattarella M, Martinelli P, Fortunato G, Di Noto R, Del Vecchio L. (2008). Comparative characteristics of mesenchymal stem cells from human bone marrow and placenta: CD10, CD49d, and CD56 make a difference. Stem Cells Dev 17:1039-41.

35. Roubelakis MG, Trohatou O, Anagnou NP. (2012) Amniotic fluid and amniotic membrane stem cells: marker discovery. Stem Cells Int 2012:107836.

36. Delorme B, Ringe J, Gallay N, Le Vern Y, Kerboeuf D, Jorgensen C, Rosset P, Sensebé L, Layrolle P, Häupl T, Charbord P. (2008). Specific plasma membrane protein phenotype of culture-amplified and native human bone marrow mesenchymal stem cells. Blood 111:2631-5.

37. Gronthos S, Franklin DM, Leddy HA, Robey PG, Storms RW, Gimble JM. (2001). Surface protein characterization of human adipose tissue-derived stromal cells. J Cell Physiol 189:54-63.

38. Sakuragawa N, Kakinuma K, Kikuchi A, Okano H, Uchida S, Kamo I, Kobayashi M, Yokoyama Y. (2004). Human amnion mesenchyme cells express phenotypes of neuroglial progenitor cells. J Neurosci Res 78:208-14.

39. Soncini M, Vertua E, Gibelli L, Zorzi F, Denegri M, Albertini A, Wengler GS, Parolini O. (2007). Isolation and characterization of mesenchymal cells from human fetal membranes. J Tissue Eng Regen Med 1:296-305.

40. Watt, V.M. and Willard, H.F. (1990). The human aminopeptidase N gene: isolation, chromosome localization, and DNA polymorphism analysis. Hum Genet 85:651–654.

41. Lai A, Ghaffari A, Ghahary A. (2010). Inhibitory effect of anti-aminopeptidase N/CD13 antibodies on fibroblast migration. Mol Cell Biochem 343:191-9.

42. Paola Mina-Osorio. (2008). The moonlighting enzyme CD13: old and new functions to target. Trends in Molecular Medicine 14:361-371.

43. Luan Y, Xu W. (2007). The structure and main functions of aminopeptidase N. Curr Med Chem 14:639-47.

44. Kawai M, Araragi K, Shimizu Y, Hara Y. (2009). Identification of placental leucine aminopeptidase and triton-slowed aminopeptidase N in serum of pregnant women. Clin Chim Acta 400:37-41.

45. Labruna G, Pasanisi F, Nardelli C, Tarantino G, Vitale DF, Bracale R, Finelli C, Genua MP, Contaldo F, Sacchetti L. (2009). UCP1 -3826 AG+GG genotypes, adiponectin, and leptin/adiponectin ratio in severe obesity. J Endocrinol Invest 32:525-9.

46. Labruna G, Pasanisi F, Nardelli C, Caso R, Vitale DF, Contaldo F, Sacchetti L. (2011). High leptin/adiponectin ratio and serum triglycerides are associated with an "at-risk" phenotype in young severely obese patients. Obesity (Silver Spring) 19:1492-6.

**Legends**

**FIG. 1. Expression of CD13 antigen in control (Co-) and obese (Ob-) pregnant women. A**: Ob-hA-MSCs expressed significantly higher amounts (at Mann-Whitney test) of CD13 surface antigen compared with Co-hA-MSCs (P=0.0043); **B**: serum levels of CD13 were significantly higher both in Ob- than in Co-not pregnant women (P=0.02) and in Ob- than in Co-women at delivery (P=0.002); **C**: Serum CD13 levels were correlated with CD13 surface expression levels in Ob-pregnant women ($r^2$=0,84; P<0.0001). The box plots provide a vertical view of the data expressed as median, 25th percentile, 75th percentile and extreme values.

**FIG. 2. Adipogenic potential in Ob-hA-MSCs and in Co-hA-MSCs.** The statistically significant higher mRNA expression levels of PPARγ (P=0.02) (**A**) and of aP2 (P=0.03) (**B**) measured 14 days after the adipogenic induction, indicated increased adipogenesis in Ob- versus Co-hA-MSCs. (**C**) The higher adipogenesis in Ob- than in Co-hA-MSCs was also confirmed by Oil-Red staining [Abs (550 nm) = 0.6 and 0.4, P=0.02, respectively].

**FIG. 3. Role of CD13 in adipogenesis.** (**A**) mRNA expression levels of CD13 were significantly higher in Ob- than in Co-hA-MSCs at day 0 (P=0.02), day 2 (P=0.02) and day 4 (P=0.04) when cultured with adipogenic medium. CD13 mRNA expression was switched-off in Ob-hA-MSCs after CD13 silencing with shRNA. (**B**) At day 4 of adipogenic induction, PPARγ mRNA expression levels that were significantly higher in Ob-hA-MSCs than in Co-hA-MSCs (P=0.01), decreased to the levels detected in Co-hA-MSCs after CD13 silencing (P=0.71), which indicates that CD13 enhances adipogenesis in hA-MSCs. n.s.: not statistically significant difference.

**Table 1.** Surface immunophenotypic profile investigated in hA-MSCs by flow cytometry

| Fluorochrome | CD Antigen | Other Names | Molecular Weight (kDa) | Cell expression | Function |
|---|---|---|---|---|---|
| **FITC** | **CD9** | Tspan-29 | 24-26 | Platelets, pre-B cells, activated T cells | Adhesion, migration, platelet activation |
| **APC** | **CD10** | CALLA | 100 | B/T precursors, stromal cells | Endopeptidase |
| **PE** | **CD13** | APN | 150 | Granulocytes, monocytes and their precursors, endothelial cells, epithelial cells, mesenchymal stem cells | Metalloproteinase |
| **PE** | **CD14** | LPS-R | 53-55 | Monocytes, macrophages | Receptor for LPS/LPB complex |
| **APC** | **CD15** | Lewis X | _ | Granulocyte, monocyte, epithelial cells | Cell adhesion |
| **PE** | **CD16** | FCγRIIIa | 50-65 | Neutrophils, NK, macrophages | Low affinity with FCγ receptor, mediates phagocytosis |
| **APC** | **CD19** | Bgp95 | 95 | B cells, not on plasma cells | Signal transduction |
| **FITC** | **CD26** | DPP IV | 110 | Mature thymocytes, T, B, NK cells | Exoprotease, co-stimulation |
| **APC** | **CD28** | Tp44 | 44 | Most T cells, thymocytes, NKs and plasma cells | Co-stimulation |
| **APC** | **CD29** | VLA β1-chain | 130 | T, B, granulocytes, monocytes, fibroblasts, endothelial cells, NKs , platelet | Adhesion activation, embryogenesis and development |
| **FITC** | **CD31** | PECAM-1 | 130-140 | Monocytes, platelets, granulocytes and endothelial cells | Cell adhesion |
| **APC** | **CD33** | My9 | 67 | Monocytes, granulocytes, mastocytes and myeloid progenitors | Cell adhesion |
| **APC** | **CD34** | My10 | 105-120 | Hematopoietic stem cells and progenitors, endothelial cells | Cell adhesion |
| **APC** | **CD36** | Platelet GPIV | 85 | Platelets, monocytes, macrophages, endothelial cells, erythroid precursors | Adhesion and phagocytosis |
| **FITC** | **CD40** | Bp50 | 48 | Monocytes, macrophages, B cells, endothelial cells, fibroblasts, keratinocytes | Co-stimulation to B cells, growth, differentiation and isotype switching |
| **APC** | **CD44** | H-CAM | 90 | Leukocytes, erythrocytes and epithelial cells | Rolling, homing and aggregation |
| **Per Cp** | **CD45** | LCA | 180-220 | Hematopoietic cells, except erythrocytes and platelets | Critical for T and B cell receptor mediated activation |
| **FITC** | **CD47** | IAP I | 50-55 | Hematopoietic, epithelial, endothelial and brain mesenchymal cells | Adhesion |
| **FITC** | **CD49d** | VLA-4 | 150 | B cells, T cells, monocytes, eosinophils, basophils, NKs, dendritic cells | Adhesion, migration, homing, activation |
| **APC** | **CD54** | ICAM-1 | 80-114 | Epithelial and endothelial cells monocyte. Low on resting lymphocytes, upregulate on activated | T cell activation |
| **PE** | **CD56** | NCAM | 175-220 | Neural, tumors, embryonic tissue, NK | Homophilic and heterophilic adhesion |
| **PE** | **CD58** | LFA-3 | 40-70 | Leucocytes, erythrocytes, epithelial endothelial cells and fibroblasts | Costimulation |
| **FITC** | **CD71** | Transferrin recepor | 95 | Reticulocytes, erythroid precursor | Controls iron intake during cell proliferation |
| **APC** | **CD81** | TAPA-1 | 26 | B and T cells, monocytes, endothelial cells | Signal transduction |
| **FITC** | **CD90** | Thy-1 | 25-35 | Hematopoietic stem cells, neurons, mesenchymal stem cells | Inhibition of hematopoietic stem cells and neuron differentiation |
| **PE** | **CD99** | MIC2 | 32 | Leucocyte, NK, monocytes, endothelial and epithelial cells | Leucocyte migration, T cell activation, cell adhesion |
| **PE** | **CD105** | Endoglin | 90 | Endothelial and mesenchymal stem cells, erythroid precursors, monocytes | Angiogenesis, modulates cellular response to TGFβ1 |
| **PE** | **CD117** | c-kit | 145 | Hematopoietic stem cells and progenitors | Crucial for hematopoietic stem cells |
| **PE** | **CD133** | Prominin-1 | 120 | Hematopoietic stem cell, endothelial, epithelial and neural precursors | Unknown function, stem cell marker |
| **PE** | **CD151** | PETA-3 | 32 | Endothelial and epithelial cells, megakaryocytes, platelets | Adhesion |
| **PE** | **CD166** | ALCAM | 100-105 | Neurons, activated T cells, epithelial cells, mesenchymal stem cells | Adhesion, T cell activation |
| **PE** | **CD200** | OX-2 | 33 | B cells, activated T cells, thymocytes, neurons endothelium | Down-regulatory signal for myeloid cell functions |
| **FITC** | **CD243** | MDR-1 | 170 | Stem cells, multi drug resistant tumors | Influences the up-take, distribution, elimination of drugs |
| **APC** | **CD271** | NGFR | 75 | Neurons, stromal and dendritic follicular cells | Low affinity for NGF receptor |
| **APC** | **CD324** | E-cadherin | 120 | Epithelial, keratinocytes, platelet | Adhesion, growth, differentiation |
| **APC** | **CD338** | ABCG-2 | 72 | Hematopoietic stem cells, liver, kidney, intestine, side population of stem cells | Absorption and excretion of xenobiotics |
| **FITC** | **HLA-ABC** | Class I MHC | 46 | All nucleated cells and platelets | Antigen presentation |
| **FITC** | **HLA-DR** | Class II MHC | 30 | B cells, monocytes, myeloid progenitors, activated T and dendritic cells | Antigen presentation |

**Table 2.** Clinical and biochemical characteristics of obese (Ob-) and normal weight control (Co-) pregnant women at delivery and their newborns.

| **A** | | |
|---|---|---|
| **Mother's parameters** | **Ob-pregnant women (n=16)** | **Co-pregnant women (n=7)** |
| Age (years) | 32.6 (0.9) | 30.7 (1.5) |
| Weight (kg) [a] | 110.1 (5.4) | 65.2 (3.6) |
| Height (m) | 163.3(1.6) | 169.0 (1.7) |
| BMI pre-pregnancy (kg/m$^2$) [a] | 40.3 (1.8) | 22.4 (1.0) |
| Weight gain in pregnancy [b] | 8.4 (1.3) | 14.3 (1.8) |
| Systolic blood pressure (mmHg) | 124.3 (2.7) | 117.1 (5.1) |
| Diastolic blood pressure (mmHg) [c] | 82.5 (2.2) | 74.2 (2.0) |
| Frequency cardiac | 79.6 (1.7) | 79.0 (3.7) |
| Gestational age | 38.4 (0.3) | 38.7 (0.2) |
| Glucose (mmol/L) | 4.3 (0.1) | 4.0 (0.3) |
| Total cholesterol (mmol/L) | 6.9 (0.4) | 7.3 (0.1) |
| Triglycerides (mmol/L) | 2.8 (0.2) | 2.3 (0.3) |
| AST (U/L) | 15 [d] (12.2-26.5[d]) | 14.8 (0.7) |
| ALT (U/L) | 13 [d] (9.2-17.7[d]) | 12.1 (1.1) |
| ALP (U/L) | 124.2 (11.1) | 115.0 (12.6) |
| GGT (U/L) | 11.0 (1.7) | 8.8 (1.5) |
| Leptin (L) (ng/ml) [a] | 38.5 (2.2) | 15.2 (3.3) |
| Adiponectin (A) (μg/ml) | 6.0 (0.7) | 7.5 (1.4) |
| L/A [a] | 7.7 (0.6) | 2.6 (0.5) |
| **B** | | |
| **Newborn features** | **Ob-newborns (n=16)** | **Co-newborns (n=7)** |
| Birth weight (kg) | 3162 (0.1) | 3401 (0.1) |
| Length (cm) | 49.6 (0.7) | 50.8 (0.7) |
| Head circumference (cm) | 34.0 (0.4) | 34.8 (0.3) |
| Apgar 1' | 7.0 [d] (7.0-8.0 [d]) | 7.8 (0.2) |
| Apgar 5' | 9.0 [d] (8.5-9.0 [d]) | 8.7 (0.1) |

Data are expressed as mean (SEM) (parametric distributions).
Statistically significant difference at Student *t* test: [a] P<0.0001, [b] P =0.025 and [c] P=0.039.
[d] median value and 25$^{th}$–75$^{th}$ percentiles (non parametric distributions).

**Table 3.** Immunophenotyping of hA-MSCs isolated from obese (Ob-) and control (Co-) pregnant women

| | | Ob-hA-MSCs | | Co-hA-MSCs | | |
|---|---|---|---|---|---|---|
| **Not expressed antigens** | | | | | | |
| **Fluorochrome** | **Antigen** | **MFI** | **25th-75th Percentiles** | **MFI** | **25th-75th Percentiles** | **p Value** |
| **FITC** | **CD31** | 364.0 | 278.3-511.3 | 306.5 | 286.8-368.0 | 0.3254 |
| | **CD40** | 444.0 | 336.5-568.3 | 388.0 | 357.0-457.8 | 0.4824 |
| | **CD243** | 363.0 | 292.3-528.3 | 307.5 | 274.0-378.3 | 0.2061 |
| | **HLA-DR** | 355.0 | 283.8-530.0 | 297.0 | 272.5-374.8 | 0.2415 |
| | **NC** | 325.0 | 250.0-516.3 | 279.0 | 218.8-418.8 | 0.4260 |
| **PE** | **CD14** | 166.5 | 125.5-197.8 | 134.5 | 124.5-157.8 | 0.2815 |
| | **CD16** | 36.0 | 11.5-71.7 | 65.5 | 50.5-72.0 | 0.2407 |
| | **CD117** | 142.5 | 109.5-189.3 | 121.0 | 116.0-176.8 | 0.6065 |
| | **CD133** | 95.5 | 80.5-112.8 | 87.5 | 76.50-110.5 | 0.5423 |
| | **NC** | 115.5 | 91.75-181.5 | 102.5 | 93.25-135.0 | 0.5427 |
| **APC** | **CD15** | 122.0 | 91.0-283.5 | 122.5 | 80.0-162.5 | 0.6065 |
| | **CD36** | 241.5 | 194.0-388.5 | 200.5 | 145.5-267.3 | 0.2417 |
| | **CD271** | 208.0 | 127.0-296.5 | 170.0 | 127.5-233.3 | 0.6065 |
| | **CD338** | 200.5 | 106.5-373.0 | 107.5 | 101.8-146.8 | 0.1223 |
| | **CD19** | 192.0 | 154.0-241.3 | 144.0 | 120.3-182.2 | 0,1012 |
| | **CD28** | 91.0 | 5.2-228.5 | 85.5 | 0-122.0 | 0.1722 |
| | **CD33** | 147.5 | 10.0-189.5 | 105.5 | 90.0-132.3 | 0.6734 |
| | **CD34** | 186.5 | 105.0-241.5 | 133.0 | 17.5-206.0 | 0.4250 |
| | **NC** | 169.0 | 99.5-244.8 | 92.0 | 64.0-204.0 | 0.2061 |
| **Per Cp** | **CD45** | 215.5 | 133.8-251.3 | 167.0 | 146.0-208.0 | 0.6734 |
| | **NC** | 305.0 | 252.0-483.3 | 288.5 | 261.3-348.8 | 0.7431 |
| **Expressed antigens** | | | | | | |
| **Fluorochrome** | **Antigen** | **MFI** | **25th-75th Percentiles** | **MFI** | **25th-75th Percentiles** | **p Value** |
| **FITC** | **CD9** | 3,538.0 | 2,172.0-6,871.0 | 2,156.0 | 1,743.0-3,495.0 | 0.2417 |
| | **CD26** | 1,287.0 | 651.8-3,235.0 | 1,308.0 | 742.3-1,920.0 | 0.9626 |
| | **CD47** | 1,339.0 | 980.3-2,312.0 | 1,287.0 | 1,106.0-1,344.0 | 0.4824 |
| | **CD49d** | 1,185.0 | 946.8-1,393.0 | 941.0 | 708.3-1,140.0 | 0.2061 |
| | **CD71** | 1,271.0 | 796.5-2,147.0 | 1,093.0 | 897.0-1,538.0 | 0.7431 |
| | **CD90** | 37,140.0 | 22,740.0-52,690.0 | 36,210.0 | 21,640.0-50,260.0 | 0.8149 |
| | **CD324** | 517.0 | 463.0-551.0 | 436.0 | 375.0-545.0 | 0.3027 |
| | **HLA-ABC** | 9,363.0 | 4,033.0-14,180.0 | 5,424.0 | 3,987.0-6,539.0 | 0.1223 |
| | **NC** | 325.0 | 250.0-516.3 | 279.0 | 218.8-418.8 | 0.4260 |
| **PE** | **CD13** | 9,802.0 | 6,786.0-17,130.0 | 3,950.0 | 3,634.0-4,961.0 | 0.0043 [a] |
| | **CD56** | 496.0 | 293.8-711.0 | 528.0 | 151.0-1,048.0 | 0.9626 |
| | **CD58** | 2,432.0 | 1,723.0-2,792.0 | 2,009.0 | 1,798.0-2,459.0 | 0.5427 |
| | **CD99** | 405.0 | 296.5-586.3 | 467.5 | 360.5-651.0 | 0.3736 |
| | **CD105** | 652.0 | 507.0-1,329.0 | 790.0 | 746.0-847.8 | 0.6734 |
| | **CD151** | 16,010.0 | 10,970.0-21,430.0 | 19,410.0 | 11,090.0-23,690.0 | 0.4260 |
| | **CD166** | 5,215.0 | 3,551.0-7,382.0 | 4,634.0 | 3,962.0-5,608.0 | 0.6734 |
| | **CD200** | 722.5 | 205.8-1,699.0 | 1,137.0 | 631.5-1,444.0 | 0.3736 |
| | **NC** | 115.5 | 91.7-181.5 | 102.5 | 93.2-135.0 | 0.5427 |
| **APC** | **CD10** | 1,247.0 | 999.3-2,319.0 | 1,890.0 | 1,122.0-3,031.0 | 0.3736 |
| | **CD29** | 45,150.0 | 25,130.0-54,610.0 | 24,240.0 | 17,660.0-40,000.0 | 0.0832 |
| | **CD44** | 11,440.0 | 8,186.0-16,290.0 | 7,259.0 | 6,613.0-9,753.0 | 0.0678 |
| | **CD54** | 9,910.0 | 5,404.0-14,260.0 | 10,660.0 | 9,486.0-24,670.0 | 0.3736 |

| | | | | | | |
|---|---|---|---|---|---|---|
| | **CD81** | 31,240.0 | 19,110.0-55,050.0 | 38,890.0 | 24,500.0-44,640.0 | 0.8149 |
| | **NC** | 169.0 | 99.5-244.8 | 92.0 | 64.0-204.0 | 0.2061 |

MFI, Median fluorescence intensity; [a] significant P value at Mann-Whitney test.

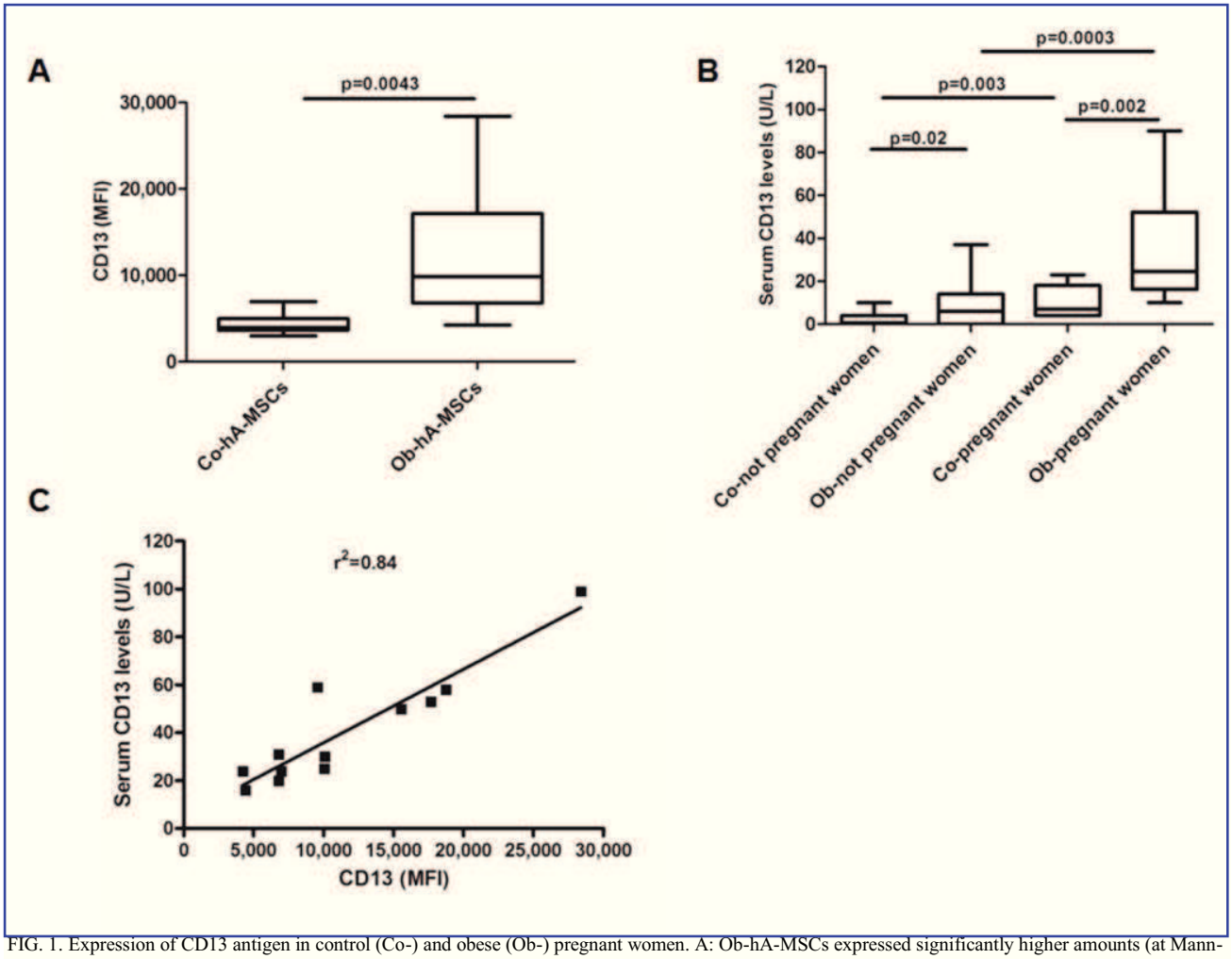


FIG. 1. Expression of CD13 antigen in control (Co-) and obese (Ob-) pregnant women. A: Ob-hA-MSCs expressed significantly higher amounts (at Mann-Whitney test) of CD13 surface antigen compared with Co-hA-MSCs (P=0.0043); B: serum levels of CD13 were significantly higher both in Ob- than in Co-not pregnant women (P=0.02) and in Ob- than in Co-women at delivery (P=0.002); C: Serum CD13 levels were correlated with CD13 surface expression levels in Ob-pregnant women (r<sup>2</sup>=0,84; P<0.0001). The box plots provide a vertical view of the data expressed as median, 25th percentile, 75th percentile and extreme values.

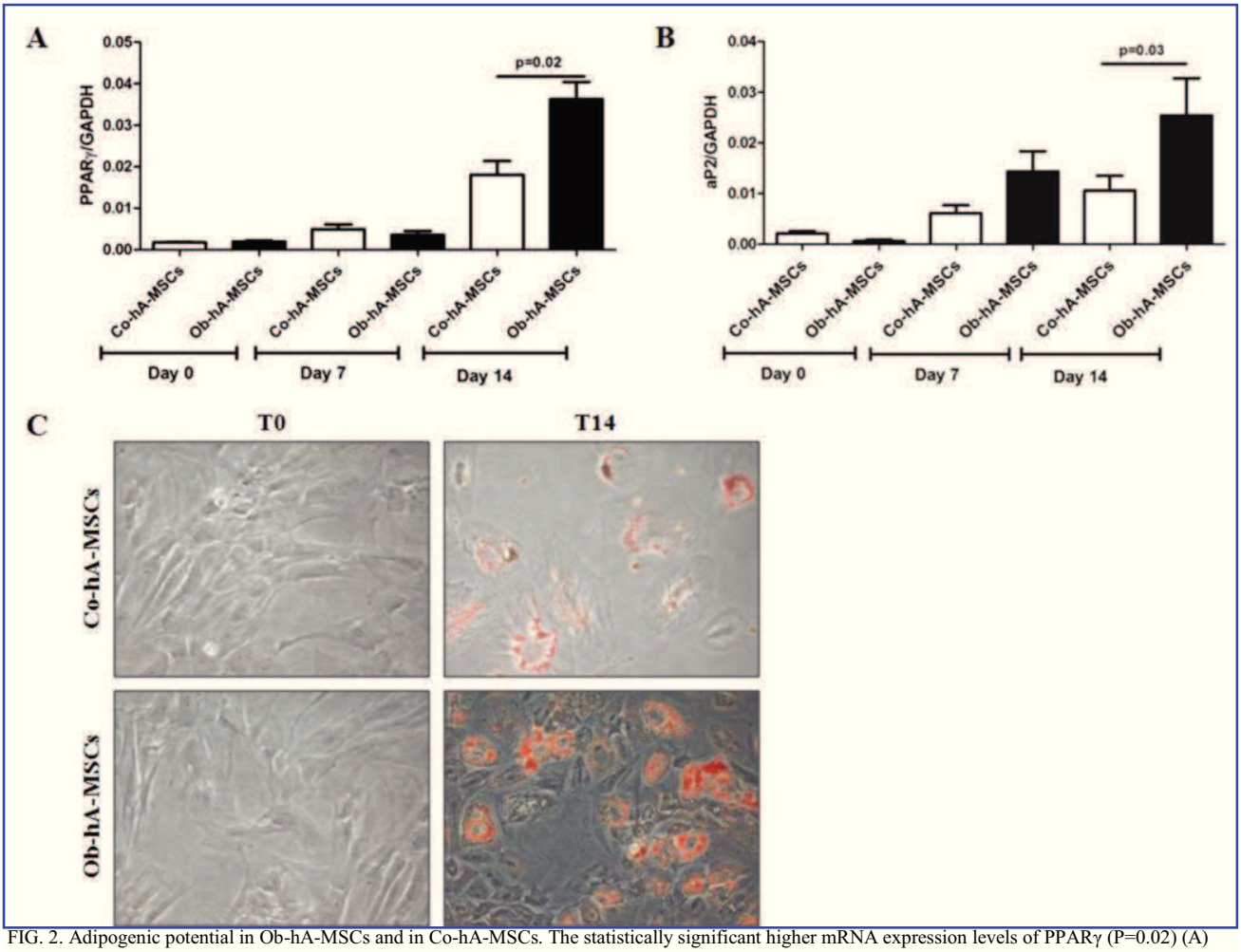


FIG. 2. Adipogenic potential in Ob-hA-MSCs and in Co-hA-MSCs. The statistically significant higher mRNA expression levels of PPARγ (P=0.02) (A) and of aP2 (P=0.03) (B) measured 14 days after the adipogenic induction, indicated increased adipogenesis in Ob- versus Co-hA-MSCs. (C) The higher adipogenesis in Ob- than in Co-hA-MSCs was also confirmed by Oil-Red staining [Abs (550 nm) = 0.6 and 0.4, P=0.02, respectively].

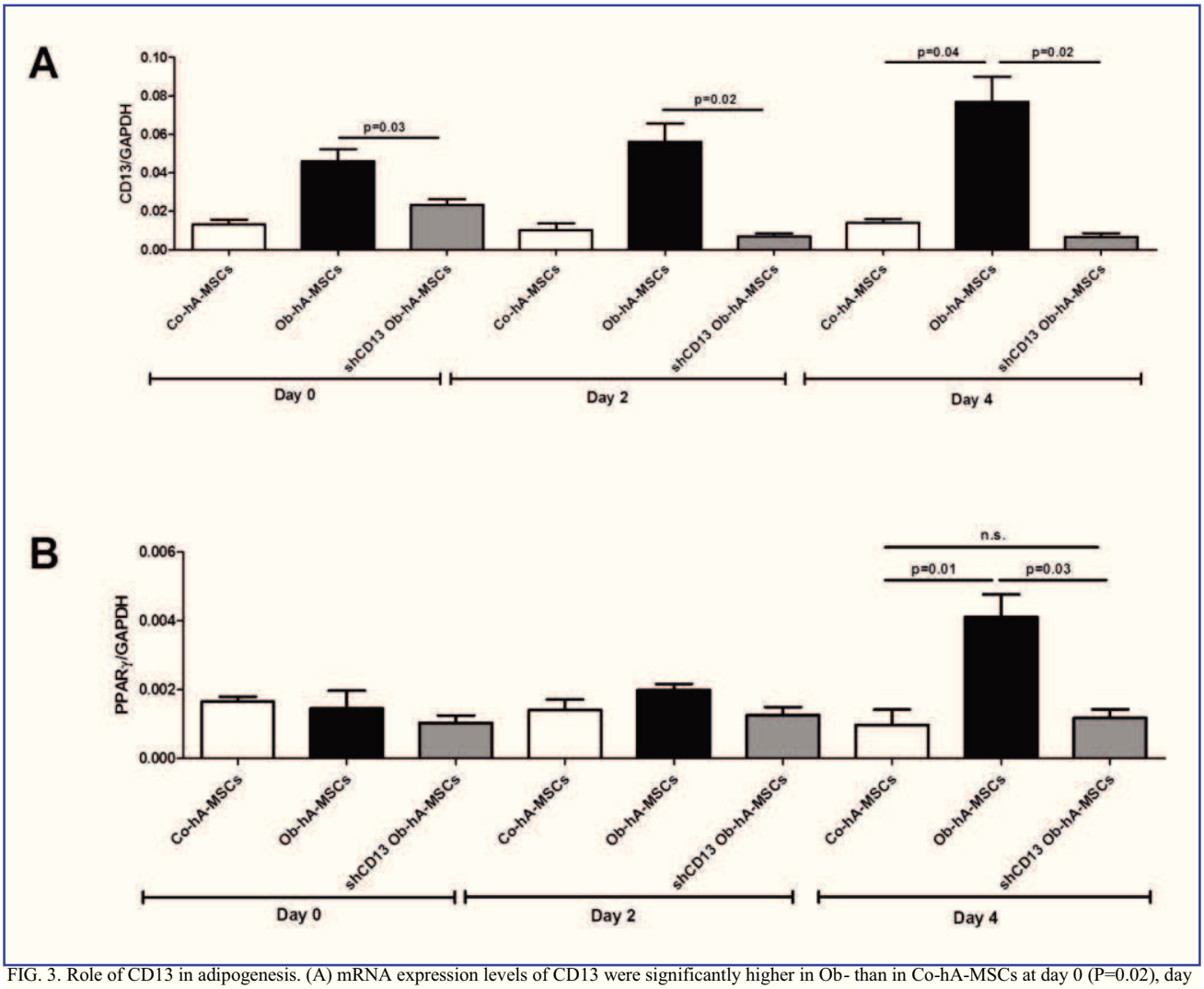


FIG. 3. Role of CD13 in adipogenesis. (A) mRNA expression levels of CD13 were significantly higher in Ob- than in Co-hA-MSCs at day 0 (P=0.02), day 2 (P=0.02) and day 4 (P=0.04) when cultured with adipogenic medium. CD13 mRNA expression was switched-off in Ob-hA-MSCs after CD13 silencing with shRNA. (B) At day 4 of adipogenic induction, PPARγmRNA expression levels that were significantly higher in Ob-hA-MSCs than in Co-hA-MSCs (P=0.01), decreased to the levels detected in Co-hA-MSCs after CD13 silencing (P=0.71), which indicates that CD13 enhances adipogenesis in hA-MSCs. n.s.: not statistically significant difference.

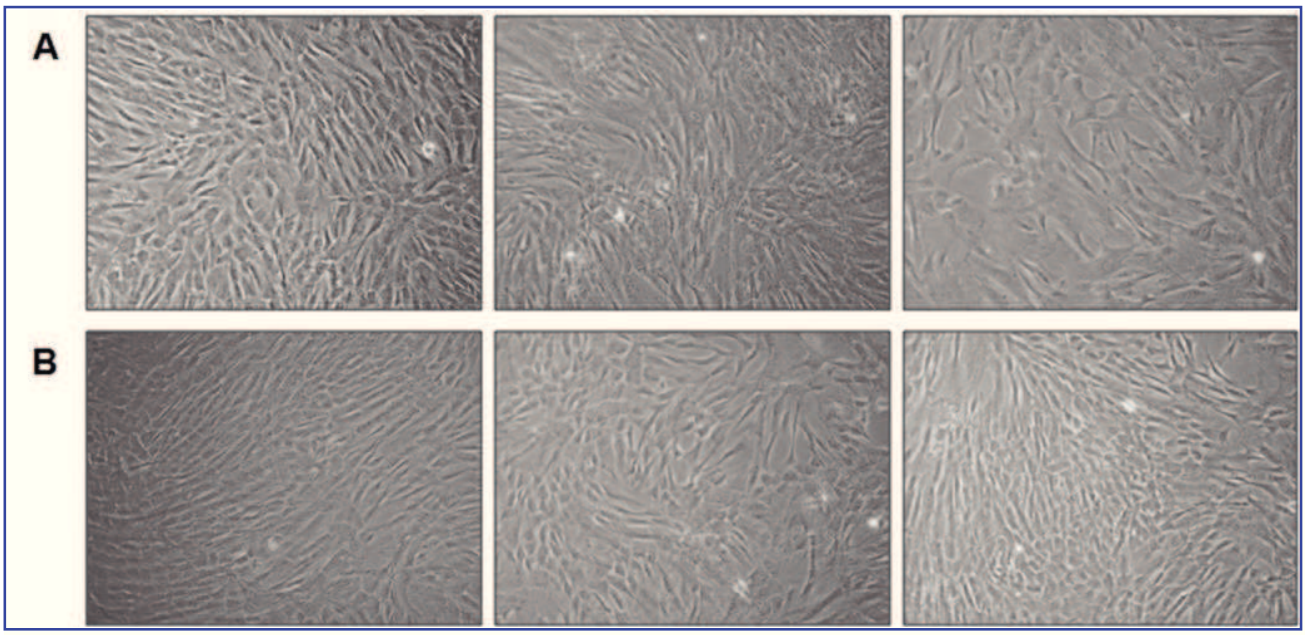

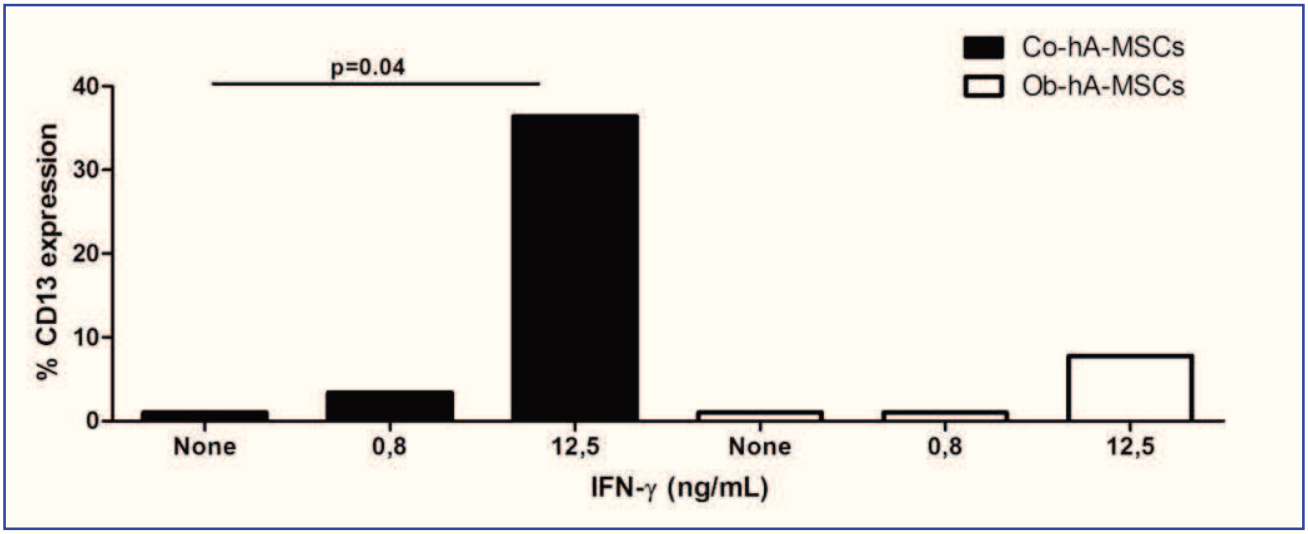

**Supplementary Figures legend**

**Supplementary Figure 1: Morphology of hA-MSCs isolated from pregnant women.** A similar fibroblastic-like shape was observed in three Ob- **(A)** and three Co- **(B)** hA-MSCs after 4 population doublings by phase contrast light microscopy (magnification 10x).

**Supplementary Figure 2: CD13 expression on Co- and Ob-hA-MSCs treated with 0.8 ng/mL or 12.5 ng/mL IFN-γ for 24 h.** CD13 expression significantly increased on membranes of Co-hA-MSCs treated with 12.5 ng/mL IFN-γ (P=0.04) versus untreated counterpart cells, whereas there was a slight, not significant increase, in treated Ob-hA-MSCs versus untreated cells.

**Supplementary Table 1:** Antibody cocktails contained in each tube for hA-MSCs immunophenotyping by flow cytometry.

| Tube | CD Antigens |
|---|---|
| 1 | Anti-CD90-FITC (clone 5E10)/anti-CD13-PE (clone L138)/anti-CD45-PerCP (clone 2D1)/anti-CD34-APC (clone 8G12) |
| 2 | Anti-HLA-DR-FITC (clone l243)/anti-CD14-PE (clone MΦP9)/anti-CD45-PerCP (clone 2D1)/anti-CD29-APC (clone MAR4) |
| 3 | Anti-CD243-FITC (clone17F9)/anti-CD56-PE (clone MY31)/anti-CD45-PerCP (clone 2D1)/anti-CD44-APC (clone g44-26) |
| 4 | Anti-CD324-FITC (clone 36)/anti-CD105-PE (clone 266)/anti-CD45-PerCP (clone 2D1)/anti-CD338-APC (clone 5D3) |
| 5 | Anti-CD71-FITC (clone L01.1)/anti-CD56-PE (clone MY31)/anti-CD45-PerCP (clone 2D1)/anti-CD28-APC (clone CD28.2) |
| 6 | Anti-CD90-FITC (clone 5E10)/anti-CD200-PE (clone MRC OX-104)/anti- CD45-PerCP (clone 2D1)/anti-CD33-APC (clone p67.6) |
| 7 | Anti-HLA-A,B,C-FITC (clone G46-2.6)/anti-CD16-PE (clone B73.1)/anti-CD45-PerCP (clone 2D1)/anti-CD36-APC (clone CB38 NL07) |
| 8 | Anti-CD90-FITC (clone 5E10)/anti-CD200-PE (clone MRC OX-104)/anti-CD45-PerCP (clone 2D1)/anti-CD34-APC (clone 8G12) |
| 9 | Anti-CD9-FITC (clone ML-13)/anti-CD133-PE (clone ACC133/1)/anti-CD45-PerCP (clone 2D1)/anti-CD10-APC (clone HI10A) |
| 10 | Anti-49d-FITC (clone R1-2)/anti-CD58-PE (clone L306.4)/anti-CD45-PerCP (clone 2D1)/anti-CD271-APC (clone ME20.4-1.H4) |
| 11 | Anti-CD31-FITC (clone WM59)/anti-CD117-PE (clone 104D2)/anti-CD45-PerCP (clone 2D1)/anti-CD81-APC (clone JS-81) |
| 12 | Anti-CD26-FITC (clone L272)/anti-CD99-PE (clone TU12)/anti-CD45-PerCP (clone 2D1)/anti-CD19-APC (clone SJ25C1) |
| 13 | Anti-CD40-FITC (clone 53C)/anti-CD151-PE (clone 14A.H1)/anti-CD45-PerCP (clone 2D1)/anti-CD54-APC (clone HA58) |
| 14 | Anti-CD47-FITC (clone B6H12)/anti-CD166-PE (clone 3A6)/anti-CD45-PerCP (clone 2D1)/anti-CD15-APC (clone HI98) |

FITC: fluorescein isothiocyanat; PE: R-Phycoerythrin; PerCP: peridinin-chlorophyll-protein complex; APC: allophycocyanin

**Supplementary Table 2**: PCR oligonucleotide primers.

| | |
|---|---|
| CD13 Forward | GGACAGCGAGTTCGAGGGGGA |
| CD13 Reverse | AGTGGCCACCACCTTTCTGACA |
| PPARγ Forward | CATACATAAAGTCCTTCCCGCTG |
| PPARγ Reverse | CGAATGGTGATTTGTCTGTTGTCT |
| aP2 Forward | GGTGGTGGAATGCGTCATG |
| aP2 Reverse | CAACGTCCCTTGGCTTATGC |
| GAPDH Forward | GTCGGAGTCAACGGATTTGG |
| GAPDH Reverse | AAAAGCAGCCCTGGTGACC |